Distribution Agreement

In presenting this thesis or dissertation as a partial fulfillment of the requirements for an advanced degree from Emory University, I hereby grant to Emory University and its agents the non-exclusive license to archive, make accessible, and display my thesis or dissertation in whole or in part in all forms of media, now or hereafter known, including display on the world wide web. I understand that I may select some access restrictions as part of the online submission of this thesis or dissertation. I retain all ownership rights to the copyright of the thesis or dissertation. I also retain the right to use in future works (such as articles or books) all or part of this thesis or dissertation.

Signature:

_____ _____

Jacob T. Beaver Date

Zika virus induced neuro-ocular pathology correlates with autoreactive anti-ganglioside antibodies and can be ameliorated with cutaneous vaccination

By

Jacob T. Beaver
Doctor of Philosophy

Graduate Division of Biological and Biomedical Science
Microbiology & Molecular Genetics

Ioanna Skountzou MD/Ph.D. Advisor	Richard Compans, Ph.D. Co-Advisor
Joshy Jacob, Ph.D. Committee Member	Bernardo Mainou, Ph.D. Committee Member
David A. Steinhauer, Ph.D. Committee Member	Arash Grakoui, Ph.D. Committee Member

Accepted:

Lisa A. Tedesco, Ph.D.
Dean of the James T. Laney School of Graduate Studies

Date

Zika virus induced neuro-ocular pathology correlates with autoreactive anti-ganglioside antibodies and can be ameliorated with cutaneous vaccination

By

Jacob T. Beaver
B.S., Coastal Carolina University, 2013

Advisor: Ioanna Skountzou, M.D./Ph.D
Co-Advisor: Richard W. Compans, Ph.D.

An abstract of
A dissertation submitted to the Faculty of the
James T. Laney School of Graduate Studies of Emory University
in partial fulfillment of the requirements for the degree of
Doctor of Philosophy
in
Microbiology & Molecular Genetics
2020

ABSTRACT

Zika virus induced neuro-ocular pathology correlates with autoreactive anti-ganglioside antibodies and can be ameliorated with cutaneous vaccination

By Jacob T. Beaver

Zika virus (ZIKV) garnered international attention between 2015-2017, initially infecting pregnant women in Brazil and later attacking indiscriminately residents of the Americas. Infection of pregnant population resulted in a newly identified fetal-maternal pathology including severe neurological impairments such as microcephaly, which is now part of the congenital ZIKV syndrome (CZS). Among adults, ZIKV caused moderate to severe neuro-ocular sequelae, with symptoms ranging from conjunctivitis to Guillain-Barré Syndrome (GBS). The lack of case reports of ZIKV since 2017 may be directly attributed to increased herd immunity and better arbovirus vector control. However, children born from mothers infected with ZIKV continue to demonstrate the long-term impacts of fetal-maternal ZIKV infection, as reports of CSZ-related brain and eye developmental abnormalities continue to emerge among children born without microcephaly.

In this dissertation, we used immunocompetent BALB/c mice, which generate robust humoral immune responses, to investigate long-term impacts of ZIKV infection. Using a high infectious dose to overcome natural interferon barriers that may hinder murine infections, we found that immunocompetent mice exhibited motor impairment such as arthralgia, as well as ocular inflammation resulting in retinal vascular damage, and corneal edema. This pathology persisted 100 days after infection with evidence of chronic inflammation in immune-privileged compartments, demyelination in the hippocampus and motor cortex regions of the brain, and retinal/corneal hyperplasia. Pathology in immunocompetent animals coincided with weakly neutralizing antibodies and increased ADE among ZIKV strains (PRVABC59, FLR, and MR766) and all Dengue virus (DENV) serotypes. These antibodies were autoreactive to GBS-associated gangliosides. This study highlights the importance of longevity studies in ZIKV infection and confirms the role of anti-ganglioside antibodies in ZIKV-induced neuro-ocular disease.

Zika virus induced neuro-ocular pathology correlates with autoreactive anti-ganglioside antibodies and can be ameliorated with cutaneous vaccination

By

Jacob T. Beaver
B.S., Coastal Carolina University, 2013

Advisor: Ioanna Skountzou, M.D./Ph.D
Co-Advisor: Richard W. Compans, Ph.D.

A dissertation submitted to the Faculty of the
James T. Laney School of Graduate Studies of Emory University
in partial fulfillment of the requirements for the degree of
Doctor of Philosophy
in Microbiology & Molecular Genetics
2020

TABLE OF CONTENTS

CHAPTER I: INTRODUCTION

ABSTRACT

Zika virus (ZIKV) became a public health emergency of global concern in 2015 due to its rapid expansion from French Polynesia to Brazil, spreading quickly throughout the Americas. Its unexpected correlation to neurological impairments and defects, now known as congenital Zika syndrome, brought urgency to characterize the pathology and develop safe, effective vaccines. ZIKV genetic analyses have identified two major lineages, Asian and African, which have undergone divergent mutations during the past 50 years. Although ZIKV has been circulating throughout Africa and Asia for the later part of the 20th century, the symptoms were mild and not associated with serious pathology until now. ZIKV evolution also lead to form of novel modes of transmission, including maternal-fetal transmission, sexual transmission, and transmission through the eye. The African and Asian lineages have demonstrated differential pathogenesis and molecular responses *in vitro* and *in vivo*. The limited number of human infections prior to the 21st century restricted ZIKV research to *in vitro* studies, but current animal studies utilize mice deficient in type I interferon (IFN) signaling in order to invoke enhanced viral pathogenesis. Indeed, there are several instances where virus evolution has guided host pathogenesis such as innate immune responses and tissue tropism. Here, we examine the molecular and pathogenic evolution of ZIKV and the impact these have had on potential vaccine candidates.

INTRODUCTION

Zika virus (ZIKV) has garnered international attention due to its rapid worldwide expansion since 2015 when an epidemic struck Brazil, resulting in a newly correlated pathology including severe neurological impairments such as microcephaly, which is now part of the congenital ZIKV syndrome, as well as Guillain-Barré syndrome afflicting adults (1). The World Health Organization declared ZIKV a Public Health Emergency of International Concern in February 2016, during which time ZIKV was spreading rapidly across South America, the Caribbean, and into the United States (1). This outbreak in Brazil spread rampant across the western continents raising critical questions pertaining to the evolution of this virus. Prior to 2015, ZIKV infections were limited geographically to Africa and Asia and were reported to be asymptomatic and approximately 20% mildly symptomatic presenting as a self-limiting febrile illness with most common symptoms including maculopapular rash, conjunctivitis, and joint pain (2). The mounting evidence that ZIKV is now causing neuropathology and fetal brain developmental disruption, as well as rising concerns over novel modes of ZIKV transmission suggests an evolutionary change in the molecular structure of ZIKV strains that has contributed to its rapid expansion, aggravated pathogenicity, and multiple routes of infections. These increasingly adverse effects depict why an analysis of the phenotypic differences between the African and Asian lineages, as well as between the many strains which have evolved under each clade, is a vital component of our ongoing effort to develop vaccines or therapeutics and fill major gaps of knowledge regarding ZIKV pathogenesis.

SECTION I.I - HISTORY OF VIRUS EMERGENCE

ZIKV was discovered in the Zika Forest of Uganda in 1947 by Alexander Haddow and George Dick during surveillance of yellow fever in rhesus macaques in Uganda (3). The virus was later isolated from *Aedes africanus* mosquitoes collected at the same site (4). The first documented human case occurred in Nigeria in 1954. It was not until 1966 that ZIKV was first detected in Asia alongside the first evidence of transmission by an urban vector, *A. aegypti* mosquitoes from Malaysia (5, 6). We know that two major lineages of ZIKV were diverged at this time, African and Asian, which is confirmed by current genetic and phylogenetic analyses (2). Zika virus silently migrated east across the Asian continent until an outbreak in 2007 on Yap Island, Micronesia, rendering 73% of residents infected (7). Despite the presence of DENV IgM in affected individuals, the unique symptomatic presentation, namely Guillain-Barré Syndrome, was definitively identified as ZIKV-induced. The next outbreak was six years later in French Polynesia, spreading to several other islands in Oceania (8). The most commonly reported symptoms in the Yap Island and French Polynesian outbreaks included rash, fever, arthralgia, and non-purulent conjunctivitis (9, 10). The first case with Guillain-Barré syndrome (GBS) as a complication of ZIKV infection was reported in the 2013 outbreak in French Polynesia (10). It was also in 2013 when it was discovered that ZIKV transmission could occur through blood or other bodily fluids, and not just through mosquito bites.

Brazil was the next location to experience an outbreak early in 2015. Phylogenetic and molecular clock analyses revealed that there was a single introduction of ZIKV to the country, which is estimated to have occurred between May and December 2013, or 12 months prior to its detection (11). The virus was likely brought to Brazil by a traveler from French Polynesia after a

stop at Easter Island (12-14). A retrospective blood bank analysis on 210 samples collected from patients during a 2013 DENV-4 outbreak (15), showed 10% had single positive qRT-PCR results for ZIKV, and only 2% positive results across triplicate samples. These data provide potential insight that ZIKV may have been present in South American countries as early as April of 2013. From the confirmed 2015 cases, it took less than one year for the virus to spread throughout Brazil into neighboring South American countries and into Central and North America. An increase in GBS cases was reported in Brazil, Colombia, Suriname and Venezuela and microcephaly cases in NE Brazil, which included neurological disorders and neonatal malformations (12, 16-25). Sequence homology studies revealed that of the two ZIKV lineages, the strains responsible for the human outbreaks throughout the Americas was phylogenetically closest to the Asian lineage (26). To better understand how ZIKV might be evolving, it is important to understand its genomic structure.

SECTION I.II - MOLECULAR BIOLOGY OF ZIKV

ZIKV genome organization

The genome organization and major protein functions of ZIKV are highly similar to all other members in the *Flavivirus* genus (26-28). ZIKV is a positive single-stranded RNA virus that belongs in the *Flaviviridae* family. This family includes the human pathogenic viruses, Japanese encephalitis virus (JEV), dengue virus type 1-4 (DENV), yellow fever virus (YFV), West Nile virus (WNV) and tick-borne encephalitis virus (TBEV). The genome is a 10.8 kb single-strand, positive-sense RNA molecule that consists of a 5' untranslated region (UTR) (~107 nt), one open reading frame (ORF) (~10.2kb), and a 3' UTR (~420 nt). The ORF encodes a polyprotein precursor

that is processed into 3 structural proteins; capsid (C), pre-membrane/membrane (prM), and envelope protein (E) as well as seven non-structural proteins (NS1, NS2A, NS2B, NS3, NS4A, NS4B and NS5). The viral polyprotein is co-translationally or post-translationally cleaved by viral NS2/NS3 protease, host signal peptidase (C/prM, prM/E, E/NS1, 2K/NS4B) and a host protease (NS1/NS2A). The pr- fragment of the prM protein is cleaved by furin in the trans-Golgi apparatus to generate mature virions. The major surface glycoprotein involved in host cell binding and membrane fusion is the E protein (29). Viral genome replication is accomplished through the nonstructural proteins (NS1-NS5) which serve as self-cleaving peptidases, along with the viral RNA-dependent RNA-polymerase.

As RNA genome viruses are strategically organized to contain the minimal number of genes required for sufficient replication and host immune evasion, many RNA viruses have evolved innovative methods for manipulating subverting molecules within their host cells (30). Among these are non-coding, subgenomic RNAs. These subgenomic flavivirus RNA components (sfRNA) have been implicated in both the reduction of type I IFN transcription, and in mediating resistance to cellular exonucleases that would degrade genomic transcripts, such as Xrn1 (31, 32). While the complete functional role of sfRNAs remains unknown, few key pieces of information have already emerged regarding ZIKV. Of these, work by Donald et al. suggests that sfRNA of ZIKV can not only inhibit the type I IFN response by means of a pseudo-knot tertiary structure, but may do so in a manner that is more broad than those of other flaviviruses, such as DENV (33). Additionally, the difference in ZIKV lineage does not impact the generation of these sfRNAs, and is unlikely to impact the predicted tertiary structure.

Genetic evolution of the virus

The MR766 (HQ234498) strain of ZIKV from Uganda is considered the classical strain and is used consistently in both *in vitro* and *in vivo* research studies to model ZIKV infections. While this strain has been passaged 147 times in insect cell cultures and suckling-mouse brain tissues, very few mutations have been detected in its genome. When genomic sequences are compared between MR766 to two other variations, AY632535 and DQ859059, which were both isolated from Uganda in 1947 from sentinel Rhesus macaques, all three variants were determined to differ in only 0.6% of nucleotide and 0.4% of amino acid sequences (34). While the correlation between low mutation rates and low human transmission may be inferred, there is no evidence of mutation rates driving transmissibility for ZIKV. Phylogenetic analysis of ZIKV genomes was analyzed using the Virus Variation software from NCBI. Using only full-length nucleotide sequences, viral strains were sorted, organized, and color coded by the source of virus isolation or by continent of origin (Figure 1 and 2, respectively). Sorting viral genomes by source reveals that 86.5% of isolates were derived from humans, 11% from mosquitoes and 2% were isolated from NHPs. Based on this sorting approach we can see that African lineage strains are limited to mosquitoes and NHPs, while Asian lineage strains are isolated from both humans and mosquitoes (Figure 1).

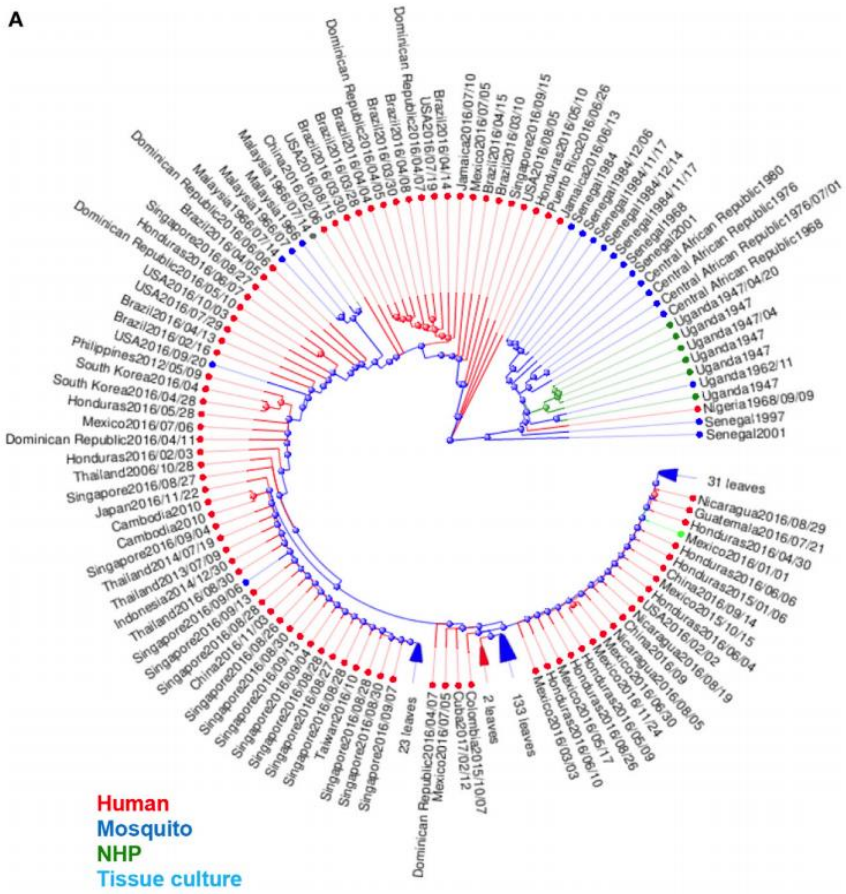

B

Host	Number of Strains	Percentage
Human	256	86.5
Mosquito	32	10.8
NHP	6	2.0
Cell Culture	2	0.7
TOTAL	**296**	**100%**

FIGURE 1. Phylogenetic analysis of ZIKV genomes by host. (A) Phylogenetic analysis of 296 available ZIKV genomes was organized according to the host species of isolation using Virus Variation analysis system available through NCBI. Only complete nucleotide genomes were screened and duplicate strains were removed to produce 296 unique strains. Strains isolated from humans, mosquitos, NHPs, and cell cultures are labeled with red (humans), blue (mosquitos), green (NHP), and aqua (cell cultures). (**B**) The total number of strains isolated per host species was used to derive the percentage of each host within the grand total.

Phylogenetic trees of ZIKV have also been used to study the movement of ZIKV strains across the globe to identify potentially serious mutations that could alter molecular mechanisms, and potentially lead to enhanced pathology (35). Phylogenetic analysis of available ZIKV genomes reveals approximately 97% of genomes published are from the Asian lineage, and 7% are of African lineage. Among these Asian lineages, 66.9% of all isolates were collected from North, South, and Central America. Of these, 38.8% of isolates were from North and Central America, and 28.1% were from South America. The remaining 26.1% of Asian lineage isolates were collected from the Asian and Oceania continents. Only 7% of all analyzed strains were from Africa (Figure 2).

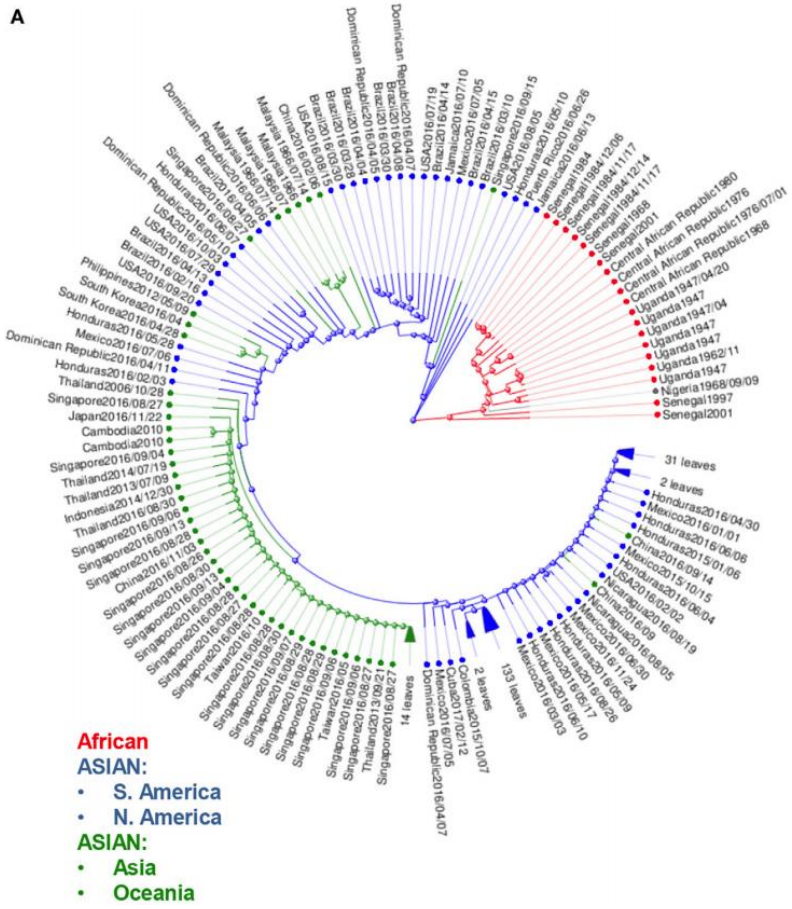

B

Continent of Origin	Number of Strains	Percentage
Africa	21	7.1
Asia/Oceania	77	26.0
N. America	115	38.8
S. America	83	28.1
TOTAL	**296**	**100%**

FIGURE 2. Phylogenetic analysis of ZIKV genomes by region.

(**A**) Phylogenetic analysis of available ZIKV genomes was organized according to lineage, followed by continent of isolation using Virus Variation analysis system available through NCBI. Only complete nucleotide genomes were screened, and duplicate strains were removed to produce 296 unique strains. Strains were clustered from Africa (red), from the Americas (Asian lineage) (blue); and from Asia and Oceania (Asian lineage) (green). (**B**) The total number of strains isolated per continent was used to derive the percentage of each host within the grand total.

A phylogenetic analysis juxtaposing MR766 strain to Asian lineage strains, particularly from Suriname and French Polynesia, revealed 50 amino acid lineage specific differences (2, 36-39). Of these, all variations occur in either the NS1 or NS5 proteins (38, 39). Yet, when Wang et al compared human to mosquito strains from the French Micronesia (FSM) outbreak in 2007 and the French Polynesia outbreak in 2013 (H/PF/2013), they identified 435 and 446 nucleotide changes in FSM and H/PF/2013 respectively (2, 27). All contemporary human strains within the Americas share higher sequence homology with the Asian lineage P6-740 (Malaysia/1966) which was the sole mosquito isolate (*A. aegypti*) than IbH-30656 (Nigeria/1968) (40). These isolates are most closely related to the H/PF/2013 strain (French Polynesia/2013) than the FSM strain (Micronesia/2007), suggesting that although the two Asian variants evolved from a common ancestor, they further diversified and the genetic distance between the 2007 and 2013 variants increased (2). A third major lineage from Africa is thought to exist based on analysis of only the

E and NS5 gene sequences (38, 41). This lineage is designated Africa II, but it is neglected due to incomplete sequencing of the whole genome.

Multiple sequence alignments using 58 complete genome and five envelope sequences of ZIKV as of April 2016, revealed conserved amino acid variations. Nineteen variations were found in the sequence of structural proteins and 47 variations in the nonstructural proteins, with the most variations in NS5 although the RNA dependent polymerase domain had no variations at conserved motifs (27, 42). Eight variation sites were located in E protein; two sites were in the stem region and one site in the transmembrane region of the E protein. Substitutions in stem and transmembrane regions affect virion assembly and membrane fusion, whereas substitutions in Domain III of E protein may affect receptor binding (29, 43).

Smith et al. (2018) found the difference between African and Asian isolates used in their analysis, to be approximately 75-100 aa residues, while the strains within each Asian and American lineage differed by approximately 10-30 aa residues, suggesting even minimal mutations could have phenotypic impact. A separate analysis by Wang et al on nucleotide sequences compared 8 African strains (7 from mosquitos, 1 from monkey) with 25 Asian strains (all human) and found 59 amino acid variations that differed between the two major lineages, but were shared within the various strains of either African or Asian ancestry (2). The highest variability (10%) between Asian human and African mosquito strain was in the pr- region of prM protein, though the effect of this structural change on viral function is unclear. Yuan et al. demonstrated differences in neurovirulence among Asian lineage strains from Cambodia and Venezuela resulted from a single amino acid substitution S139N in the pr region of prM (44). The authors hypothesized that this substitution may contribute to a neurovirulent phenotype but did not propose a mechanism. These data are important because they demonstrate not only variances

among strains of the same lineage, but also shed critical insight on intra-lineage strain-specific evolutionary differences. Comparison of protein sequences using P6-740 as the Asian reference and FSM showed over 400 variations at the nucleotide level and 26 unique substitutions at the protein level. Comparison of FSM, H/PF/2013 and the Brazilian strains from 2015-16 showed that all these strains acquired changes at an additional 8 positions for a total of 34 amino acid changes compared to P6-740. All isolates showed identical amino acids at these positions except for T2634M/V in the NS5 protein.

Of note, no known ZIKV mosquito strain has the same nucleotide sequence as the human strains, though this could be due to sampling bias or ZIKV transmission through alternative routes (2). Nonetheless, nucleotide sequence changes can have an impact on viral pathology, replication, transmissibility, and fitness. One such example is the impact on post-translational modification of the E protein. Faye O. et al in 2014 reported a N154-glycosylation site deletion event of E protein in African isolates that did not exist in Asian lineage strains (42). Neurovirulence may depend on glycosylation of the Env protein (Asn 154) (45, 46). Naik and Wu reported that a mutation of putative N-glycosylation sites on DENV NS4B decreased RNA replication suggesting that glycosylation may play important roles in infectivity, maturation and virulence of flaviviruses (47).

Similar to DENV, ZIKV evolution depends on worldwide spread of the mosquito vector, growing human population size, and increased foreign travel and commerce (37). Sequence analyses demonstrate that the virus originated in Africa within two distinct groups; Uganda and Nigeria, mostly isolated from non-human vectors, and share a common ancestor in the MR-766 strain. The Asian cluster was isolated in Malaysia shows evolutionary descent from a prototype strain, P6-740, which includes strains from other Southeast Asian countries, such as Cambodia and French Polynesia. The American clade, which includes strains from Brazil and other American

or Caribbean strains, evolved from this Asian cluster and expanded rapidly among naïve populations (37). As ZIKV evolves, it diversifies and creates new interactions with vectors and hosts that impact pathology, which exhibit unique lineage and strain specific pathological profiles. To this date 416 fully sequenced African and Asian isolates have been characterized have been deposited in GenBank.

SECTION I.III - ZIKV TRANSMISSION AND TISSUE TROPISM

Vector influence on viral evolution.

While the African lineage contained eight mosquito isolates, the P6-740 (Malaysia/1966) was the sole mosquito isolate in the Asian lineage. In 2007, human sera from patients with painful febrile disease and *A. albopictus* mosquitos were sampled from West Africa and tested positive for ZIKV (48). At the same time, the Micronesia outbreak identified *A. (stregomyia) hensilli* as the likely principal vector (7). In 2013, ZIKV reached French Polynesia, with subsequent spread to Oceanian islands (New Caledonia, Cook islands and Easter island) which contained *A. aegypti* and *A. Albopictus* throughout most of this region (8). Eleven percent of the population was infected causing symptoms such as low-grade fever, rash, conjunctivitis and arthralgia, as well as GBS (49). *Aedes aegypti* has not only expanded to Central-South America, but is also regarded as the most common vector for DENV (50). The New World strains of *A. aegypti* and *A. albopictus* which are the most common in USA are poor transmitters of ZIKV (51) suggesting that divergence of the Asian lineage can impact human to human transmission without impacting how the virus behaves in a vector. Indeed, while *Aedes* is widely accepted as the vector for ZIKV (52-54), work by Guedes et al. has demonstrated that ZIKV can infect and replicate in the midgut, salivary glands, and can be detected in saliva of *Culex spp (55)*. This work suggests, while still a contentious topic

requiring further investigation, the transmission vector range for ZIKV may be greater than anticipated.

Non-Vector transmission. ZIKV and other Flaviviruses (with the exception of Hepatitis C) are transmitted by mosquito bite, but ZIKV has clearly diverged from other flaviviruses. Since the 2015 epidemic, the mirth of published data has made it apparent that ZIKV can be transmitted from human to human through sexual transmission, blood transfusion, ocular transmission, or vertical transmission from mother to fetus (20, 23, 56). While the African strains are better transmitted through mosquitos, the American strains with Asian ancestry may have obtained enhanced transmission capabilities through sexual intercourse. This is supported by the numerous clinical cases of sexual transmission from male to female partners, and the limited data regarding female to male transmission (57-68). Of these clinical cases, originally infected individuals are reported to have traveled to South American countries or Pacific island nations, where they are believed to have contracted ZIKV (69). Recent findings from Mead et al. reveal that while ZIKV can be detected in semen from infected men for up to 9 months after infection, sexual transmission of ZIKV typically occurs within 20 days of infection, and the amount of infectious ZIKV in semen decreases rapidly within the first 3 months of infection. In a recent study aiming to standardize *in vitro* techniques for detection of Asian lineage strains of ZIKV, Barreto-Vieira et al. demonstrated that monkey epithelial cells are more susceptible to ZIKV infection than insect cells (70).

Human infection studies

Fetal-placental infections. The new routes of transmission demonstrate a novel tissue tropism for the virus. As such, tropism for the human placenta allowing infection of the fetus is unique for

ZIKV, even though it should be noted that other flaviviruses that are not human pathogens do infect placental tissue in their respective hosts. Asian strains of ZIKV attracted global attention for their impact on maternal and fetal health (71, 72). Infectivity studies have shown South American strains of Asian lineage are capable of infecting human decidua and umbilical cord tissues, and are responsible for apoptosis of chorionic villi, which function in fetal/maternal blood/nutrient exchange (73, 74). In Brazil, mothers giving birth to newborns with microcephaly reported fever, rash and conjunctivitis during pregnancy, the most commons signs and symptoms of ZIKV infection (75). However, diagnosis beyond the earliest stage of acute disease is nearly impossible in the dengue-endemic regions and since the majority of exposures to ZIKV may cause asymptomatic infections, large numbers of infected pregnant women may have gone undiagnosed or misdiagnosed (23). Importantly, the severity of these responses varies greatly between patients, indicating that while studies on human immune responses to ZIKV infection are important, there is a large knowledge gap yet to be filled regarding the diversity of ZIKV infections among human demographics. An excellent example of how ZIKV pathogenic severity is dependent on individual genetic backgrounds is the study published by Caires-Junior et al., which compared twins where one was diagnosed with congenital Zika virus syndrome (CZS) (76). This study demonstrated that upon infection of neural tissues with ZIKV, stem-cells from the CZS twins grew slower and exhibited increased viral replication. Importantly, the transcriptome results of the study revealed a significant difference in the level of an mTOR inhibitor protein, DDIT4L, between CZS and unaffected twins. This finding is significant because it indicates an individual genetic disposition for increased mTOR signaling. Also, mTOR signaling pathways are critical for autophagy-mediated viral clearance (77), suggesting a reason why ZIKV infections are intensified in individuals with mTOR mutations.

Fetal brain infections. ZIKV's proclivity for neural cells is not a novel finding among flaviviruses, as members of this viral family are known for their neurovirulent qualities (78). Several studies have sought to investigate the neuro-invasiveness and pathogenesis of ZIKV within both human-specific cell cultures and in neonatal mice. One example is the work done by van den Pol et al., which investigated ZIKV cellular targeting within the brain (79). Here, *in vivo* mouse studies on neonatal brains revealed ZIKV infection of specific regions of the brain as early as 4 days post infection, and can be resolved by *in-situ* hybridization by 7 days post infection. Additionally, human cell culture work by van den Pol et al. revealed a 24-hour virus incubation period in human astrocytes before shedding active virus into culture media. Importantly, a study by Lin et al. using cultured human fetal brain tissues suggests that ZIKV enters the brain via the subventricular zone and actively infects and replicates in committed neural cells, and thus as cells propagate to develop the brain, they result in an increase of viral presence (80). The authors speculated that the immune response to this neural infection may drive microcephaly.

Urogenital tract infections. Viral RNA can persist at high levels for months in the sperm of infected men even after resolution of symptoms and persists in the vaginal secretions of infected females for weeks after symptoms resolve (5, 62). This type of persistence in the reproductive tract and sexual transmission is not observed with other flaviviral infections (81).

Ocular infections Ocular infections are also unique to ZIKV and likely transmitted through conjunctival fluids, tears and lacrimal glands. Although the reported cases of African lineage infections were too few to identify similar symptomatology, ocular infections by the Asian lineage

have been documented in humans and recapitulated in animal models. Inner retinal vasculopathy (82) or other ocular infections have been reported linked to international travel into South American and Caribbean island nations (82, 83). Ocular abnormalities have been documented in infants with CZS. In a report by Fernandez et al., *post-mortem* examination of fetuses from terminated pregnancies revealed micro-calcifications of the retina, increased amount of autolysis of tissues at the front of the ocular tract, detachment of retinal and retinal epithelial layers, and a distinct lack of neural differentiation of retinal neurons (84). This study by Fernandez et al. corroborates clinical cases where 34.5% of all ZIKV microcephalic infants reported in the first two months of 2016 had ocular abnormalities, such as retinal mottling, optic nerve degeneration, and a lack of differentiation of retinal neurons (85-93).

Animal infection studies

Ocular infections. Small animals have been used to investigate the pathogenic variability of ZIKV lineages during active infections. Noteworthy among these are murine models, which have been well characterized for use studying other flaviviruses (94). A129 and AG129 mice that are deficient in interferon (IFN) receptor signaling when infected with ZIKV, showed specific cellular tropism of ZIKV in retinal cell layers of the eye (95). A129 mice are deficient in IFN alpha/beta receptors, while AG129 mice are deficient in IFN alpha/beta and gamma receptors. Muller cells and retinal astrocytes infected with the virus resulted in a sustained proinflammatory microenvironment within the ocular tract that contributed to conjunctivitis and uveitis in these mice (96). In a NHP model for ocular and uteroplacental pathogenesis, Mohr et al. demonstrated lack of retinal neuron maturation, anterior segment dysgenesis, and notable chorioretinal lesions

in fetal macaques (97). Different ZIKV strains display divergent tropism within host tissues. Miner et al. showed that ZIKV infections induced purulent viral panuveitis in AG129 mice and that Asian lineage ZIKV from South America had higher viral burden than those from Oceania in ocular tissues (98).

Previous studies investigating the molecular mechanisms by which ZIKV gains access to the eye and causes inflammation, have revealed a role of retinal epithelial infection and cell death in allowing for ZIKV to cross the blood barriers of immune-privileged tissues (95, 99). These investigations are often limited to *in vitro* studies of human primary cells or juxtapose cell culture studies with ZIKV infection in wild-type (WT) C57BL/6 and immune-compromised animals. Singh et al. provides a thorough analysis of transcriptional responses after intravitreal inoculation of ZIKV into either WT or ISG15 deficient animals and shows a rapid induction of inflammatory responses during ZIKV infection (95). These findings coincide with retinal lesions and chorioretinitis that present within 24 hours of infection and last up to 96 hours after infection. While this insight into ZIKV pathogenesis of immune-privileged tissues is beneficial, the mechanism behind systemic ZIKV entry into the eye and ZIKV infection synergy between eye and brain remain to be determined.

Brain, spleen and testicular infections. Regarding tissue tropism by the Asian and African strains in animal models, the reports are conflicting. Dowall et al. demonstrated that viral RNA and ZIKV-induced histopathology with both MP1751 (African lineage) and PRVABC59 (Asian lineage) were highest in brain, spleen and testis of A129, although the histological changes were more prominent in animals infected with the African lineage. The histopathology was minimal in heart, liver, kidney and lung, although the Asian lineage caused no measurable clinical features (100).

The natal RGN strain from northeastern Brazil was isolated from the brain of a fetus with microcephaly and contained half of all mutations in the NS1 gene, suggesting tissue-specific evolution of ZIKV has contributed to the emergence of CZS (2).

Lineage-Dependent Differences in Animal and Cell Culture Models.

There are limited studies characterizing ZIKV strains and the majority utilize one strain exclusively. Phenotypic differences among African and Asian isolates have been reported in both *in vitro* and *in vivo* models, demonstrating the importance of considering ZIKV isolate, passage history, cell type, or mouse model when interpreting results (1, 101). Asian strains of ZIKV have been analyzed for differential infectivity in many human and non-human cell lines (28, 102). These include cells from ovary, kidney, liver, brain, lung, and keratinocytes. Keratinocyte involvement is important to explore as the skin is the first barrier encountered during mosquito bites, and the first line of defense against ZIKV entry (28, 102). Analyses from these *in vitro* studies demonstrate that infection after 48 hours produced differences between cell lines in the amount of intracellular NS1, as well as amount of virus release, and the extent of infection did not directly correlate to IFN response (103).

Substantial differences are also found between African and Asian strains *in vitro* among mammalian and insect cell lines (28). A low-passage African isolate from mosquito reached higher titers than two low-passage Asian strains at all observed time points (0-36 dpi) in cell lines from four diverse vertebrate hosts and five insect cell lines (28). Vielle et al reported strain specific infection profiles in Vero cells, Aedes cells and human monocytic DCs (MoDCs) (102). The authors used five African and Asian lineage strains isolated from various hosts; MR766 (U-1947) from monkey, MP1751 (U-1962) from a pool of *A. africanus* mosquito, PF13/25013-18: FP-2013

(French Polynesia) from human serum, PR-2015 (Puerto Rico) from human serum and G-2016 (Guadaloupe) from human semen. The low passage U-1962 and U-1947 are very distant phylogenetically. The African lineage U-1962 and the Asian lineage PR-2015 showed highest rates of infection in Vero cells compared to the other strains (101). Similar findings for the U-1962 were observed in the mosquito cell line. In contrast, *in vitro studies* of human MoDCs showed similar susceptibility to infection, activation/maturation, expression of type I and III IFNs or cell death between lineages (101). The authors reported that NS5 of U-1962 showed polymorphism compared to the other strains of the study, but none of the residues were putative STAT2 binding residues, suggesting that the levels of expression of mutations were independent of mutations in the NS5 sequence of the U-1962 strain (102).

Additionally, infectivity studies comparing the two lineages revealed that African strains of ZIKV can infect human neural progenitor cells and produce both higher titers of progeny virus, and also induce higher levels of cellular apoptosis (39, 101, 104). A study by Hamel et al., demonstrated similar findings using human astrocyte cell cultures, where they found African ZIKV strain HD78788 can reach higher infectious titers 24 hours post infection of human astrocytes, and also induces less innate antiviral gene transcription than Asian strain H/PF/2013 (105). This trend was further confirmed in human dendritic cells, which are one of the primary cell types naturally infected by ZIKV (102).

While mice may not naturally become infected by ZIKV, they can be used as models for pathogenesis, and similar reports of differential lineage-specific infection characteristics have been published regarding *in vivo* mouse experiments. Zhang et al. conducted a study juxtaposing an older Asian lineage strain from Cambodia, with a more contemporary American strain from Venezuela to investigate potential differences in neuro-virulence between the two (106). They

found that compared to the Cambodia strain, neonatal mice infected with Venezuelan strain of ZIKV demonstrated more neuronal cell death, obliteration of oligodendrocyte development, and an increase in the amount of CD68 and Iba1 positive microglia/macrophages in brain tissues. On the other hand, Qian et al. reported that African and Asian lineages showed similar levels of brain-development disruption in an organoid development model, thus prompting further questions regarding further analyses within the Asian lineages (107). This change between Asian and American, or alternatively between pre-epidemic and epidemic stains of ZIKV, may be attributed to new mutations between the two (108). Indeed, sequencing data comparing over 20 strains of ZIKV reveals at least 15 amino acid changes between epidemic and pre-epidemic strains, as well as the generation of a 9 amino acid bulge, rather than an external loop structure at the 3-prime UTR region of the NS5 sequence.

Mouse background strain and treatment play a major role in pathogenesis, as infections using the same dose and strain of ZIKV from either lineage. The animal model chosen for a study is a potential complication of comparing the phenotypes of ZIKV isolates, as is the *in vitro* and/or *in vivo* passage history of isolates. There is a tradeoff between passage number and viral fitness in either vertebrate or insect hosts. A study by Haddow et al. suggests that high passage number of traditional African strains, such as MR766, in both Vero cells and suckling mouse brains has resulted in a distinct loss of glycosylation sites, which may thus affected pathology in other organs (34). The pathology of a low-passage African isolate from mosquito and two low-passage Asian strains were compared *in vivo* using two mouse models, the A129 mouse (deficient in type-I interferon receptor, Ifnar1$^{-/-}$) and the IFN-I antibody blockade mouse. The A129 mouse is commonly used to study ZIKV because the virus infects cells by targeting human STAT2 to suppress IFN signaling and it has been proposed that lack of murine STAT2 binding impairs

infection unless the type I IFN receptor is knocked out or blocked (1). Of additional note, the majority of investigations that utilize ZIKV grow their viral stocks in Vero cells, which do not produce IFN type I in response to a viral infection, and thus makes them permissive to ZIKV infections (109, 110).

According to Smith et al, the African isolate caused more severe clinical pathology and lethality in both mouse models, suggesting enhanced virulence of the African strain compared to both Asian strains. Significant phenotypic differences were also observed between the two Asian strains (CPC-0740 and SV0127-14) used in the study; SV0127-14 produced 10-100 fold lower titers in all cell types compared to CPC-0740, and it produced only mild clinical symptoms and 10% mortality in Ifnar1$^{-/-}$ mice versus 90% mortality with the more virulent CPC-0740 (28). The IFN-I antibody mouse model was far less susceptible than the Ifnar1$^{-/-}$ model, producing zero mortality and no clinical symptoms with CPC-0740. The same result was found using a more recent Asian isolate from Puerto Rico, PRVABC59 in the IFN-I antibody blockade mouse (28).

Similar to previous studies comparing African and Asian strains, Dowall et al. reported that A129 mice tolerated infections with an Asian strain well, while an African strain was lethal, with morbidity and mortality worsening in a dose-dependent manner. Interestingly, although the Asian strain produced no clinical symptoms, viral RNA levels were detected in various tissues, including brain, spleen, lungs, and kidneys and viral burden was detected in secretions, albeit the magnitude and time course of the Asian and African strain differed, with detection levels produced earlier using African infections. Moreover, seroreactivity revealed detectable antibody responses in the Asian infected A129 mice despite no clinical signs of illness (1).

Correlates of Inflammation during ZIKV infection in Eyes and Brain.

GBS has been correlated with antibody cross-reactivity to host gangliosides in other flaviviruses (111), and correlate with motor-neural pathology (112). Gangliosides are vital to synaptic transmissions, intercellular adhesion and communication, equilibrium, immune signaling, and nervous system and motor/neural network maintenance (113). Anti-ganglioside antibodies have been previously shown to lead to the absence or fragmentation of MBP, myelin PLP, and vimentin all contributing to persistent neuroinflammation within the brain by acting as damage associated molecular patterns (DAMPs). Myelin or myelin debris signal in macrophages via complement/opsonization or phagocytosis and facilitate M1 (macrophage type-1) polarization and proinflammatory secretion (114). Protracted neuroinflammation by M1 microglia is mediated by locally secreted inflammatory factors, such as TNF-α (114). Thus, using transcriptional quantification of neural cells can be used to evaluate chronic inflammation.

The persistent neuroinflammation and severe pathology has been shown in published data, which report that chronic neuroinflammation potentiates severe motor/cognitive diseases among flavivirus infections as seen in GBS cases (115). COX2 stimulates glial cell IL-1β and TNF-α secretion resulting in a paracrine and autocrine signaling cascade (116). This cycle of persistent inflammation and pain-sensitivity is established through a COX2 and IL-1β positive feedback loop, via NF-κB signaling (117) (118).

MMPs are endopeptidases with vital functions such as neural network remodeling, tissue formation, and blood-brain barrier (BBB) integrity regulation. M2 microglia (type 2 macrophages), which function in tissue remodeling and anti-inflammatory responses, secrete MMP2 to permeabilize the BBB (114) and allow macrophages infiltrate the brain, phagocytose, and clear dead cells (119, 120). Increased permeability of the BBB via elevated transcription of

MMP2 and MMP9 corresponds with increased inflammatory leukocyte trafficking into the brain (121, 122). Wang et al., where MMP2 and MMP9 were upregulated in brain tissues following West Nile virus (WNV) infection, thus mediating infiltrating leukocyte trafficking into the brain (116).

Collectively, proinflammatory markers and anti-inflammatory markers can be monitored to discern responses to ZIKV in immune privileged compartments by showing M1 or M2 skew. Additionally, COX2, MMP2, and MMP9 can be used to correlate with systemic infiltration in the brain and also as a measure of BBB integrity. When supplemented with data of auto-ganglioside antibodies, these parameters can be used to evaluate the severity of ZIKV pathology.

SECTION I.IV - CURRENT UNDERSTANDING OF ZIKV AND THE HOST IMMUNE RESPONSE

Cases of ZIKV infections are believed to have either been subclinical or misdiagnosed as a different flavivirus infection, such as DENV (34). As ZIKV spread from Africa across Asia and into the Polynesian and Micronesian islands, ZIKV shifted from a mild pathogenesis and largely subclinical symptomatology to the neuro-virulent Asian lineage with a higher incidence of congenital abnormalities. The specific pathways activated by viral infection inevitably steer the innate immune response towards differential patterns and intensities of cellular and humoral responses. Zika virus is a member of the flavivirus family, and thus shares similar cell signaling pathways with other viruses within this group, which directly antagonize the interferon (IFN) response system of the host innate immune response, but through a species-specific mechanism (Figure 3). Thus, to fully comprehend the challenges that ZIKV poses to human immunity and to

recognize fully efficacious vaccine candidates, a detailed understanding of how ZIKV directly evades and antagonizes host innate and adaptive responses is vital.

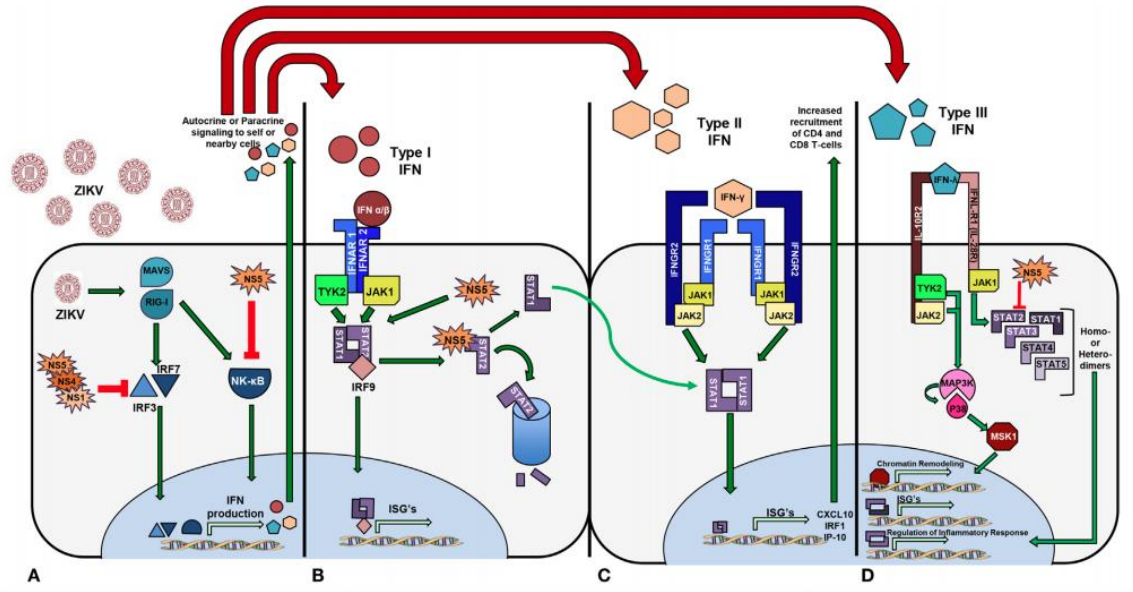

FIGURE 3. ZIKV activates signaling pathways that promote transcription of IFN genes differentially.

(**A**) The NS5 protein from African lineage binds and prevents NF-kB function. Asian lineage nonstructural proteins NS5, NS4, and NS1 act to inhibit IRF3 and IRF7 functionality, thus inhibiting IFN production. (**B**) IFN Type I phosphorylates STAT1 and STAT2 and NS5 targets STAT2 for degradation. (**C**) Activation of Type II IFN signaling upon receptor binding phosphorylates STAT1 heterodimers and thus increases chemoattractant ISG's. (**D**) STAT2 is targeted for proteasomal degradation by NS5 resulting in an increased rate of STAT homo-dimerization, and upregulation of anti-inflammatory cytokines.

Type I interferon responses

Type I IFN refers to the classic IFN α/β signaling pathway, whereby viral antigen, or a pathogen associated molecular patterns (PAMP), are recognized by pathogen recognition receptors (PRR) initiating an intracellular protein cascade that culminates in protein translocation into the nucleus

and subsequent transcriptional activation of DNA for IFN-α and IFN-β (123). When nearby cells have IFN α/β bind to their surface receptor, IFN alpha receptor (IFNAR), a series of phosphorylation events, involving Janus kinase 1 (JAK1), tyrosine kinase 2 (TYK2), and the many signal transducer and activator of transcription (STAT) proteins ultimately result in the transcription of IFN stimulated genes (ISG's) which have antiviral properties through a broad variety of mechanisms.

Lineage similarities. Many flaviviruses directly antagonize different stages of the type I IFN pathway via species independent and diverse mechanisms that all centrally rely on genomic non-structural protein 5 (NS5). Of the seven genomic NS proteins and sub-proteins, the NS5 protein functions as the viral polymerase enzyme, and in RNA capping (124-126). Dengue virus NS5 protein has been shown to inhibit human STAT2 function by means of an E3 ubiquitin ligase, called UBR4 that targets STAT2 for proteasomal degradation. Dengue virus NS5 protein has been shown to inhibit human STAT2 function by means of an E3 ubiquitin ligase, called UBR4 that targets STAT2 for proteasomal degradation. ZIKV similarly inhibits human STAT protein, but can do so independently of UBR4 (127, 128). ZIKV inhibition of STAT2 has been demonstrated in several studies where primary human dendritic or endothelial cell infections resulting in lower expression of pro-inflammatory cytokines, such as interleukin 6 (IL-6), IFN α/β, and chemokine C-C ligand 5 (CCL5) (129, 130). Additionally, NS1 and NS4b have both demonstrated the ability to inhibit the production of IFN α/β after direct stimulation with polyI:C (synthetic double stranded RNA) by blocking the formation of the TBK1 (TANK binding kinase 1) complex, which allows for oligomerization of interferon regulator factors (IRF's) (77, 125, 131).

Primary human skin fibroblasts infected with the French Polynesia isolate H/PF/2013 mounted innate immune responses by increasing the expression of RIG-I, MDA5, TLR3 leading to upregulation of Type I IFNs and ISGs as well as CXCL10 and CCL5 (132). The same strain led to IFN-β production and induced apoptosis of infected lung epithelial cells A549 (133). Overall both lineages have demonstrated similar mechanisms of Type I IFN activation and upregulation, and similar pathways of STAT2 inhibition and targeting for degradation.

Importantly, Zika virus inhibits human STAT2 function via a mechanism similar to DENV, but does not similarly inhibit murine STAT2. These two proteins share 64% sequence homology, which may account for the dissimilar protein interactions. This single protein non-homology between human and mouse STAT2 has led to a domination of immune deficient murine models as the primary model for pathogenic and vaccine studies (134, 135). These models are primarily A129 and AG129 systems, which lack the IFNAR protein, required for the production of ISG's. Despite many investigators' claims that immune competent models for ZIKV will lack symptomatic expression, replication, and similarity to human infections, several recent publications have demonstrated that ZIKV can be modeled in immune competent mice using either a C57BL/6 or BALB/c background (136). The success of immune competent systems may be directly attributed to ZIKV inhibitory effects on STAT3, 4, 5, or 6, although this knowledge, however, still requires investigation and remains a knowledge gap in the field.

Lineage differences.

Bowen et al. found that dendritic cells from donors are productively infected *in vitro* by both lineages, but with different kinetics (129). The African lineage had faster replication and infection magnitude, and unlike the Asian linage, caused cell death. All strains antagonized STAT1 and

STAT2. Asian strains used included PRVABC59 and P6-740, while African strains included the Ugandan prototype strain (MR766) and a low-passage Senegalese strain (DakAr41524). They found that the viral kinetics varied with the source of the monocyte isolate, but that related strains varied similarly. All strains induced IFNB gene transcription, and a decrease in STAT2 phosphorylation was seen in both, but more pronounced in the African lineage (129).

In a study by Simonin et al who infected human primary neural cells with African and Asian lineage strains, the African strain induced upregulation of at least 19 genes including RIG-I, MDA-5 and TLR-3 and induction of type 1 and 2 interferon (IFN) was higher, associated with enhanced levels of inflammatory cytokines such as IL-6 or tumor necrosis factor (TNF). The only downregulated gene was CXCL8, a mediator of inflammatory responses. The Asian strain did not show any significant upregulation of genes; instead, four genes (CXCL8, CXCL10, CASP1, and CTSS) were downregulated. Even at higher MOIs, the cytokine response to Asian strain was weak. In addition, neural cell infection by both strains showed similar differences in viral infectivity and cytokine production (104). In contrast, when McGrath et al. infected human neural stem cells from two individual patients with Asian and African lineages of ZIKV and conducted a transcriptomics analysis they found increased expression of IFN-α, IL-2, TNF-α, IFN-γ genes as well as genes involved in complement, apoptosis and STAT5 signaling pathways in cells infected with the Asian isolate (137). Patients displaying neurological symptoms during the ZIKV epidemic in Brazil demonstrated higher blood concentrations of pro-inflammatory cytokines, such as IL-6, IL-7, and IL-8, as well as higher levels of chemotactic molecules, such as IP-10 and MCP-1 (138). These findings were recapitulated in a non-human primate model (139) and in mouse studies modeling ZIKV infections using homologous strains.

Ultimately, this inhibition of type I IFN production and signaling results in an attenuated innate response to infection, and may alter T cell specific responses (140, 141). A handful of reports have examined the host-induced immune responses to genetically evolved ZIKV. Tripathi et al. examined strain specific differences using Ifnar1$^{-/-}$ and Stat2$^{-/-}$ C57BL/6 mice. They looked at 3 viruses from the Asian lineage (P6-740, FSS13025, and PRVABC59) and 2 from the African lineage (MR766; DakAr41519). They found that the African strains induced faster onset of disease and higher mortality and in both mouse models. Infection with the African strains was marked by more severe neurological symptoms, while neurological symptoms in Asian infections were more prolonged. While both strains induced host inflammatory responses, the African isolates elicited higher levels of several cytokines and markers of T cell infiltration (IL-6, CXCL10, TNF-a, IFN-γ, CCL3, CCL4, CCL5, CXCL9, GZMB, CCL2, CCL7, CXCL1, CXCL2, IL-1b, IL-15, CD4, CD8, CCR5, CXCR3, CCR2, CCR5) (142).

Foo et al. infected human blood monocytes with the Uganda strain MR766 or the French Polynesia strain H/PF/2013 (74). They found that both strains productively infected CD14 monocytes, but that infection with Asian viruses led to the expansion of non-classical monocytes, resulting in a M2-skewed immunosuppressive phenotype, marked by IL-10 production. African lineages on the other hand, induced pro-inflammatory M1-skewed responses, inducing CXCL10. They also found that blood from pregnant women was more susceptible to infection. Infection with virus from the African lineage led to higher viral burdens, and increased levels of IFN-β, STAT, OAS, IRF, and NF-kB. The Asian lineage had higher expansion of CD14^{lo}CD16^{+} non-classical monocytes, despite having a lower viral load. In general, the African strain promoted cytokines and immunomodulatory genes involved with inflammation (CXCL10, IL-23A, CD64, CD80, IL-18, IDO, SOCS1, CCR7), while the Asian strain was associated with the activation of

immunosuppressive genes (IL-10, Arg1, CD200R, CD163, CD23, CCL22, VEGFa). These results were confirmed using a second strain of Zika virus from each lineage (IbH30656 for African and PRVABC59 for Asian). Pregnancy enhanced infection of both lineages in CD14 monocytes, and they found a similar pattern with the African lineage having a higher viral load. Blood from women in first and second semester of pregnancy demonstrated considerably higher $CD14^{lo}CD16^{+}$ non-classical monocyte number upon infection with the Asian strain, but blood from third trimester of gestation had similar numbers to non-pregnant blood. The African strain however, produced a slight increase in non-classical monocytes during all 3 trimesters. Unlike monocytes from non-pregnant women, monocytes from pregnant women were more reactive to the Asian lineage than the African one. The Asian strain additionally induced genes associated with adverse pregnancy outcomes in the first two trimesters of pregnancy (ADAMTS9 and fibronectin 1) (74).

While both Asian and African lineages have demonstrated similar agonism and antagonism in Type I IFN signaling, Asian lineage strains have additionally shown a secondary method of IFN antagonism. Asian strains isolated from South American countries appear to directly activate IRF3, IRF7, and IRF9 through NS1, NS4, and NS5 viral proteins (130). African lineages have not demonstrated this ability as of yet, which implicates the differential amino acid residues as key binding factors for innate immune mediators.

Type II Interferon Responses

Unlike the type I IFN response which inhibits ZIKV infection, Chaudhary et al. demonstrated that IFN-γ (a type II IFN) does not only decrease ZIKV infectivity in mammalian cell culture but can also upregulate transcription of innate inflammatory and chemo-attractant cytokines, such as IRF1 and CXCL10, respectively. This suppression of type I responses, but activation of type II responses

is also demonstrated by the NS2A and NS4B proteins. This phenomenon of variable activation of type I and type II IFN responses has also been documented in human clinical cases of ZIKV infections (143). A study performed by Kam et al., sought to fully characterize immune biomarkers that were associated with ZIKV infections in 95 human clinical cases from Brazil. The authors demonstrated an increase of IFN-γ among human febrile cases of ZIKV and differential cytokine expression between febrile patients and those with neurological complications. Between these two groups, patients with neurological complications showed similar levels of IFN-γ, and decreased levels of anti-inflammatory cytokines, such as IL-10 and IP-10 (138). Zika virus NS5 was shown to generate the differential type I and type II responses during infection, by specifically inhibiting IFN-β signaling, and simultaneously functioning as a prominent activator of IFN-γ signaling.

Interferon-γ plays a critical role in host antiviral responses and increased levels of IFN-γ can be associated with host natural killer (NK) cell response, as they secrete high levels of this cytokine during infection (143). A study by V. Costa et al. proposed that DENV infection is controlled by NK cells specifically through the production of IFN-γ, and that these NK cells are activated by DENV-infected dendritic cells (DC's) (144). While this specific mechanism of IFN-γ inhibition has not been demonstrated yet for ZIKV, it has been shown that ZIKV does infect antigen-presenting cells (APCs) upon infection via mosquito bite. Cimini et al. found that the amount of IFN-γ secreted by $CD4^+$ T-cells is reduced (145). Given that $CD4^+$ and $CD8^+$ T-cells have proven to be the dominant drivers in ZIKV clearance during human infection (146), this alteration in cell cytokine secretion raises several questions regarding the mechanisms that ZIKV uses to subvert the host immune response and facilitate its replication.

Ngono et al. compared CD8 T cell responses to two Zika strains from the African (MR766) and Asian (FSS13025) lineages in wild-type C57BL/6 mice treated with an IFNAR blocking

antibody, and in LysMCre^{+}IFNAR$^{fl/fl}$ C57BL/6 (H-2^{b}) mice (lacking IFNAR in certain myeloid cells) (141). They found that the viral load of the African lineage strain decreased 3 days post infection, but that the Asian lineage strain did not. Both strains elicited similar levels of granzyme B^{+} CD8^{+} T cells in both mouse models. They additionally identified epitopes recognized by IFN-γ secreting CD8^{+} T cells and found that in both strains the major epitope was E protein derived. In LysMCre^{+}IFNAR$^{fl/fl}$ mice, they identified 14 peptides specific to the African lineage, 3 specific to the Asian, and 12 shared by both, with all proteins being targeted, except for NS1 and NS2b in the Asian lineage. The Asian and African strains both resulted in a 6 and 5-fold increase in CD44^{+}CD62L^{-}CD8^{+} T cells respectively, indicating a strong CD8 response. Both strains showed similar CD8^{+}T cell kinetics, with the percentage of IFN-γ^{+} CD8^{+} T cells being highest at day 7 post-infection. It is important to note that the MR766 isolate was serially passaged in mouse brains, possibly affecting its behavior (141).

Collectively, the majority of the investigations regarding ZIKV and the Type II IFN response have been done using Asian lineage viruses. Thus, there is an immense knowledge gap concerning African lineage ZIKV strains and how they may directly affect the Type II IFN response. While it can be inferred that both African and Asian lineages benefit from the increase in STAT1, being freely able to generate homodimers and thus promote ISG's, African lineage ZIKV strains have not specifically demonstrated this ability, and thus it remains to be investigated.

Type III Interferon Responses

Discovered in the early 2000's, type III IFNs comprises four variants of IFN-λ (numbered 1-4). The receptor for this type of IFN is unique because, rather than being ubiquitously expressed on nucleated cells like IFNARs, it is selectively expressed on epithelial cell surfaces. Thus, IFN-λ

plays a distinct role in the protection of epithelial barriers. Additionally, while expressed on epithelia surfaces, other cell types can respond to type III IFN signaling, such as those in the central nervous system (147, 148). While the role of IFN-λ has been studied during WNV and YFV infections, there is limited information regarding IFN-λ and ZIKV infections. During DENV and YFV infection, the depletion of type III interferons results in impaired $CD4^+$ and $CD8^+$ T-cell activation, and thus also negatively impacts viral clearance. Additionally, in mouse models deficient for type III IFN signaling infected with YFV, type III IFN signaling resulted in reduced blood/brain barrier intactness, thus allowing for viral neuro-invasion (149). Of the studies for ZIKV infections investigating type III IFN responses to infection, many focus on maternal and fetal infections with emphasis on the fetal/maternal blood barrier (75, 150-153).

The placenta is the organ that separates the fetal and maternal blood supply, primarily through the chorionic villi, where fetal and maternal blood are spatially separated by 3-4 cell layers. After blastocyst implantation in the uterine wall, trophoblast cells multiply and differentiate into variable cell types. One such cell type, the syncytiotrophoblast, forms the outer epithelial layer of the chorionic villi where the majority of fetal/maternal blood exchange occurs (154). The syncytiotrophoblast layer is the primary epithelial defense in the fetal/maternal blood barrier and the first cells ZIKV encounters during fetal infection. Indeed, the type III interferons produced by syncytiotrophoblasts allow for autocrine protection, and subsequently prevent ZIKV from infecting the fetus (155).

Provided that the cells of the fetal/maternal blood interface are resistant to ZIKV infections based on their ability to secrete IFN-λ, several studies have focused on uncovering the mechanism(s) by which ZIKV gains entry into the amniotic space and thus can infect the fetus (156). These studies focused on a specific type of fetal macrophage cells called Hofbauer cells

(HBC) that derive from the fetus; are of monocytic origin and are commonly found through the chorionic villi. (157). These cells first appear early during human pregnancy (within the first 3 weeks), and then diminish in numbers between the 4th and 5th month of gestation. Among mothers and fetuses infected with ZIKV however, HBCs have been seen to linger longer into the 3rd trimester of pregnancy at a density higher than normally observed (158). Not only do HBCs persist at increased density, they are also capable of direct infection by ZIKV. It is speculated that they can move freely between the chorionic tissues where blood exchange occurs in the placenta (159-161). Thus, by traversing from the chorionic fetal/maternal blood interface to the amniotic sac and fetus, HBCs can act as a shuttle for ZIKV to bypass the fetal/maternal blood barrier and infect the fetus.

Asian lineage strains have shown the ability to upregulate Type III IFN production and mRNA translation in both cell culture and in primary human clinical cases. African lineage strains have only demonstrated this ability to a lesser extent only in cell cultures. *In vitro* studies with ZIKV AF (MR-766) and AS 9 (FSS13025) infected human choriocarcinoma JEG-3 cells showed induction of anti-viral type III IFN responses and the ISG 2'-5' oligoadenylate synthetase suggesting that IFN type III responses produced by human placental trophoblasts confer protection against ZIKV infection (159). Interestingly, while both lineages have demonstrated an increase in both translation and transcription, there is not an increase of the amount of active Type III IFN proteins produced and detected in culture medium.

ZIKV Vaccine development

Since the outbreaks that garnered international attention for ZIKV in 2015, the race for a vaccine to combat ZIKV has yielded several candidates, currently at various stages of development. A

successful ZIKV vaccine must confer strong protection in healthy and pregnant populations, while also proving safe and efficacious regarding fetal/neonatal health. Important features to consider for a vaccine should include both enhanced magnitude and quality of neutralizing antibodies and minimal cross-reactivity to DENV to prevent antibody dependent enhancement (ADE) (162-165). Antibody dependent enhancement is perhaps the most critical of these features, as flaviviruses are antigenically and structurally similar, and non-neutralizing antibodies generated by one flavivirus can result in fatal outcomes upon secondary infection with a different flavivirus.

Recombinant envelope (E) protein subunit vaccines have been tested as either whole protein or single domain subunit candidates. Many of the published E protein subunit vaccines have required multiple booster administrations to achieve high antibody titers and rely on the use of adjuvants to augment the humoral response (166, 167). The use of domain III alone of the E protein has proven sufficient to neutralize ZIKV in cell culture systems and in multiple mouse models when proteins are generated using the French Polynesian strain of ZIKV, Asian lineage, as a template (168). Combining the knowledge of how T-cells mediate viral clearance of ZIKV infections with epitope predictions, Pradhan et al., demonstrated that subunit vaccines using the NS2B, NS3, and NS4A proteins have potential as neutralizing vaccines that mediate a strong $CD4^+$ T-cell response through *in silica* analyses (169).

Another candidate ZIKV vaccine is lipid encapsulated mRNA. While multiple publications have demonstrated that lipid enclosed mRNA vaccines are capable of antibody-based neutralization, only the work of Richner et al. addressed the issue of cross-reactive antibodies by specifically deleting the domain II of the fusion loop on the ZIKV E protein (170). Removal of this fusion loop domain resulted in minimal cross-reactivity between ZIKV and DENV, serotype 1. DNA vaccines have also been evaluated for ZIKV candidates, and one has progressed to clinical

trials. DNA vaccines provide an economic advantage with their ease of production, and Larocca et al. has demonstrated a ZIKV DNA vaccine using the E and matrix (M) proteins can induce strong T-cell responses (171). An additional study by Muthumanni et al. evaluated the efficacy of a DNA vaccine in both immunocompromised mice and non-human primates and demonstrated the successful generation of neutralizing antibodies and high antibody titers (172). Of DNA vaccine candidates, all rely on host synthesis of viral conserved proteins among MR766 and Brazilian strains, in an attempt to generate the largest cross-protective response. Despite this effort, data regarding non-homologous challenges and evaluations against different strains and lineages remains scarce. This is true for the majority of vaccine candidate studies published to date.

Live attenuated vaccines and chimeric vector vaccines offer alternative candidate vaccines against ZIKV, as they provide a strong cellular immune response due to their active infections, and a humoral response that more closely recapitulates natural infection. Live attenuated vaccines also have the benefit of generating a natural cellular response without the risk of a generating disease. Shan et al. has demonstrated that deletions within the 3'-UTR of the RNA genome can generate an attenuated ZIKV clone that fails to replicate, and that this vaccine can induce sufficient protection to prevent ZIKV from causing disease (173, 174). Whole inactivated virus vaccines are the front-runner candidates for future ZIKV vaccines, based on the clinical trials occurring within the United States, 75% of which are whole inactivated particles from the PRVABC59 strain of ZIKV, which poses the largest threat to the US (175).

Knowledge gaps and future studies

Despite the major concern that ADE and ZIKV antibody cross-reactivity among flavivirus plays in the development of vaccines, few studies have successfully demonstrated that the neutralizing

antibodies produced by a particular vaccine candidate are not cross-reactive to other flaviviruses. Thus, while the quest for neutralization is important, the future risk of ZIKV mediated DENV ADE should not be overlooked. A third consideration is that few, publications directly investigate the binding avidity of these antibodies, but instead focus on neutralization capacity, although the data strongly suggest low avidity and affinity antibodies have a higher chance of generating ADE for other flaviviruses, presenting another potential complication (168, 176, 177).

Additionally, despite the known disparities between different lineages of ZIKV, a lack of clarity remains regarding the mechanism behind neutralizing antibodies produced by a candidate vaccine or the protection conveyed against non-homologous vaccine strains. Neutralization assays should ideally include multiple strains from each of the three lineages: African, Asian, and American. This information is highly significant, because representative viruses from these lineages demonstrate differential neuroinvasive and inflammatory capabilities, as well as different infection profiles.

Few studies exist that focus on the impacts of ZIKV vaccination during pregnancy and even less address the issue of ZIKV sexual transmission. This is particularly important for areas with high prevalence of DENV where ZIKV cases can often be misdiagnosed and untreated for the infection. It is therefore of paramount importance to design effective vaccines conferring strong mucosal immunity in these high-risk groups.

CONCLUSIONS

Zika virus continues to pose an international threat as a neuroinvasive virus with potentially lethal consequences especially to pregnant mothers and their fetus. While ZIKV has demonstrated a continual geographic and phylogenetic expansion, the levels of genetic mutations between ZIKV

strains is surprisingly limited between lineages. African lineages have shown to be more infectious and elicit stronger inflammatory responses in a number of *in vitro* and *in vivo* experiments. It is unclear why neurological complications and fetal disruption in the Americas is produced by strains with Asian ancestry. It is also puzzling why African strains are not found in recently reported human cases. One possibility is that surveillance of infected humans in Africa is insufficient to detect severe cases of infection with the African strain.

Moreover, African lineages exhibit an inhibitory mechanism on IFN production and signaling, which has been well documented in other flaviviruses (102, 129). The Asian and American lineages, however, have developed a secondary mechanism to prevent IFN transcription by IRF3 and IRF7 binding and preventing their translocation into the nucleus. Hence, while the African lineage has been shown to be more infectious than the Asian, it often presents as a self-limiting febrile disease, whereas the Asian and American lineages have exhibited persistent infections, with some human cases shedding active virus for upwards of 6 months (178).

Vaccine candidate research for ZIKV continues to be limited, providing little insight into potential differences in vaccination responses between circulating lineages. Additionally, these investigations have not prioritized the critical relationship between ZIKV and other flaviviruses, such as DENV, as the antibodies proven protective against ZIKV may promote more severe infections for DENV, rather than provide cross-protective benefits. While our understanding of ZIKV has increased profoundly, extensive investigations are still required for a better understanding of lineage-specific dynamics and the host immune response in terms of their evolutionary trajectory as they continue to expand geographically. Improved understanding of these topics, which currently present knowledge gaps in the field of ZIKV research, will serve as

the cornerstones for designing future vaccines and antivirals that not only efficacious for ZIKV, but also safe against other flaviruses.

SECTION I.V - Introduction to Dissertation Research

In this dissertation, I investigated differential viral pathogenesis among immunocompetent and immunocompromised mice and then evaluated immune correlates of protection generated via systemic or cutaneous vaccination routes. In Chapter II, I characterized the development and convalescence of neuro-ocular pathology following ZIKV infection among immunocompetent mice at both early and late timepoints. As infections among mice treated with a functional IFNAR blockade were 90% lethal, we focused our evaluation on immunocompetent mice, which have well-characterized innate and adaptive immune responses to viruses. In Chapter III, I characterized cellular and humoral immune responses following prime and booster vaccination prior to infectious challenge and I evaluated the protective efficacy of systemic and cutaneous vaccination to prevent non-resolving ocular pathology and chronic brain inflammation. I also studied antibody-based breadth of immunity to Asian and African lineage ZIKV strains and cross-reactivity to Dengue virus strains (DENV).

CHAPTER II : ZIKA VIRUS-INDUCED NEURO-OCULAR PATHOLOGY IN IMMUNOCOMPETENT MICE CORRELATES WITH ANTI-GANGLIOSIDE AUTOANTIBODIES

Jacob T. Beaver*[1], Lisa K. Mills[1], Dominika Swieboda[1], Nadia Lelutiu[1], Edward S. Esser[1], Olivia Q. Antao[1], Eugenia Scountzou[2], Dahnide T. Williams[1], Nikolaos Papaioannou[3], Elizabeth Q. Littauer[1], and Ioanna Skountzou[1,#]

[1] Department of Microbiology & Immunology, Emory University School of Medicine, Atlanta, GA, 30322, USA

[2] EyeVetSurgery-Small Animal Clinic, Athens, 15561, Greece

[3] Faculty of Veterinary Medicine, Aristotle University of Thessaloniki Thessaloniki, 54124, Greece

Accepted May 23, 2020. Published August 6, 2020.

DOI: 10.1080/21645515.2020.1775459

Running Title: ZIKV autoantibodies mediate neuro-ocular pathogenesis.

#Address correspondence to Ioanna Skountzou: iskount@emory.edu

* First Author.

ABSTRACT

A severe consequence of adult Zika virus (ZIKV) infection is Guillain-Barré Syndrome (GBS), where autoreactive antibodies attack peripheral and central nervous systems (CNS) resulting in neuro-ocular pathology and fatal complications. During virally induced GBS, autoimmune brain demyelination and macular degeneration correlate with low virus neutralization and elevated antibody-mediated infection among Fcγ-R bearing cells. The use of interferon-deficient mice for ZIKV studies limits elucidation of antibody-dependent enhancement (ADE) and long-term pathology (≥120 days), due to high lethality post-infection. Here we used immunocompetent BALB/c mice, which generate robust humoral immune responses, to investigate long-term impacts of ZIKV infection. A high infectious dose ($1x10^6$ FFU per mouse) of ZIKV was administered intravenously. Control animals received a single dose of anti-IFNAR blocking monoclonal antibody and succumbed to lethal neurological pathology within 13 days. Immunocompetent mice exhibited motor impairment such as arthralgia, as well as ocular inflammation resulting in retinal vascular damage, and corneal edema. This pathology persisted 100 days after infection with evidence of chronic inflammation in immune-privileged tissues, demyelination in the hippocampus and motor cortex regions of the brain, and retinal/corneal hyperplasia. Anti-inflammatory transcriptional responses were tissue-specific, likely contributing to differential pathology in these organs. Pathology in immunocompetent animals coincided with weakly neutralizing antibodies and increased ADE among ZIKV strains (PRVABC59, FLR, and MR766) and all Dengue virus (DENV) serotypes. These antibodies were autoreactive to GBS-associated gangliosides. This study highlights the importance of longevity studies in ZIKV infection and confirms the role of anti-ganglioside antibodies in ZIKV-induced neuro-ocular disease.

INTRODUCTION

Zika virus (ZIKV) is a mosquito-borne flavivirus discovered in 1947 in a rhesus macaque within the Zika Forest of Uganda. Outbreaks of human ZIKV were occasional until an epidemic in 2015 with more than 37,000 cases in the US and US territories, and more than 1 million in Latin America(179).

ZIKV can spread via multiple modes of transmission: transplacentally to developing fetuses, via breastfeeding to infants, to adults through sexual intercourse, or cutaneously via mosquito bite. Congenital Zika syndrome (CZS), associated with microcephaly and birth defects, has been demonstrated in infants of infected pregnant women (16, 180, 181), and more recent reports point to impaired visual and neurological development among infants born with CZS independent of microcephaly (182-184). Flaviviruses persist up to 6 months in immune-privileged compartments such as brain, eyes, and genitals after the virus has been systemically cleared (63, 185, 186).

While infected adults can end up with permanent ocular damage, such as macular degeneration and retinal edema, the most severe consequence of adult infections is Guillain-Barré Syndrome (GBS), a disease attacking the nervous system. GBS initially manifests gastrointestinal and respiratory symptoms (187), and as autoantibodies develop, symptoms shift to the notable motor/neural impairment hallmarks. Diagnostic criteria for GBS include progressive symmetric weakness of one or more limbs, hyporeflexia or areflexia, and a full progression within 4 weeks (188). Recent studies suggest that ZIKV-induced GBS develops during the course of infection, and not post-infection, as commonly seen with other GBS-inducing pathogens, such as *Campylobacter jejuni* (189-191). While the role of T cells in GBS-associated demyelination and neuroinflammation has been well studied (192, 193), there is limited information on the putative

role of ZIKV-specific antibodies in initiating or sustaining these symptoms. These facets of GBS necessitate the use of animal models enabling the long-term study of ZIKV-induced pathology.

Commonly used murine models for ZIKV infection are deficient in type-I interferon (IFN) receptors (IFNAR-/- such as A129/AG129 strains), as flavivirus infections are intricately linked to the host IFN response. These murine models are either deficient in IFN receptors (194), or IFN signaling is inhibited by blocking receptors with antibodies to facilitate susceptibility to infection and enable extreme viremia(96, 100, 195). Consistent with human infections, ZIKV-infected IFNAR-/- mice develop purulent ocular discharge with detectable viral RNA (vRNA) in lacrimal glands and tears, and active ZIKV virions in Müller glial cells and optic tract tissues (195), with symptoms persisting after viral clearance (96). However, these animals do not survive beyond 10 days post-infection, which limits studies of long-term infectious impacts.

Previous studies investigating the molecular mechanisms by which ZIKV gain access to the eye and causes inflammation have revealed the role of retinal epithelial infections and cell death in allowing for ZIKV to cross the blood-barriers of immune-privileged tissues (95, 99). These investigations are often limited to *in vitro* studies of human primary cells, or juxtapose cell culture studies with ZIKV infection in wild-type (WT) C57BL/6 and immune-compromised animals. Singh et al. provides a thorough analysis of transcriptional responses after intravitreal inoculation of ZIKV into either WT or ISG15 deficient animals and shows a rapid induction of inflammatory responses during ZIKV infection (95). These findings coincide with retinal lesions and chorioretinitis that present within 24 hours of infection and last up to 96 hours after infection. While this insight into ZIKV pathogenesis of immune-privileged tissues is beneficial, the mechanism behind systemic ZIKV entry into the eye and ZIKV infection synergy between eye and brain remain to be determined.

In this study, immunocompetent BALB/c mice were intravenously infected (195) with a high dose of ZIKV-PRVABC59 suitable for this model (196). BALB/c mice were selected over C57BL/6 mice for their ability to generate robust humoral responses and their use in vaccination studies. Similar studies in C57BL/6 mice require intracranial or intravitreal injection in order to achieve similar ZIKV neuro-ocular pathology (95, 197). This study seeks to build on previous studies by examining the development and convalescence of neuro-ocular pathology over 120 days using a less traumatic form of inoculation. To assess infection-induced pathology, we adapted two ocular reflex assessments, and two motor/neural and joint tests. We evaluated the magnitude and quality of immune responses after infection.

METHODS AND MATERIALS

Cells and virus stocks

Vero cells (ATCC, CCL-81) for virus propagation and titration were maintained in DMEM (Mediatech, 10-013-CV) containing 10% fetal bovine serum (FBS; Hyclone, Thermo Scientific, SH3007103), 5% HEPES (Corning, H3537) and 1% Penicillin/Streptomycin (Corning, 30-002-CI). ZIKV stocks were generated from the African lineage Uganda strain (MR766, B.E.I. resources, NR-50085) and the Asian lineage, Caribbean isolate from Puerto Rico (PRVABC59, generously provided by Dr. Scott Michael and Dr. Sharon Isern at Florida Gulf Coast University). The FLR strain from Colombia was obtained from B.E.I resources (NR-50183). Dengue virus strains (DENV1/Hawaii/1944, DENV2/16681/Thailand/1964, DENV3/H87/Philippines/1956, and DENV4/UNC4019/ Colombia/2006) were generously provided by Dr. Joshy Jacob of Emory University. All viruses were propagated in Vero cells for 7 days at 37°C. After the tenth passage, culture supernatants were collected and cell debris was cleared by centrifugation at 3,000xg for 10

minutes at 4°C. Viral harvest was then filtered using 0.22-micron filters (Sigma, Z741966). Culture supernatants were concentrated using Amicon centrifugal concentration filters (EMD Millipore, C7715) by centrifugation at 4,000xg for 30 minutes. As the ZIKV virion is approximately 50 nm in diameter, we used the 100 NMWL variant filters to maximize the recovery. Finally, viral supernatants were purified by discontinuous 20-60% sucrose gradient, where they were diluted 1:5 with FBS before final storage at -80°C (198).

Virus titration

Viral stocks were titrated by plaque assay performed in Vero cells as previously described (199). Focus-forming assays were performed as previously described (200). Blue foci were counted, and titers were calculated by foci numbers in infectious volume (# of foci x infectious volume x conversion factor to ml x dilution factor). FFU and PFU are equivalent in that both are quantification methods. In this study, PFU assays and FFU assays resulted in similar titers.

Trans-well Focus-Forming Assay: To evaluate if live virus can be isolated from systemic and privileged tissues and bodily fluids, we adapted a trans-well infectious system similar to a monocyte chemotaxis assay used for Japanese Encephalitis Virus (201). Tissue homogenates and cell suspensions were then added onto 0.4µm trans-well insert systems (Corning, CLS3396) overtop sterile Vero cells. Live virus released from cells in contact with the insert filtered through the membrane to infect permissive Vero cells growing as a monolayer in the lower well. This provided a measure of tissue-specific live viral load as opposed to quantifying the amount of vRNA present in tissues.

Animal strains and housing

Female BALB/c mice (Charles River Laboratories) were housed in a biosafety level 1 facility at Emory University's Division of Animal Resources and viral infection experiments were performed on animals housed in a Biosafety Level 3 facility at Emory University's Division of Animal Resources. All experiments were conducted in accordance with protocols approved by Emory University's Institutional Animal Care and Use Committee (IACUC) in accordance with guidelines with the United States Federal Animal Welfare Act (PL 89-544) and subsequent amendments.

Animal infection, tissue and biological fluid sampling

Mice were infected with $1x10^6$ FFU of ZIKV-PR virus intravenously (IV) (202). Serum or platelet-poor plasma (PPP) was collected 0, 3, 6, 10, 30, 40, 60, 80, 100, and 120 days post-infection; plasma was collected in citrate buffer and stored at -20^{o}C until use. Small groups of mice were euthanized at the same time points and tissues were collected and processed for histology or, homogenized in protease inhibitors and RNase inhibitors (ThermoFisher Scientific, Waltham, MA) for infectivity and qRT-PCR studies. In the remaining mice, tears were collected via PBS gavage 100 DPI and after euthanasia. Tissues (brain, eyes, genital organs, liver and spleen) were collected and processed for infectivity experiments, histology, and inflammatory markers. Ocular tissues were not perfused prior to harvest to avoid structural and cellular changes induced by the perfusion process (203), as functional morphology of the retina correlates directly with fluid pressure in the choroid. For both FFA and qRT-PCR quantification methods, tissues were homogenized after mincing and passaged through 40µm cell strainers (Fisher Scientific, 08-771-1). They were further digested with 1 mg/ml of Collagenase IV (Worthington, LS004189) for 30

minutes at 37°C, and the purified through 40µm cell strainers. Homogenates were separated using a Percoll (Millipore Sigma, P1644) density gradient (204, 205), and cell suspensions were isolated for qRT-PCR and FFA trans-well studies. One eye from each animal was used for FFA and qRT-PCR experiments, and the other was used for tissue sectioning for microscopy studies.

Anti-IFNAR administration: Immunocompetent mouse infections were compared to a second cohort of animals that which received a one-time administration of anti-mouse IFNAR-1 functionally blocking monoclonal antibody (mAB) (MAR1-5A3, Leinco Technologies, #I-401). Each mouse received 1 mg of anti-IFNAR mAB via intraperitoneal injection 24 hours prior to infection (206). The projected half-life of this dosage is 2.6 days.

RNA isolation and qRT-PCR

Total RNA was extracted from tissues using Trizol (Ambion, 15596018). Tissues were homogenized into Trizol reagent using the FastPrep-24 5G homogenizer (MP Biomedicals). Total RNA was isolated using the PureLink RNA mini-kit (Ambion, 12183025). Purified RNA was quantified, checked for quality assurance, and then reverse transcribed with the qScript Reverse Transcription kit (QuantaBio, 95047). For quantification of vRNA, a standard curve was generated using 10-fold serial dilutions of ZIKV RNA standard. qRT-PCR for ZIKV prM-E was performed with TaqMan Gene Expression Master Mix, ZIKV Primers, and probe as previously described (207). The standard curve had an R value greater than 0.99. vRNA copies were interpolated from the standard curve using the average Ct value obtained from samples run in triplicate. qRT-PCR for *GAPDH, IL-1β, TNF-α, IL-10, SOCS3, MMP2, MMP9,* and COX2 were performed with PerfeCTa SYBR Green SuperMix Low Rox (Quantabio, #95056-500). Primers for *GAPDH, IL-1β, TNF-α, IL-10, SOCS3,* and *COX2* were as previously described (208). MMP2 primers were as

follows; forward 5'-AACGGTCGGGAATACAGCAG-3'; reverse 5'-GTAAACAAGGCTTCATGGGGG-3'. MMP9 primers were as follows; forward 5'-AACCTCCAACCTCACGGACA-3'; reverse 5'- AGGTTTGGAATCGACCCACG-3'. Data was analyzed using the ΔΔCt method to determine normalized relative expression.

Ocular and Brain Symptomatology

At the same time points of blood collection post-infection, animals were assessed for ocular and motor/neural symptomatology. Behavioral tests to characterize pathogenesis in our mouse model were adapted from the Department of Molecular & Comparative Pathobiology's 2015 Lab Manual from Johns Hopkins University School of Medicine (209). These assessments were identified and further researched with the explicit aim to evaluate visual and motor function following ZIKV infection.

Visual Placement Reflex: A reaching reflex test, or visual placement assessment, measures optic function and can also potentially indicate inflammation in parietal and occipital lobes of the brain (210, 211). It is performed by holding the mouse gently by the tail suspended approximately 1-2 feet above a solid cage grate surface (209). The mouse is then vertically lowered slowly toward the grate, taking note not to allow whiskers to contact the surface. A mouse with normal, average visual capabilities will attempt to reach toward the surface. A mouse that is blind, with impaired vision, or spatio-temporal problems will not attempt to reach until the whiskers contact the surface. Alternatively, the impaired mouse may also try to bend backwards on itself, in attempt to right itself using its awareness of gravity.

Palpebral Reflex: Alternatively called the corneal reflex, it measures optic function and indicates potential inflammation in central nervous tissue connected to the optic tract, such as the trigeminal

nerve, occipital lobe, and parietal lobes of the brain (212, 213). It is performed by using a teased-out cotton tipped applicator. The mouse is held steady, and the cotton is gently touched against the cornea (209). The blinking response is assessed on a scale of 0 to 3. On this scale, 3 represents a hyper-repetitive blinking in response to corneal stimulation; 2 equivocates to a normal, quick blink response; 1 corresponds to a slow blink or a closure response to stimuli; and a score of 0 indicates there was no response to corneal stimuli. Impaired or absent reflex responses suggests deteriorated motor/neural capabilities, eye function, and potential neurological inflammation.

Rear Limb Withdrawal: The limbic withdrawal test measures motor neuron responses in mice, and can indicate arthralgia in limb joints, and/or inflammation of motor neurons (214, 215). The mouse is allowed to grip onto a surface and steadied by the tail (209). One of the hind limbs is gently picked up and pulled taut at a 45˚ angle. The limb is then released, and the withdrawal of the limb is scored on a scale 0 to 3. On this scale, 3 represents a hyper-active response; 2 equivocates to a normal quick withdrawal of the limb back to normal position; 1 corresponds to a slow response to stimulus; and a score of 0 indicates no response, with the leg dropping to the ground and not returning to normal position.

Grip Time Assessment: The grip time assessment quantitatively evaluates mouse muscular capabilities and indicates potential arthralgia and muscular coordination issues (216, 217). The test was performed by placing a mouse on a grated cage lid, and the grate was suspended 1-2 feet above the bench-top or cage (209). The mouse and grate were gently shaken for 1 minute, and then rapidly inverted to bring the mouse into an upside-down position. The time the mouse could successfully hold on without falling off the grate was recorded. Healthy mice are expected to be able to hold onto the grate for a minimum of 1 minute. Any recordings less than 60 seconds was considered abnormal.

Histopathology and immunofluorescence of eyes and brain

To evaluate tissue infectivity, viral burden, and infection-induced histopathology; eyes and brains were harvested from 5 out of 20 total mice per group at 10 DPI and the remaining15 mice at 100 DPI. The tissues were fixed in 10% formalin solution, followed by paraffin embedding for 8 µm sectioning. Sectioning of brain tissues was performed at the Neuropathology/Histochemistry core of the Emory NINDS Neurosciences Core Facility (P30 NS055077), sectioning and H&E staining of eye tissues was performed by the L.F. Montgomery Ophthalmology Pathology core.

Immunofluorescent staining: Slides were de-waxed and rehydrated using sequential washes of xylene, ethanol, and distilled water. Antigens were unmasked and retrieved by submersion in sodium citrate buffer (10mM, pH 6.0) for 10 minutes at 56°C. Aldehyde auto-fluorescence was quenched in a humidified chamber using 3M glycine solution, and lipofuscin auto-fluorescence was quenched using Sudan-Black B. Slides were then blocked in bovine serum albumin (2% BSA)-TBS. Primary antibody diluted in 1% BSA in PBS buffer was added directly on top of each section, and slides were incubated overnight at 4°C. The 4G2 antibody (Millipore, MAB10216) was used for viral infectivity analysis. Myelination studies utilized anti-MBP-Alexa Fluor488 (SantaCruz, sc-271524), anti-Vimentin (Rabbit anti-Mouse, Abcam, ab92547), and anti-Myelin PLP (Rabbit anti-Mouse, Abcam, 28486) antibodies. Secondary antibodies were fluorescently conjugated (Anti-Mouse Alexa594, Biolegend #405326; Anti-rabbit Alexa547, Abcam, ab150167; Anti-mouse Alexa488, Invitrogen, A10667), diluted in 1%BSA in PBS solution and incubated for 2 hours at room temperature. Prolong Gold Antifade mounting medium with DAPI (Thermo-Fisher, P36931) was applied, and slides were covered with a coverslip. Images were

taken on Zeiss AxioScope microscopes via SPOT-advanced imaging software. Images were processed in Fiji/ImageJ.

TUNEL staining: TUNEL stain was selected because it identifies infection-induced cell death via DNA fragmentation irrespective of specific cell death pathways i.e. apoptosis, necroptosis, or pyroptosis (218-220). Terminal deoxynucleotidyl transferase dUTP nick end labeling, or TUNEL, staining was performed according to manufacturer protocol (Abcam, ab66110). Slides were de-waxed and rehydrated using sequential washes of xylene, ethanol, and distilled water. Antigens were unmasked and retrieved by submersion in sodium citrate buffer (10mM, pH 6.0) for 10 minutes at 56°C. Aldehyde auto-fluorescence was quenched in a humidified chamber using 3M glycine solution, and lipofuscin auto-fluorescence was quenched using Sudan-Black B. Slides were then blocked in bovine serum albumin (2% BSA)-TBS. Slides were then washed in PBS and blocked using a proteinase K solution for 5 minutes at room temperature. Wash slides with PBS and then label fragmented DNA using TdT enzyme, enzyme buffer, and Br-dUTP (Abcam, ab66110). Prolong Gold Antifade mounting medium with DAPI (Thermo-Fisher, P36931) was applied, and slides were covered with a coverslip. Images were taken on Zeiss AxioScope microscopes via SPOT-advanced imaging software. Images were processed in Fiji/ImageJ.

Quantification of MBP, Myelin PLP, and 4G2 positive cells: Corrected total cellular fluorescence (CTCF, also called normalized MFI) was determined as described by Lourenço et al. for both MBP, myelin PLP, and vimentin stains (221). Similarly, to determine the percentage of 4G2 positive cells, DAPI foci and 4G2 cells were enumerated both manually and automatically, using the "Threshold" and "Analyze particles" functions in FIJI/ImageJ. The percent of infected cells was then calculated as the number of 4G2 positive cells was divided by the number of DAPI positive foci.

Antibody Titration and Characterization

ELISAs: Anti-ZIKV specific antibodies were determined by coating flat bottom, 96-well Nunc MaxiSorp plates (Thermo-Fisher, 44-2404-21) with 4µg/ml of inactivated virus stocks, diluted in sodium bicarbonate buffer. Plates were incubated overnight at 4°C, washed with PBS-Tween 0.5%and blocked with 2% BSA in PBS for 1 hour. Individual PPP samples were run in duplicate and incubated for 2 hours at 37°C. The standard curves were generated with appropriate purified mouse immunoglobulins and isotype-specific HRP-labeled detection antibodies (Southern Biotech, Birmingham, AL). Sample IgG concentrations were determined by interpolation from standard curves. Anti-ganglioside specific antibody concentrations were determined similarly. Flat bottom, 96-well Nunc MaxiSorp plates were coated with 2µg/ml of either GD1a, GD1b, or GT1a ganglioside (SantaCruz, sc-202621, sc-202622, sc-202629, respectively). Standard wells were coated as described above. PPP samples were diluted. Standard curve antibodies and development of plates was performed as described previously (222).

Focus-forming Reduction by Neutralization Assay (FFRNT): Heat-inactivated PPP samples were diluted serially and combined with 100 FFU live virus. Antibody dilutions and virus were co-incubated for 1 hour at 37˚C, and then added over Vero cells for 24 hours. The focus-forming assay was performed as described (200).

Antibody-Dependent Enhancement Assay: ADE assay protocol was performed as described using U937 cells (200). The cells were maintained in suspension in complete RPMI medium. Cells were stained with 4G2 antibody (EMD Millipore). Samples were run on a CytoFLEX LX system at Pediatrics/Winship Flow Cytometry Core of Winship Cancer Institute of Emory University, Children's Healthcare of Atlanta and NIH/NCI, which is supported under the award number P30CA138292.

Statistical Analysis

Correlation analysis was performed on vRNA titers determined by qRT-PCR for brain and eyes to determine a relationship with raw reflex scores. Pearson's correlation coefficient with a two-tailed p-value were calculated for each of the four reflexes. For ELISA assays, linear regression tests to interpolate OD values into concentrations. For co-culture assays and qRT-PCR, two-way ANOVA was used to analyze differences between infected and uninfected infections were followed by Sidak's Post Hoc test for multiple comparisons. Two-way ANOVA with Sidak's post-hoc was also used to determine differences between uninfected and infected groups. For immunofluorescence assays, two-way ANOVA was used to compare differences in hippocampal and cortical regions, as well as between early and late time points. Non-linear regression analysis was performed to determine the IC_{50} (95% confidence interval) for avidity and neutralization assays. A p-value less than 0.05 was considered significant.

RESULTS

ZIKV-PRVABC59 infection in immunocompetent mice results in distinct neurological and ocular pathology.

Current mouse models for ZIKV are insufficient for long-term studies because they utilize low infectious dosages (less than $1x10^3$ FFU) to generate acute pathology and mortality within 1 week of infection. When immunocompetent animals were infected with $1x10^6$ FFU of virus, symptoms and pathology typical of ZIKV infections presented within 3 days post infection (DPI). While the moribund weight loss of 25% or greater seen in IFNAR-/- models was not observed, infected BALB/c mice lost 10% of their starting weight by 6 DPI, and never recovered to match uninfected animals (Fig 1A). To evaluate how immunocompetent BALB/c mice compare to similar immune compromised models, we administered 1 mg of anti-IFNAR mAB by intraperitoneal injection 24-hours prior to infection. These animals lost approximately 20% of their initial body weight, and were euthanized due to seizures at 3, 4, 5, 10, 11, and 12 DPI (Fig 1B). Only 1 animal the received anti-IFNAR block survived beyond 12 DPI.

ZIKV has demonstrated persistence in human organs and fluids for ≥200 days(223). Thus, we quantified viral burden in tissues and secretions with a focus-forming assay (FFA) co-culture, where homogenized tissues were used in a trans-well system over permissive Vero cells 4. Homogenized tissues would then shed live virus through the membrane pores, infect permissive sterile cells below, and where the readout of this assay is FFU/ml. Homogenates were not added directly to monolayers because it does not discriminate if the cells are permissive to infection or a productive infection. Previous concerns were raised that ZIKV would not propagate in WT BALB/c tissues due to STAT non-homology. Thus, they were evaluated here to specifically

identify if live virus was being shed from the tissues. Among immunocompetent mice, the maximum viral load in systemic organs was similar, between $1.4x10^4$ and $1.3x10^4$ FFU/ml in liver and spleen. Mice which received anti-IFNAR treatment showed a maximum of $2.2x10^4$ and $1.9x10^4$ FFU/ml in these same tissues (Fig 1C). Viral burden in their immunoprivileged tissues, eye and brain, were $1.3x10^4$ FFU/ml and $9.3x10^3$ FFU/ml, respectively. In contrast, anti-IFNAR recipients showed a maximum of $1.8x10^4$ and $1.7x10^4$ FFU/ml in identical tissues. Viral load in immunocompetent animals was 1.7-fold greater in plasma *vs* tears. Among anti-IFNAR mice, tears exhibited an average of $1.7x10^4$ FFU/ml and plasma a maximum of $2.9x10^4$ FFU/ml (Fig 1C). To correlate live virus isolations to the amount of vRNA present within immune-privileged tissues, qRT-PCR was performed at 10 and 100 DPI in brain, eyes, and plasma in both immunocompetent and immunocompromised mice and showed that anti-IFNAR administration resulted in elevated viral load in all tissues (Fig 1D). Animals that received anti-IFNAR injection demonstrated a maximum vRNA concentration of $1x10^4$, $7.1x10^3$, and $1.7x10^4$ ng/ml in brain, eyes, and plasma respectively. Immunocompetent animals demonstrated maximum infectivity levels of $5.8x10^3$, $4.2x10^3$, and $1x10^4$ ng/ml of vRNA in the same tissues, respectively.

Our model demonstrated vision and motor-function abnormalities following ZIKV infection similar to those observed in humans infections and in other published IFNAR-/- murine models (224). We standardized palpebral and visual placement reflex tests to evaluate ocular pathology and intracranial inflammation, and rear-limb withdrawal and grip tests to evaluate motor/neural pathology. Palpebral reflex deficits can indicate inflammation in facial, ocular, and cranial nerves (225, 226). Among infected immunocompetent mice, 55% lost normal palpebral reflex responses 3 DPI. Symptoms reached their nadir 6 DPI, where 75% of mice exhibited aberrant or loss of normal reflexes ($p<0.0001$ for all time-points) (Fig 2A). Palpebral reflexes appeared to recover in

60% of the animals in the remainder of the time-course, whereas 40% of mice demonstrated a persistent loss of normal reflexes until the end of monitoring period (120 DPI). Among anti-IFNAR mice, palpebral reflexes declined within 3 DPI, reaching a nadir where all animals had lost palpebral/corneal reflexes 30 DPI. This loss persisted up to 120 DPI (Fig 2A).

Visual placement reflex deficiencies can suggest abnormalities in optic and cranial nerve function. For this assessment, hyporeflexia indicates an animal's reflexes are reduced or slowed to a debilitating degree. Similar to palpebral reflex kinetics, hyporeflexia in immunocompetent mice was observed as early as 3 DPI, and appeared to reach a nadir between 6 and 10 DPI where 50% of all animals demonstrated loss of visual placement reflexes ($p<0.0001$ for all time-points) (Fig 2B). Thirty percent of mice demonstrated persistent hyporeflexia 120 DPI, indicating non-resolving neurological/ocular infectious sequelae. Among anti-IFNAR mice, the remaining animals demonstrated hyporeflexia at 30 DPI which persisted until 120 DPI.

Rear-limb withdrawal reflexes assess joint pain, inflammation, and motor/neural pathology. Among immunocompetent infected mice, 70% lost normal withdrawal reflex 3 DPI. Symptoms reached their nadir 6 DPI, where 80% of mice exhibited aberrant or loss of withdrawal reflex ($p<0.0001$ for all time-points) (Fig 2C). Reflexes among this cohort appeared to recover across the remainder of the time-course with a notable relapse 60 DPI. At 120 DPI, 30% of mice demonstrated a persistent loss of withdrawal reflexes. Anti-IFNAR animals exhibited a constant and steady decline of withdrawal reflexes until the remaining animal because unresponsive at 30 DPI (Fig 2C).

Similar to rear limb withdrawal assessments, immunocompetent mice evaluated via grip time demonstrated motor/neural impairment as early as 3 DPI, evident by the 2.7-fold reduction in average grip time of infected animals. Hyporeflexia reached the nadir 6 DPI, with a 5.8-fold

reduction in average grip time ($p<0.0001$ for all time-points) (Fig 2D). While symptoms appeared to convalesce, a secondary drop in grip time occurred between 60 and 80 DPI, potentially indicating a periodicity of symptoms or recurrence of infection. The average grip time among infected mice remained 35% lower than uninfected animals 120 DPI. Anti-IFNAR treated animal showed an immediate decline in grip abilities that persisted and did not recover through 120 DPI.

Correlation analyses were performed to determine the relationship between viral burden and reflex clinical assessment scores 100 DPI in immunocompetent mice (Fig 2E). Palpebral and visual placement clinical assessments primarily evaluate ocular functionality, pain, and inflammation. Scores from these tests were plotted against the concentration of ZIKV RNA per gram of eye tissue as determined by qRT-PCR. Both palpebral and visual placement scores demonstrated a strong negative correlation (palpebral $r = -0.7505$ and $p<0.0001$; visual placement $r = -0.6199$ and $p<0.0001$) between increasing viral load and ocular reflex scores (Fig 2E-i and ii). Rear limb withdrawal and grip time tests were used to evaluate motor/neural inflammation, function, and pain. Scores from these two clinical assessments were plotted against the concentration of ZIKV RNA per gram of brain tissue as determined by qRT-PCR. Rear limb withdrawal and grip time evaluations both exhibited a strong negative correlation between increasing viral load and decreasing motor/neural responses (withdrawal $r = -0.7078$ and $p<0.0001$; grip times $r = -0.7972$ and $p<0.0001$) (Fig 2E-iii and iv). Collectively, these data demonstrated that immunocompetent mice infected with high doses of ZIKV, suffered from mild weight loss and reduced recovery resulting in distinct neurological and ocular pathology that significantly correlated with viral burden.

ZIKV infection-induced antibodies have limited cross-protection and enhance infection among ZIKV and DENV strains.

To characterize and evaluate kinetics of ZIKV-specific IgG antibody subtype production and evaluate antibody maturation progression, we collected PPP up to 120 DPI from immunocompetent mice. ZIKV-specific IgG total concentrations were low within the first 40 DPI, never exceeding 77 ng/ml. After 40 DPI, IgG total concentrations increased until 80 DPI, where they plateaued at 647.5 ng/ml and reached a maximum of 714.1 ng/ml (Fig 3A). ZIKV-specific IgG1 concentrations never exceeded 116.8 ng/ml during the length of the study (Fig 3B), and IgG2a concentrations demonstrated increasing titers until 60 DPI, with a maximum of 110.3 ng/ml followed by a sharp spike in concentrations reaching a maximum of 332.2 ng/ml (Fig 3C). This data demonstrates that there was a sharp increase in antibody titers around 60 DPI, and that the majority of these antibodies were IgG2a.

As antibody cross-reactivity has been well documented between ZIKV and DENV, we next aimed to characterize antibody quality, based on the ability to neutralize ZIKV strains and DENV serotypes, and to potentiate infection of non-permissive cell types 100 DPI. Neutralizing virus titer was determined using a contemporary South American ZIKV strain from Colombia, FLR; and an ancestral African lineage strain from Uganda, MR766 (Fig 3D). Of ZIKV strains, PRVABC59 demonstrated 50% neutralization at a titer of 628, while neither FLR nor MR766 demonstrated neutralization beyond a titer of 16. Four DENV strain serotypes were selected for neutralization analysis (Fig 3E). Of these four serotypes, only DENV-1 and DENV-2 exhibited antibody-mediated neutralization with titers of 61 and 33, respectively. This data demonstrates that antibodies generated by ZIKV infection were specific to the strain of infection, and had little to no neutralization capacity to other strains of ZIKV or to DENV serotypes.

Flavivirus antibody cross-reactivity is a double-edged sword; often antibodies can neutralize different viruses at high concentrations but also enhance infection via incomplete neutralization at lower concentrations. Antibody-dependent enhancement (ADE) is a well-studied phenomenon where poorly neutralizing antibodies against one flavivirus or virus strain can increase infectivity of another virus or strain (227). Here, we evaluated the ability of antibodies generated against PRVABC59 to enhance infectivity of homologous and non-homologous ZIKV strains and DENV using non-permissive U937 cells that will only be infected by through ADE. Antibodies generated by ZIKV infection demonstrated some autologous neutralization capabilities at high antibody concentrations and became enhancing at a titer of 320. Among ZIKV strains, both FLR and MR766 demonstrated an endpoint titer of 40, which resulted in 92% and 86% of cells becoming infected, respectively (Fig 3F). Despite the lineage differences, FLR and MR766 infection is a direct product of antibody concentration as evinced by infectivity and antibody concentration decreasing simultaneously. This also points to potential differences among E-protein sequences where FLR and MR766 have a common sequence distinct from PRVABC59. Among DENV serotypes, DENV-2 and DENV-4 demonstrated similar peaks of infectivity at titers of 160 and 80, respectively, with a maximum of 85% of all cells infected for both viruses. DENV-1 infected 71% of all cells at an endpoint titer of 20, and DENV-3 exhibited 74% of cells infected at a titer of 320 (Fig 3G). The trend observed for DENV-1 ADE in (Figure 2G) demonstrates that virus neutralization is a product of antibody concentration and not epitope specificity, as ADE decreases as antibody concentration decreases. Collectively, these data demonstrate that antibodies generated by ZIKV infection were both poorly neutralizing and highly enhancing to non-homologous viruses and strains.

Corneal and retinal hyperplasia among infected mice coincides with elevated cell death and persistent inflammation in the eye.

Conjunctivitis and uveitis are common symptoms among humans infected with ZIKV, and ocular pathology comparable to them has been observed in IFNAR-/- mouse models of ZIKV pathogenesis (96, 98). We documented macroscopic conjunctivitis by facial imaging of the same immunocompetent mouse across infectious time-points in effort to detail animal pain according to the mouse grimace scale (228, 229) (Fig 4A, top-row). Unilateral swelling and orbital tightening was evident 3 DPI and progressed to bilateral swelling with purulent discharge 10 DPI. Both eyes showed intense purulent discharge at 30 DPI, and swelling was persistent up to 100 DPI (Fig 4A, top row). Fundoscopy was performed simultaneously and showed intense vascular inflammation 3 DPI. Retinal edema and vascular inflammation developed 10 DPI, persisted up to 30 DPI, and was not fully resolved by 100 DPI (Fig 4A, bottom-row).

Eye tissues were sampled 10 and 100 DPI to determine infection-induced morphological changes during early and late stages (Fig 4B-C). Within 10 DPI, infected =mice demonstrated chemotic conjunctiva, minor edema of corneal epithelia, and increased leukocyte infiltration within corneal stroma (Fig 4B, left side). ZIKV infections also presented edematous retinal pigmented epithelial (RPE) layers which contributed to further retinal degeneration, and notable immune infiltration of sclera and ganglionic layers (evident by increased nuclei present in these layers) (Fig.4B, right-column). Through 100 DPI, animals showed non-resolving warping of corneal epithelia, and hyperplasia within the cuboidal and squamous layers (Fig.4C, left column), with persistent leukocytes within the stroma. Retinal layers of infected animals showed bifurcation of the ganglionic layer and distinct edema of RPE (Fig.4C, right-column).

Active virus and vRNA could be isolated from eyes of infected animals 100 DPI. Thus, we aimed to identify cell tropism within the eye, possible changes in tropism as infection progresses, and whether morphologically affected tissues demonstrated increased infection or infection-induced cell-death. Viral proteins were detected as early as 10 DPI in lacrimal glands and cornea of infected mice and persisted 100 DPI (Fig 4D; S2A-B). The number of infected cells increased 1.2-fold between 10 and 100 DPI ($p=0.006$) (Fig 4E). To quantify infection-induced cell death, we fluorescently labeled apoptotic and necrotic cells using terminal deoxynucleotidyl transferase dUTP nick end labeling (TUNEL); we and observed increased levels of cell death in cornea and lacrimal glands (Fig 4F; S2C-D). When compared to uninfected animals, ZIKV-infected eyes exhibited 5-times higher cell death after 10 DPI, and 12.6-times greater levels of cell death after 100 DPI. Between 10 and 100 DPI, cell death within infected eyes increased 1.3-fold ($p=0.004$), which correlated with the fluorescent infectivity data (Fig 4G).

IL-1β and *TNF-α* transcription were 1611-fold and 964-fold greater in ZIKV-infected eyes compared to uninfected eyes (Fig 4H). *COX2* expression among infected eyes was 111-times greater than in uninfected eyes. MMP transcription was also elevated, with *MMP2* showing 1,861-fold higher expression and *MMP9* exhibiting 1,313-fold increased transcription. Transcription of the anti-inflammatory cytokines *IL-10* and *SOCS3* was increased 1,007- and 108-fold respectively. Collectively, these data demonstrate that ZIKV infection-induced ocular hypo- and areflexia may be the manifestation of direct infection and cell death of eye tissues, which subsequently mediate leukocyte infiltration, tissue morphology changes, and pan-uveitis inflammation.

ZIKV infection reduces myelin expression and results in prolonged inflammation in the brain.

We observed decreased neurological and motor reflexes and elevated concentrations of anti-ganglioside autoantibodies after infection of immunocompetent mice with PRVABC59. The severity of pathology correlated strongly with viral load in brain tissues, and the antibodies generated by infection were characterized as poorly neutralizing, broadly cross-reactive, and able to robustly induce infection in non-permissive Fcγ-R bearing leukocytes. These data in conjunction with established literature linking anti-ganglioside antibodies with aberrant myelin expression among GBS patients (230) led us to investigate ZIKV-induced myelin expression alterations in the brain. Murine tissues were harvested from immunocompetent 100 DPI and processed for immunofluorescent histochemistry using dual stains for pan-flavivirus group antigen and myelin glycoproteins common on myelin-bearing cells, such as oligodendrocytes and Schwann cells.

ZIKV infectivity immunofluorescence was performed to determine if viral antigen was isolated to specific regions of the brain; the total amount of infected foci were normalized against the total number of cells present in the optic field. Both the hippocampus and cortex showed 35-40% infectivity (Fig 5A). Myelin basic protein (MBP) and myelin proteolipid protein (mPLP) are the most abundant proteins in the CNS which contribute to the myelin sheath (231). Thus, we stained brain sections for MBP in cortex sections, which revealed that infected mice had 2.5 times lower MBP expression than uninfected animals ($p<0.0001$) (Fig 5B and C; S1A). Hippocampus and cortex regions stained for mPLP showed a 2.3- and 1.9-fold lower expression, respectively, compared to uninfected mice ($p=0.0001$, $p=0.001$) (Fig 5D-F; S1B and C). GBS patients have not only demonstrated antibody-mediated reduction in MBP and mPLP, but also a reduction in intermediate neuro-filament and glial cell body proteins, such as vimentin (Vim) (230).

Hippocampus and cortex regions from infected animals demonstrated 2.1- and 2.0-fold less Vim expression compared to uninfected animals (both $p<0.0001$) (Fig 5G-I; S1D and E).

Chronic inflammation plays a critical role in mediating the long-term consequences of GBS (230), thus we characterized transcription of immune proteins 100 DPI from brains of immunocompetent mice. ZIKV infection increased *IL-1β* and *TNF-α* levels by 500 and 660-fold, respectively (Fig 3J). *IL-1β* expression can be regulated by cyclooxygenase 2 (*COX2*), a pain mediator, via a positive feedback loop (118). We quantified transcription of *COX2* via qRT-PCR and observed 75-fold greater levels within infected brains. Matrix metalloproteinases (MMPs) are capable of mediating blood-brain barrier (BBB) permeability, and thus we evaluated transcription levels of *MMP2* and *MMP9*. *MMP2* expression increased 466-fold after infection, while *MMP9* increased 290-fold. Finally, we sought to quantify transcription of the anti-inflammatory proteins *IL-10* and *SOCS3*, as these play prominent roles in controlling neuroinflammation and in regulating anti-inflammatory phenotypes of resident microglia. We observed that these proteins had 15 and 12-fold greater expression after infection. The elevated anti-inflammatory expression is expected at late time points, as these correlate with wound healing. Our transcriptional data suggests that ZIKV infection results in persistent neuroinflammation with high levels of MMPs, which may result in systemic leukocyte infiltration and contribute to both neurological symptoms and observed demyelination (120).

Antibodies generated during ZIKV infection are auto-reactive to GBS-associated neural markers.

Current researching regarding GBS and ZIKV-induced GBS points to auto-antibodies generated against glycosylated pathogen proteins that which mimic ganglioside residues on neurons. As our

observed neuro-ocular pathology resembles GBS, we next wanted to characterize the ganglioside reactivity of the antibodies generated during ZIKV-infection of immunocompetent mice. Thus, we quantified the total amount of IgG that bound to GD1a, GD1b, and or GT1a gangliosides (Fig 6Ai-iii). Each of these gangliosides correlates with a specific variety of GBS. GD1a reactive IgG correlates with acute motor axonal neuropathy; GD1b corresponds to a sensory ataxic variant; GT1a is connected to Miller-Fisher Syndrome, a variant of GBS affecting the eyes (232). To understand what quantity of these antibodies are auto-reactive, we took the percentage of each ganglioside concentration as a proportion to the total ZIKV-specific IgG (Fig 6Bi-iii). As early as 3 DPI, 30-46% of all ZIKV-induced IgG showed reactivity to one of the three gangliosides. Both GD1a and GD1b demonstrated similar peaks at 60 DPI with a maximum of 72% of all ZIKV-IgG being autoreactive. GT1a reached a peak of 56% 100 DPI. Our data demonstrate that highly autoreactive antibodies generated in immunocompetent mice are primarily against GD1a and GD1b gangliosides.

DISCUSSION

In this study, we successfully recapitulated ocular and neurological symptomatology and pathology observed in human ZIKV infections (16) and in A129/AG129 murine models using fully immunocompetent BALB/c mice (98, 100). Importantly, we established precise clinical scoring methods to detail symptom kinetics, severity, and convalescence. We demonstrated that infection-induced sequelae persist among immune privileged tissues up to 100 DPI, and that the demyelination generated following by ZIKV infection correlates strongly with viral burden and persistence, decreased ocular and motor/neural clinical scores, and non-resolving inflammation. These findings were associated with virus-specific antibodies that, despite being long-lived, were

weakly neutralizing and highly enhanced infection, while also perpetuating tissue pathology during ZIKV infection due to autoreactivity. These antibodies were able to neutralize homologous virus but no other ZIKV strains of Asian and African lineages, or DENV serotypes. Notably, they mediated robust infection among non-permissive cells by means of ADE.

Importantly, our study utilized BALB/c mice rather than C57BL/6. Immunocompetent BALB/c mice were preferable for this study because they generate robust humoral responses, and thus are more suitable for investigations about antibody-mediated pathology. While BALB/c have shown retinal degeneration due to normal husbandry lighting, a study by Bell et al. found that standard lighting in animal facilities ranges between 130 and 325 lumens, and induced retinal lesions only in animals ≥20 weeks old (233). Our results are similar to those reported in C57BL/6 mice that developed retinal and corneal pathology, such as retinal edema and hyperplasia, following ZIKV infection (98, 234). Manangeeswaran et al. found that retinal lesions and ocular pathology persists in C57BL/6 up to 90 days and correlates with elevated cytokine levels, but was performed in suckling neonatal mice (235). Our data in the BALB/c model agree with the findings in C57BL/6 mice, and expand in the field of ZIKV neuro-ocular pathology and the underlying mechanisms, providing further insight into current knowledge gaps.

Our study is the first to report on ZIKV-induced autoreactive antibodies to GD1a, GD1b, and GT1a gangliosides that contribute to myelin degradation in immunocompetent BALB/c mice following infection (111). GBS has been correlated with antibody cross-reactivity to host gangliosides in other flaviviruses. We observed that 25-75% of all antibodies generated by and specific to PRVABC59 were also reactive to GD1a and GD1b gangliosides, which may correlate to our observed motor-neural pathology (112). Gangliosides are vital to synaptic transmissions, intercellular adhesion and communication, equilibrium, immune signaling, and nervous system

and motor/neural network maintenance (113). Anti-ganglioside antibodies have been previously shown to lead to the absence or fragmentation of MBP, myelin PLP, and vimentin all contributing to persistent neuroinflammation within the brain by acting as damage associated molecular patterns (DAMPs). Myelin or myelin debris signal in macrophages via complement/opsonization or phagocytosis and facilitate M1 (macrophage type-1) polarization and proinflammatory secretion (114). Protracted neuroinflammation by M1 microglia is mediated by locally secreted inflammatory factors, such as TNF-α, which is consistent with our transcriptional data (114).

The persistent neuroinflammation and severe pathology we observed is consistent with published data reporting that chronic neuroinflammation potentiates severe motor/cognitive diseases among flavivirus infections as seen in GBS cases (115). COX2 stimulates glial cell IL-1β and TNF-α secretion resulting in a paracrine and autocrine signaling cascade (116). This cycle of persistent inflammation and pain-sensitivity is established through a COX2 and IL-1β positive feedback loop, via NF-κB signaling (117) (118). Our data confirmed this in ZIKV-infected mice, showing elevated transcription of COX2, IL-1β, and TNF-α up to 100 days after infection while simultaneously exhibiting persistently hypo- and areflexia.

MMPs are endopeptidases with vital functions such as neural network remodeling, tissue formation, and BBB integrity regulation. M2 microglia (type 2 macrophages), which function in tissue remodeling and anti-inflammatory responses, secrete MMP2 to permeabilize the BBB (114) and allow for infiltrating macrophages to enter the brain, phagocytose, and clear dead cells (119, 120). Increased permeability of the BBB via elevated transcription of MMP2 and MMP9 corresponds with increased inflammatory leukocyte trafficking into the brain (121, 122). Our findings on MMP2 and MMP9 elevation following ZIKV infection are similar to those of Wang

et al., where MMP2 and MMP9 were upregulated in brain tissues following West Nile virus (WNV) infection, thus mediating infiltrating leukocyte trafficking into the brain (116).

TNF-α and IL-6 production by local resident and infiltrating immune cells in the CNS induces IL-10 production, which has an anti-inflammatory function via SOCS3 signaling pathways (236). Importantly, IL-10 has demonstrated the ability to protect astrocytes from excessive inflammation and in regulating adult neurogenesis after brain injury, being implicated as an important mediator of intracellular cross talk between microglia, astrocytes, neurons, and oligodendrocytes (237, 238).

In eyes, COX2, IL-1β, TNF-α, MMP2, and MMP9 transcription profiles among infected animals were elevated through 100 DPI. Interestingly, IL-10 and SOCS3 expression were also elevated in this cohort, suggesting an alternative route of ocular pathogenesis in addition to the primary route resulting from infection and inflammation. High intraocular concentrations of IL-10 and SOCS3 have resulted in pathological angiogenesis via Müller-cell mediated neovascularization (239). Additionally, SOCS3 works by blocking intracellular signaling of IL-6 and IL-23, namely preventing STAT3 phosphorylation and directly influencing ocular T cell repertoires (240). This constraint on T_{H1} and T_{H17} differentiation during infection and inflammation also provides insight into a novel pathway for ZIKV pathogenesis in the eye.

Our study addresses a current gap in the field regarding antibody-specific mechanisms that underlie the initiation of ocular and neurological pathology persistence and damage, and point to the need for a more comprehensive, systems biology approach to understand how antibodies influence long-term neurological pathogenesis of flaviviruses. Collectively, our data suggests that autoreactivity of ZIKV antibodies may initiate a demyelination cascade that ultimately results in chronic neuroinflammation and persistent neuro-ocular impairments. Importantly, we demonstrate immunocompetent animals can serve as models for pathogenesis and long-term infection studies.

These findings underscore the need of exploring alternative vaccination platforms and imposing stringent qualifications for ZIKV vaccine candidates that would confer breadth and longevity of protection while minimizing the risk of autoimmunity or ADE. Future studies should include investigation of demyelination sequelae after passive transfer of ZIKV-induced antibodies, and the putative role of maternal antibodies on vertically transmission. Additionally, future studies duplicating this work in C57BL/6 mice will determine if similar pathology can be observed in a Th1-skewed background.

Acknowledgements

We thank Dr. Sharon Isern, Dr. Scott Michael, and Lauren Paul for providing the ZIKV PRVABC59 strain for propagation. We thank Dr. Micah Chrenek, Dr. Hans Grossniklaus, and Dr. John Nickerson from Emory Ophthalmology Clinic for their advice on optic histology and staining. We thank Dr. Eugenia Scountzou and Dr. Nikolaos Papaioannou for their expertise in veterinary ophthalmology and for detailed assistance in evaluating animal ocular pathology. We thank Vidisha Singh and Aaron Scanlon for assistance running qRT-PCR experiments.

Funding Source

This work was supported by NIAID and CEIRS – HHSN272201400004C NIAID

Author contribution

J.T.B., N.L., I.S., E.S. Project conceptualization and experimental design

J.T.B., L.K.M., E.S.E., D.S., N.L., O.Q.A., E.Q.L., I.S.: Execution of experiments

E.S. and N.P. Assessment of ocular pathology

J.T.B, N.L., D.S., and I.S. Data analysis.

J.T.B., D.S. and I.S. Manuscript preparation

R.W.C. Manuscript feedback.

All authors read and provided feedback prior to submission

Competing financial interests

J.T.B., L.K.M., E.S.E., D.S., N.L., O.Q.A., E.S., N.P., D.T.W., and I.S. declare that they have no conflicts of interest.

FIGURE 1

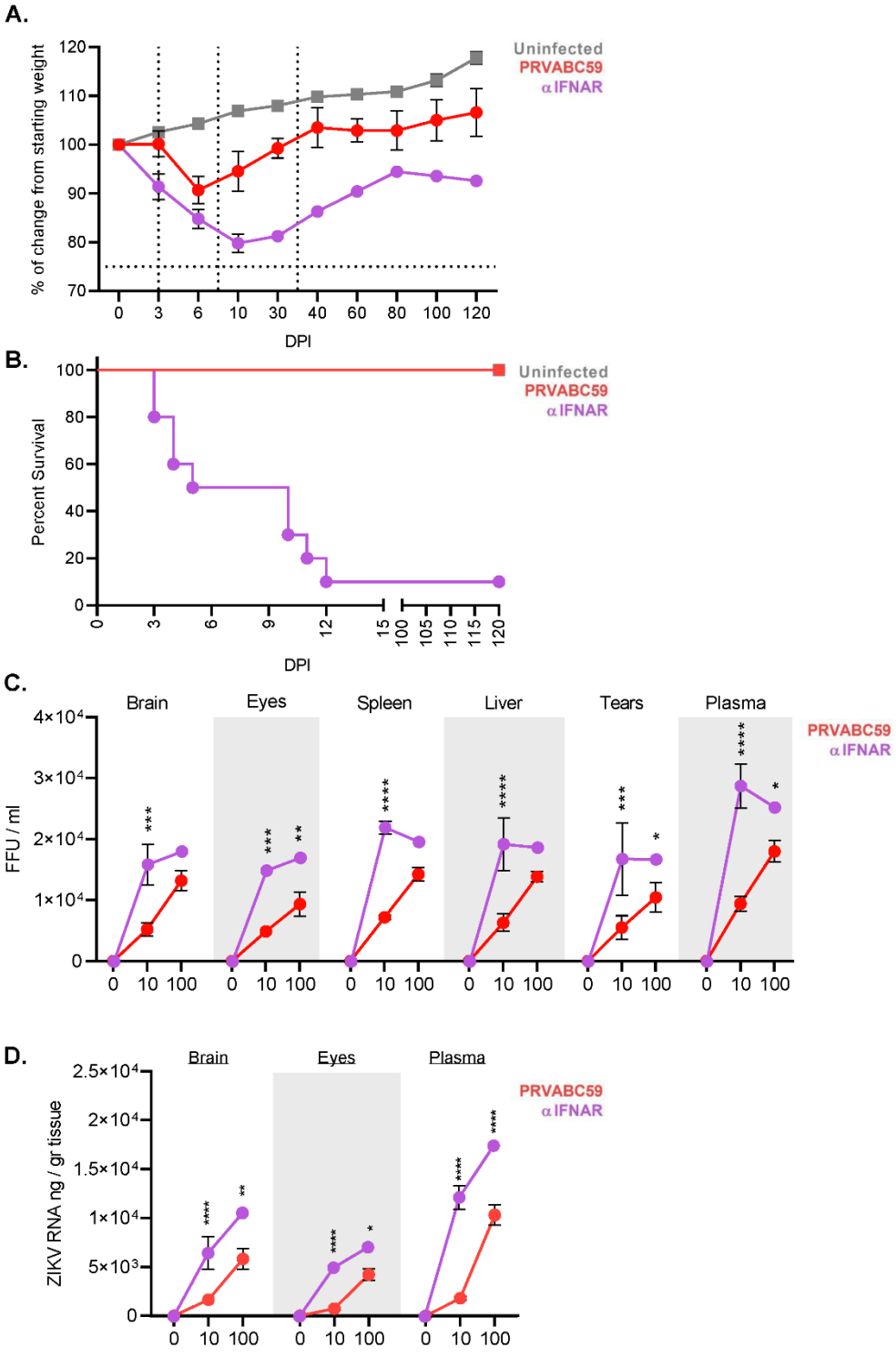
A.
% of change from starting weight
120
110
100
90
80
70
0 3 6 10 30 40 60 80 100 120
DPI
Uninfected
PRVABC59
αIFNAR
B.
Percent Survival
100
80
60
40
20
0
0 3 6 9 12 15 100 105 110 115 120
DPI
Uninfected
PRVABC59
αIFNAR
C.
Brain
Eyes
Spleen
Liver
Tears
Plasma
FFU / ml
4×10⁴
3×10⁴
2×10⁴
1×10⁴
0
0 10 100
PRVABC59
αIFNAR
D.
Brain
Eyes
Plasma
ZIKV RNA ng / gr tissue
2.5×10⁴
2×10⁴
1.5×10⁴
1×10⁴
5×10³
0
0 10 100
PRVABC59
αIFNAR

Figure 1. PRVABC59 can infect systemic and privileged organs in immunocompetent mice. (A) Body weight changes were monitored for 120 DPI. (N=10). PRVABC59 infected mice were immunocompetent, while mice denoted as αIFNAR (anti-IFNAR) received a single administration of monoclonal antibody that functionally blocks IFNAR signaling 24 hours prior to infection. The N for αIFNAR mice decreased from 10 to 5 between 3 and 6 DPI, and further decreased from 5 to 1 between 10 and 30 DPI. These loses are denoted by vertical lines. The horizontal dotted line represents lethal weight loss endpoint. (B) Survival of mice infected with ZIKV with and without prior administration of αIFNAR mAB. (C-D) Active viral replication was determined by infectious co-culture (C) at 0, 10, and 100 DPI. Total ZIKV genomic RNA was quantified by qRT-PCR (D; N=5) at 0, 10, and 100 DPI. For panels C and D, N=3 at 0 and 3 DPI, and for PRVABC59 group at 100 DPI. N=1 for αIFNAR at 100 DPI. All error bars in all panels reflect Standard Deviation. Data was analyzed by Two-way ANOVA using Sidak post-hoc correction. For all panels, * is $p<0.05$, ** is $p<0.01$, *** is $p<0.001$, and **** is $p<0.0001$.

FIGURE 2

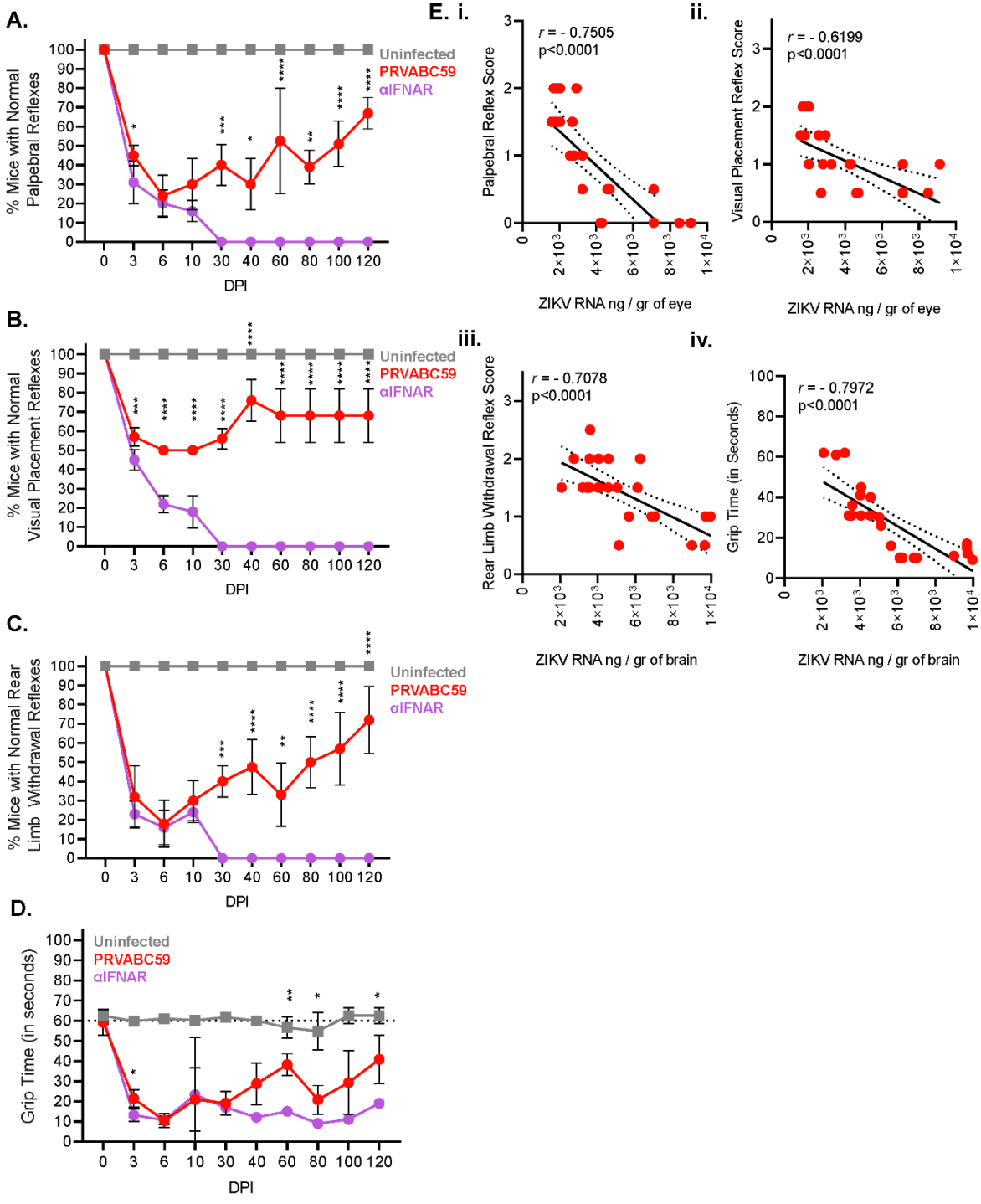
A.
% Mice with Normal Palpebral Reflexes
Uninfected
PRVABC59
αIFNAR
DPI
B.
% Mice with Normal Visual Placement Reflexes
C.
% Mice with Normal Rear Limb Withdrawal Reflexes
D.
Grip Time (in seconds)
E. i.
Palpebral Reflex Score
r = - 0.7505
p<0.0001
ZIKV RNA ng / gr of eye
ii.
Visual Placement Reflex Score
r = - 0.6199
p<0.0001
ZIKV RNA ng / gr of eye
iii.
Rear Limb Withdrawal Reflex Score
r = - 0.7078
p<0.0001
ZIKV RNA ng / gr of brain
iv.
Grip Time (in Seconds)
r = - 0.7972
p<0.0001
ZIKV RNA ng / gr of brain

Figure 2. Competent mice infected with ZIKV-PRVABC59 demonstrate distinct ocular and motor/neural symptomatology that correlate with viral load.

Ocular clinical scores were determined via palpebral (A) and visual placement (B) reflexes. (Two-way ANOVA with Bonferroni's post-hoc correction; N=10). Motor/neural clinical scores were evaluated by rear-limb withdrawal reflex tests (C) and by grip time tests (D). The dotted line among grip time tests indicates the standard time a healthy animal should endure test conditions. (Two-way ANOVA with Bonferroni's post-hoc correction; N=10). (E) Symptom severity and viral load at 100 DPI in the affected tissue were analyzed by Pearson's test to determine potential correlations for palpebral (i), visual placement (ii), and rear limb withdrawal reflexes (iii) and for grip time tests (iv). Dashed lines represent 95% confidence interval bands; Pearson's correlation coefficient and p-values are listed for each graph. All correlation analyses used infectious and symptom data (N=25). For all panels, * is $p<0.05$, ** is $p<0.01$, *** is $p<0.001$, and **** is $p<0.0001$. All error bars in all panels reflect standard deviation.

FIGURE 3

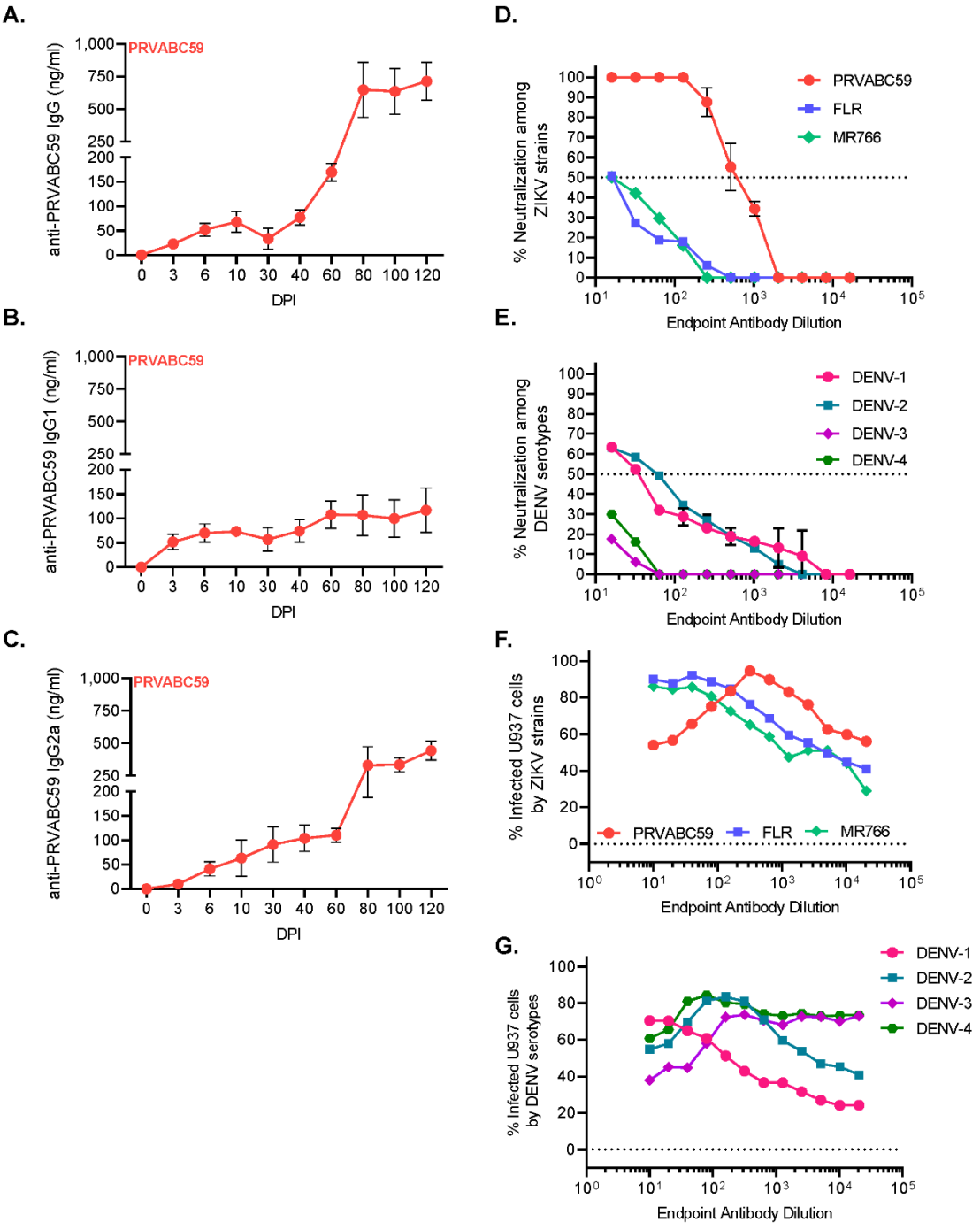
A.
anti-PRVABC59 IgG (ng/ml)
PRVABC59
DPI
B.
anti-PRVABC59 IgG1 (ng/ml)
PRVABC59
DPI
C.
anti-PRVABC59 IgG2a (ng/ml)
PRVABC59
DPI
D.
% Neutralization among ZIKV strains
PRVABC59
FLR
MR766
Endpoint Antibody Dilution
E.
% Neutralization among DENV serotypes
DENV-1
DENV-2
DENV-3
DENV-4
Endpoint Antibody Dilution
F.
% Infected U937 cells by ZIKV strains
PRVABC59
FLR
MR766
Endpoint Antibody Dilution
G.
% Infected U937 cells by DENV serotypes
DENV-1
DENV-2
DENV-3
DENV-4
Endpoint Antibody Dilution

Figure 3. PRVABC59-induced antibodies are weakly neutralizing and enhance non-homologous infection.

Antibody kinetics for IgG total (A), IgG1 (B), and IgG2a (C) that are specific to PRVABC59 were determined up to 120 DPI via ELISA using whole, inactivated virus particles. (N=5). (D-E) Antibody neutralization was evaluated by determining the endpoint antibody titer necessary to neutralize 50% of live virus (IC50) among homologous and non-homologous ZIKV strains (D; N=5) and a representative strain from all four DENV serotypes (E; N=5). The horizontal line indicates when 50% of live virus has been neutralized. (F-G) Antibody-mediated infection was evaluated among homologous and non-homologous ZIKV strains (F) and a representative strain from all four DENV serotypes (G; N=5). Background fluorescence, denoted by the horizontal dotted line, was determined by combining virus, no antibody sample, and cells. All error bars in all panels reflect standard deviation.

FIGURE 4

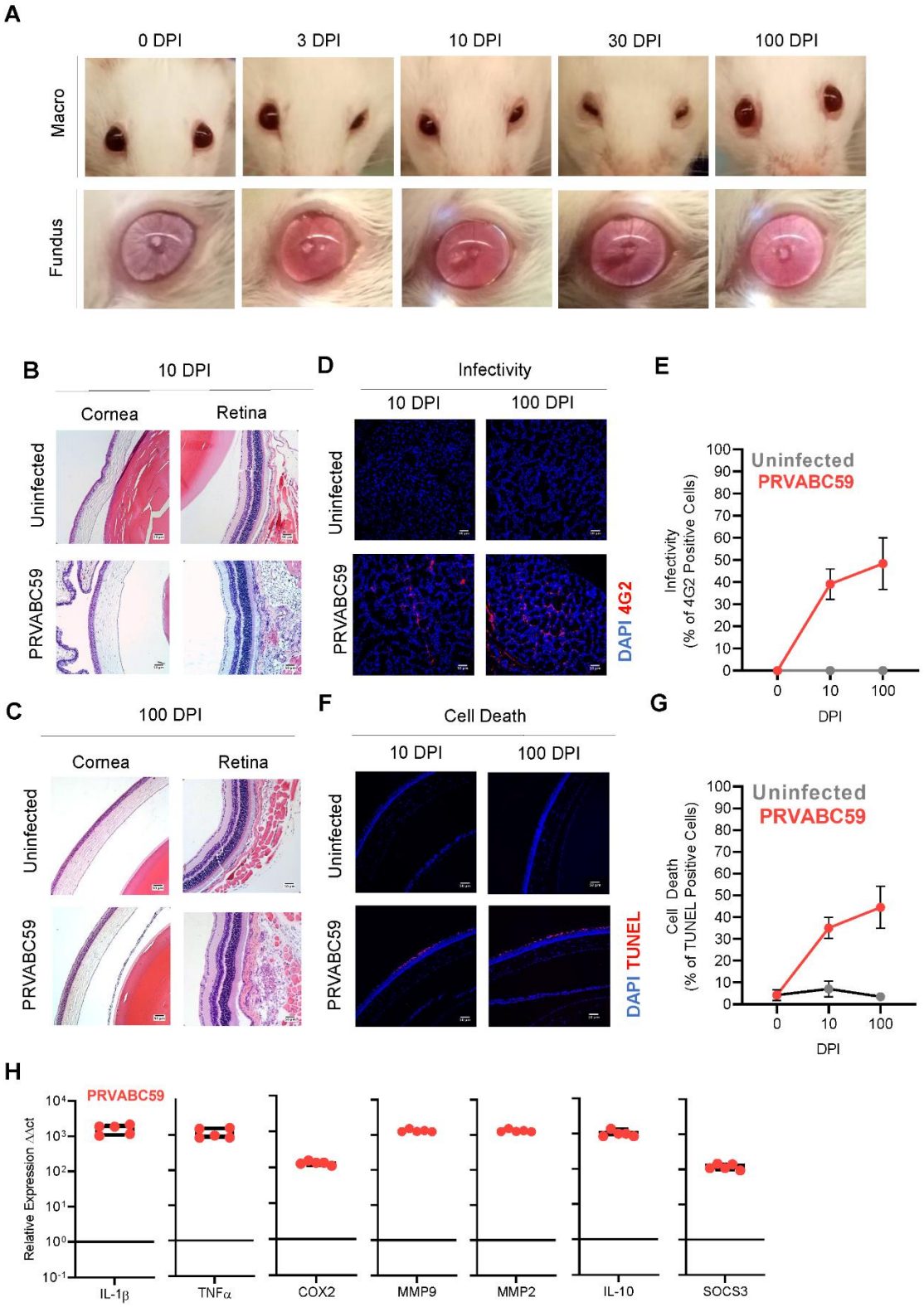
A
0 DPI
3 DPI
10 DPI
30 DPI
100 DPI
Macro
Fundus
B
10 DPI
Cornea
Retina
Uninfected
PRVABC59
C
100 DPI
Cornea
Retina
Uninfected
PRVABC59
D
Infectivity
10 DPI
100 DPI
Uninfected
PRVABC59
DAPI 4G2
E
Uninfected
PRVABC59
Infectivity
(% of 4G2 Positive Cells)
DPI
F
Cell Death
10 DPI
100 DPI
Uninfected
PRVABC59
DAPI TUNEL
G
Uninfected
PRVABC59
Cell Death
(% of TUNEL Positive Cells)
DPI
H
PRVABC59
Relative Expression ΔΔct
IL-1β
TNFα
COX2
MMP9
MMP2
IL-10
SOCS3

Figure 4. Tenacious corneal and retinal hyperplasia coincides with persistent ocular infection, increasing levels of cell death, and chronic inflammation.

(A) Macroscopic (top) and fundus (bottom) imaging was done at 0, 3, 10, 30, and 100 DPI to visualize ocular pathology. (B-C) Eyes from infected and uninfected mice were harvested 10 (B) and 100 (C) DPI for H&E and immunofluorescent staining. H&E images of corneal and retinal layers were taken at 20x to assess pathology. (D-E) ZIKV infectivity was determined by immunofluorescent staining for flavivirus antigens (Two-way ANOVA with Bonferroni's post-hoc; N=10). (F-G) Similarly, TUNEL staining for cell death was performed at 10 and 100 DPI (Two-way ANOVA with Bonferroni's post-hoc; N=10). (G) qRT-PCR on pro-inflammatory proteins, pain mediators, MMPs, and anti-inflammatory proteins among infected brains were normalized to GAPDH and then to expression levels of uninfected controls using the ΔΔCt method (N=5). For all panels, * is $p<0.05$, ** is $p<0.01$, *** is $p<0.001$, and **** is $p<0.0001$. All error bars in all panels reflect standard deviation.

FIGURE 5

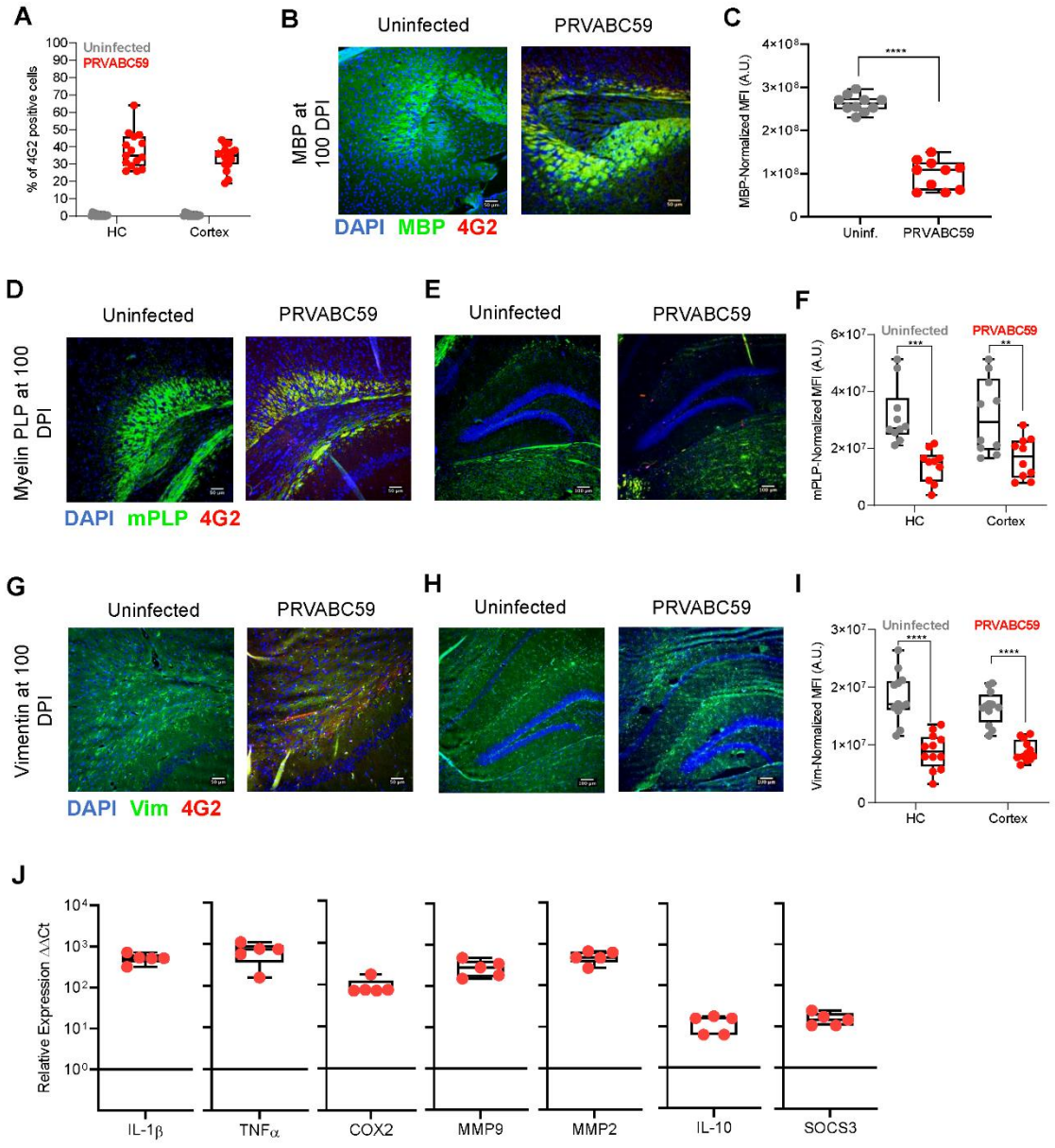
A
Uninfected
PRVABC59
% of 4G2 positive cells
HC
Cortex
B
Uninfected
PRVABC59
MBP at 100 DPI
DAPI MBP 4G2
C
MBP-Normalized MFI (A.U.)
****
Uninf.
PRVABC59
D
Uninfected
PRVABC59
Myelin PLP at 100 DPI
DAPI mPLP 4G2
E
Uninfected
PRVABC59
F
mPLP-Normalized MFI (A.U.)
Uninfected
PRVABC59
***
**
HC
Cortex
G
Uninfected
PRVABC59
Vimentin at 100 DPI
DAPI Vim 4G2
H
Uninfected
PRVABC59
I
Vim-Normalized MFI (A.U.)
Uninfected
PRVABC59
****
****
HC
Cortex
J
Relative Expression ΔΔCt
IL-1β
TNFα
COX2
MMP9
MMP2
IL-10
SOCS3

Figure 5. PRVABC59 infection in the hippocampus and cortex corresponds to decreased levels of myelin and persistent inflammation.

(A) Brains were sectioned and stained for ZIKV antigen 100 DPI. Foci were counted in hippocampal (HC) and cortical regions (N=15). (B-C) MBP expression was determined by immunofluorescent staining in mid-brain cortex regions of mice (B), expression was normalized to background using the CTCF calculation and is presented as normalized MFI (C; student's t-test; N=10). (D-F) mPLP expression among mid-brain sections was normalized to background using the CTCF calculation and is presented as normalized MFI in both hippocampus and cortex regions (Two-way ANOVA with Bonferroni's post-hoc analysis; N=10). (G-I) Vim expression was similarly quantified among hippocampus and cortex regions from infected mice. (Two-way ANOVA with Bonferroni's post-hoc analysis; N=10). (J) qRT-PCR on pro-inflammatory proteins, pain mediators, MMPs, and anti-inflammatory proteins among infected brains were normalized to GAPDH and then to expression levels of uninfected controls using the ΔΔCt method (N=5). For all panels, * is $p<0.05$, ** is $p<0.01$, *** is $p<0.001$, and **** is $p<0.0001$. All error bars in all panels reflect standard deviation.

FIGURE 6

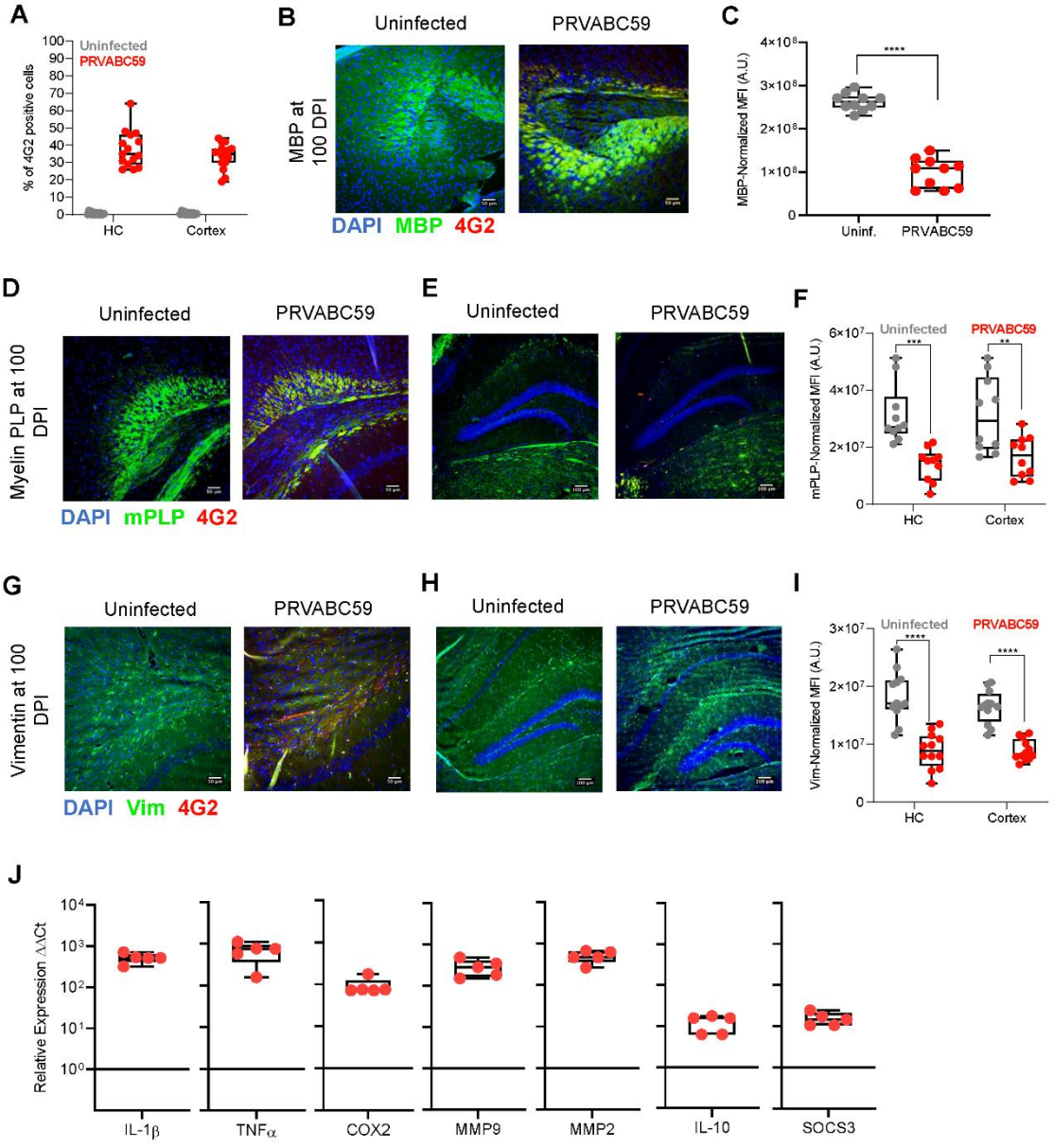
A
Uninfected
PRVABC59
% of 4G2 positive cells
HC
Cortex
B
Uninfected
PRVABC59
MBP at 100 DPI
DAPI MBP 4G2
C
MBP-Normalized MFI (A.U.)
****
Uninf.
PRVABC59
D
Uninfected
PRVABC59
Myelin PLP at 100 DPI
DAPI mPLP 4G2
E
Uninfected
PRVABC59
F
mPLP-Normalized MFI (A.U.)
Uninfected
PRVABC59
***
**
HC
Cortex
G
Uninfected
PRVABC59
Vimentin at 100 DPI
DAPI Vim 4G2
H
Uninfected
PRVABC59
I
Vim-Normalized MFI (A.U.)
Uninfected
PRVABC59
****
****
HC
Cortex
J
Relative Expression ΔΔCt
IL-1β
TNFα
COX2
MMP9
MMP2
IL-10
SOCS3

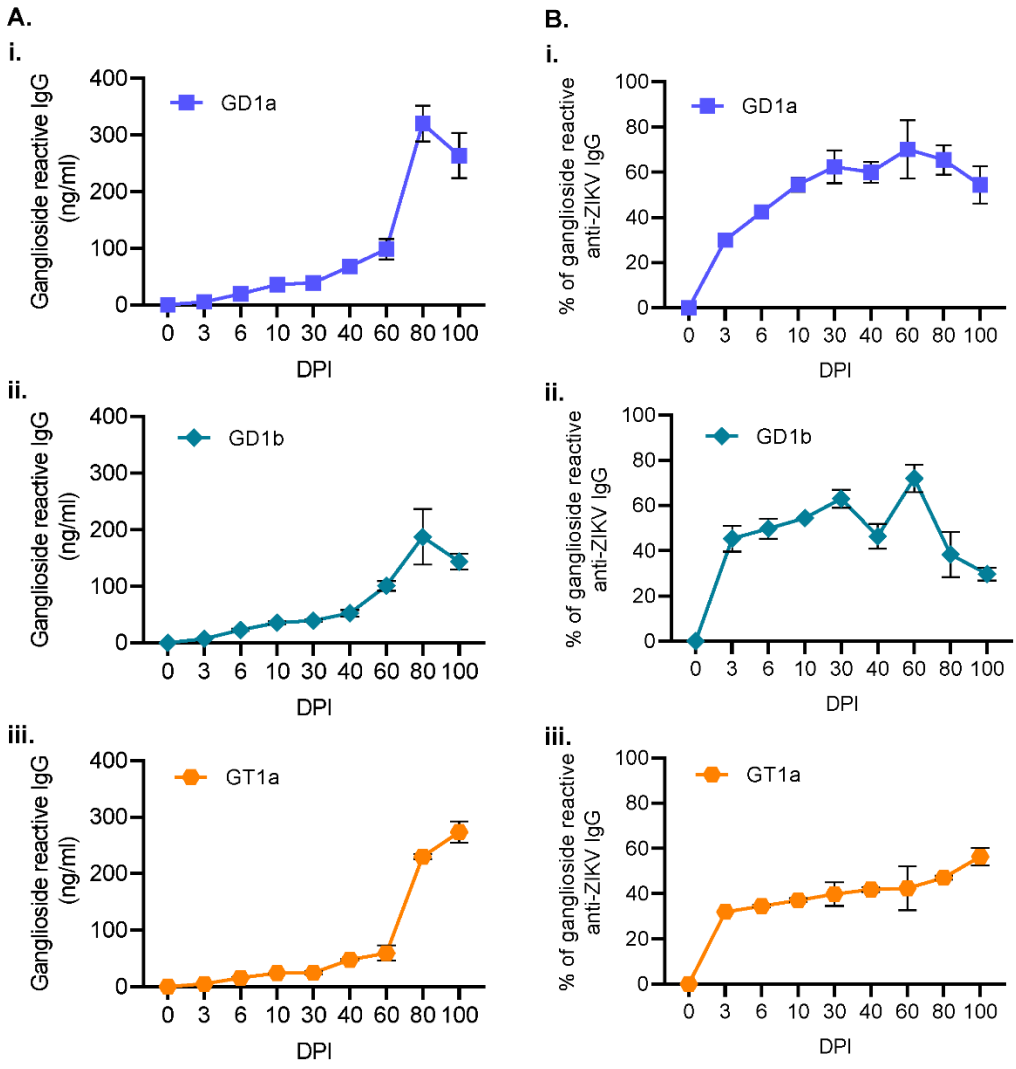

Figure 6. IgG produced during ZIKV infection are cross-reactive to host gangliosides. Antibodies generated during ZIKV infection were also evaluated for their reactivity to GD1a, GD1a, and GT1a gangliosides (Ai, ii, and iii, respectively) via ELISA. The proportion of ganglioside-reactive antibodies to ZIKV-specific IgG was then determined for 0, 3, 10, 60, 80, and 100 DPI. (N=5). All error bars in all panels reflect standard deviation.

SUPPLEMENTARY FIGURE 1

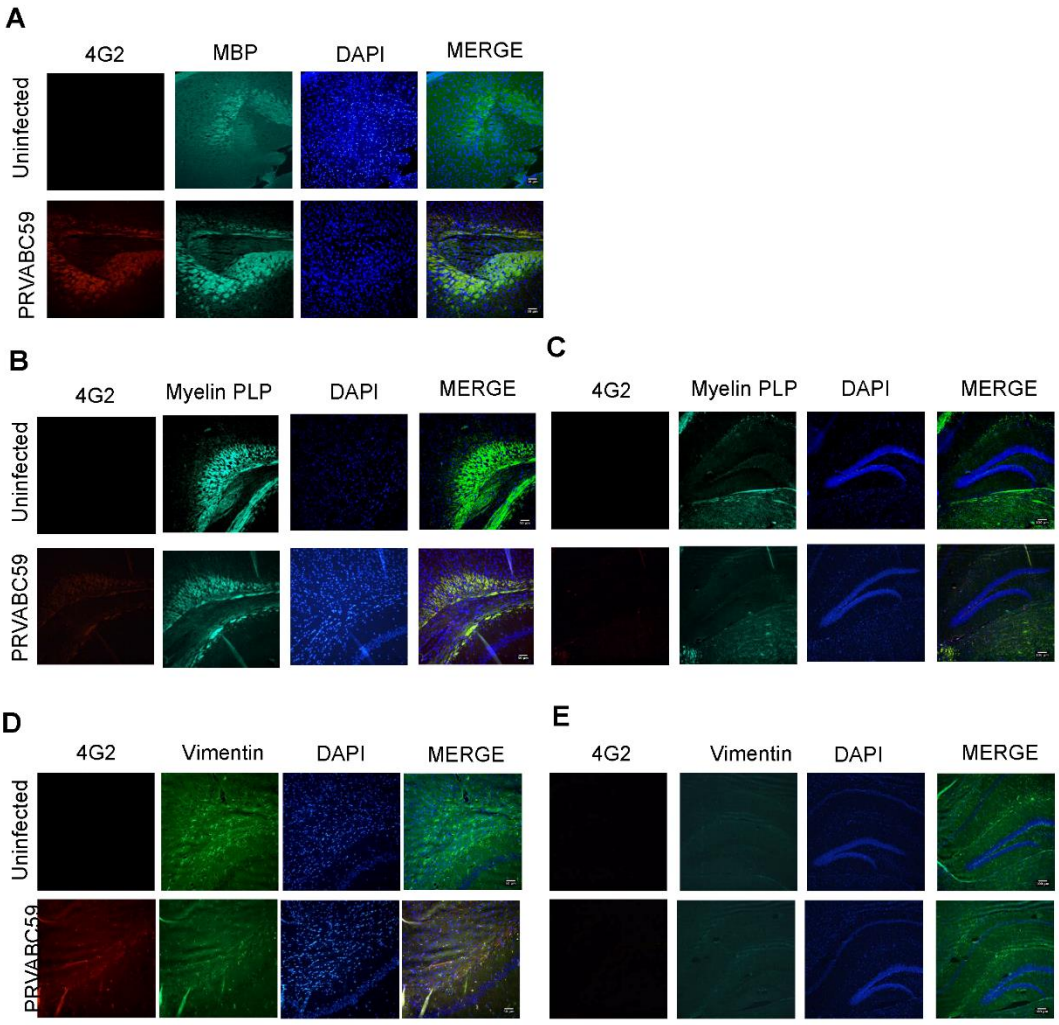

Supplementary Fig 1. ZIKV-PRVABC59 demyelinates cortex and hippocampus.

(A) Individual fluorescent panels show MBP expression in cortex regions of infected animals 100 DPI. Images were taken at 20x magnification with a scale-bar of 100 μm (bottom right corner). (B-C) Individual fluorescent panels show myelin PLP expression in cortex (B) and hippocampus (C) regions of infected animals 100 DPI. Images were taken at 20x magnification with a scale-bar of 100 μm (bottom right corner). (D-E) Individual fluorescent panels show vimentin expression in cortex (D) and hippocampus (E) regions of infected animals 100 DPI. All images were stained with DAPI (blue); MBP, myelin PLP, or vimentin (green); and the ZIKV E-protein via 4G2 (red). Images were taken at 20x magnification with a scale-bar of 100 μm (bottom right corner).

SUPPLEMENTARY FIGURE 2

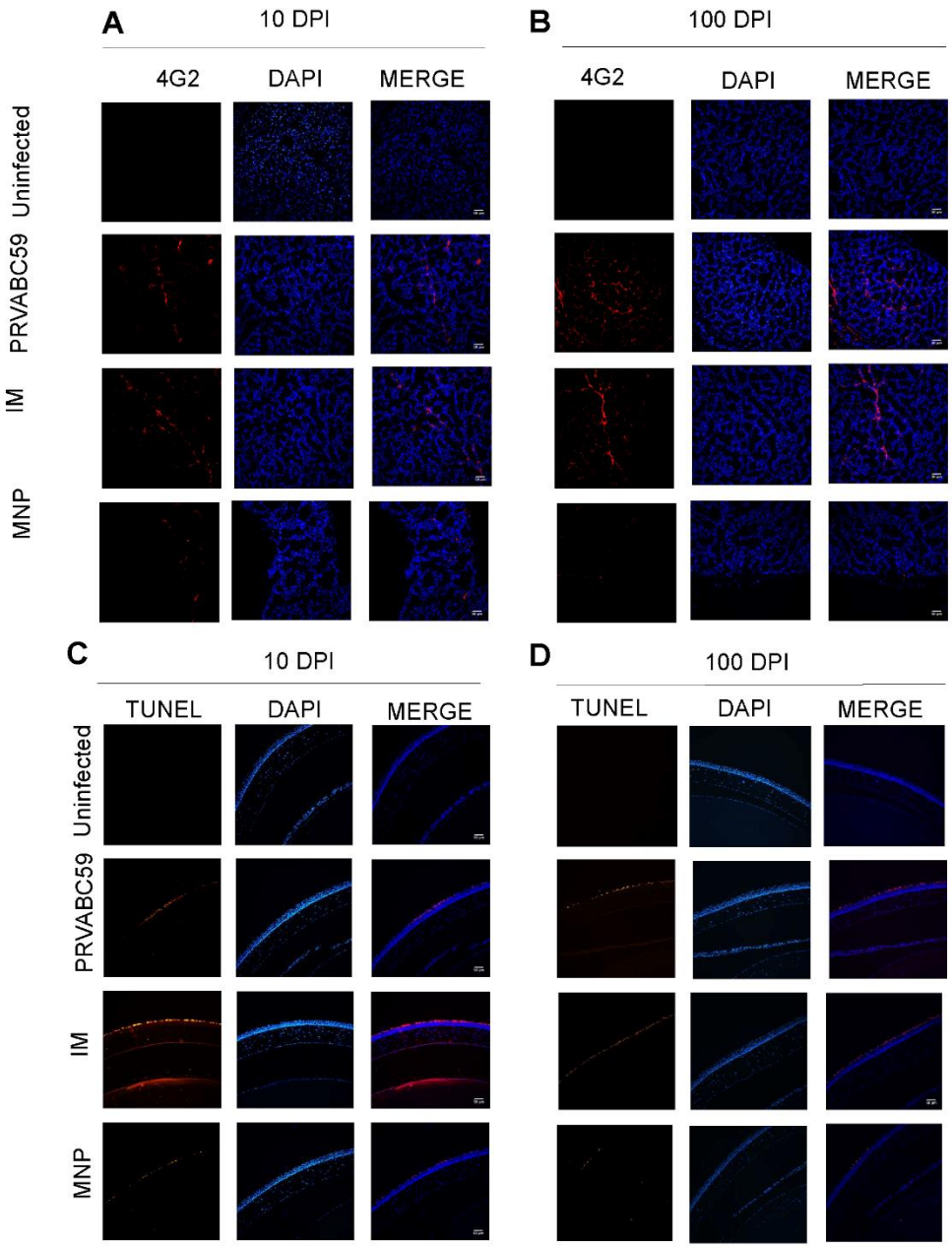

Supplementary Fig 2. Intraocular infection increases apoptosis and necroptosis.

(A-B) Infectivity among eye tissues was determined via 4G2 immunofluorescent labeling of ZIKV E-protein in cells at 10 (A) and 100 (B) DPI. Individual panels show 4G2 ZIKV-antigen in red,

DAPI in blue, and a final merge. (C-D) Immunofluorescent cell death was determined via TUNEL stain for fragmented DNA at 10 (C) and 100 (D) DPI. Individual panels show TUNEL-positive cells in red, DAPI in blue, and a final merge. Images were taken at 20x magnification with a scale-bar of 100 μm (bottom right corner).

CHAPTER III : CUTANEOUS VACCINATION AMELIORATES ZIKA VIRUS-INDUCED NEURO-OCULAR PATHOLOGY VIA REDUCTION OF ANTI-GANGLIOSIDE ANTIBODIES

Jacob T. Beaver*[1], Lisa K. Mills[1], Dominika Swieboda[1], Nadia Lelutiu[1], Edward S. Esser[1], Olivia Q. Antao[1], Eugenia Scountzou[3], Dahnide T. Williams[1], Nikolaos Papaioannou[4], Elizabeth Q. Littauer[1], Andrey Romanyuk[2], Richard W. Compans[1], Mark R. Prausnitz[2], and Ioanna Skountzou[1,#]

[1]Department of Microbiology & Immunology, Emory University School of Medicine, Atlanta, GA, 30322, USA

[2] School of Chemical and Biomolecular Engineering, Georgia Institute of Technology, Atlanta, GA, 30332, USA

[3]EyeVetSurgery-Small Animal Clinic, Athens, 15561, Greece

[4] Faculty of Veterinary Medicine, Laboratory of Pathologic Anatomy, Aristotle University of Thessaloniki, 54124, Greece

Accepted May 23, 2020. Published August 6, 2020.

DOI: 10.1080/21645515.2020.1775460

Running Title: Cutaneous vaccination ameliorates ZIKV-induced autoantibodies.

#Address correspondence to Ioanna Skountzou: iskount@emory.edu

* First Author

ABSTRACT

Zika virus (ZIKV) causes moderate to severe neuro-ocular sequelae, with symptoms ranging from conjunctivitis to Guillain-Barré Syndrome (GBS). Despite the international threat ZIKV poses, no licensed vaccine exists. As ZIKV and DENV are closely related, antibodies against one virus have demonstrated the ability to enhance the other. To examine if vaccination can confer robust, long-term protection against ZIKV, preventing neuro-ocular pathology and long-term inflammation in immune-privileged compartments, BALB/c mice received two doses of unadjuvanted inactivated whole ZIKV vaccine (ZVIP) intramuscularly (IM) or cutaneously with dissolving microneedle patches (MNP). MNP immunization induced significantly higher B and T cell responses compared to IM vaccination, resulting in increased antibody titers with greater avidity for ZPIV as well as increased numbers of IFN-γ, TNF-α, IL-2 and IL-4 secreting T cells. When compared to IM vaccination, antibodies generated by cutaneous vaccination demonstrated greater neutralization activity, increased cross-reactivity with Asian and African lineage ZIKV strains (PRVABC59, FLR, and MR766) and Dengue virus (DENV) serotypes, limited ADE, and lower reactivity to GBS-associated gangliosides. MNP vaccination effectively controlled viremia and inflammation, preventing neuro-ocular pathology. Conversely, IM vaccination exacerbated ocular pathology, resulting in uncontrolled, long-term inflammation. Importantly, neuro-ocular pathology correlated with anti-ganglioside antibodies implicated in demyelination and GBS. This study highlights the importance of longevity studies in ZIKV immunization, and the need of exploring alternative vaccination platforms to improve the quality of vaccine-induced immune responses.

INTRODUCTION

The most severe consequence of adult Zika virus (ZIKV) infection is Guillain-Barré syndrome (GBS), a disease attacking peripheral nerves that can result in permanent neuro-ocular damage, such as macular degeneration (20, 56, 181). As ZIKV and other flaviviruses persist up to 6 months in immune-privileged tissues such as brain, eyes, and genitals, these organs present a crucial focus for ZIKV vaccination research (63, 185, 186). Indeed, ZIKV infections are spread via multiple modes of transmission; transplacentally to developing fetuses, via breastfeeding to infants, and through sex, or mosquito bite. Infants that acquire ZIKV often present congenital Zika syndrome (CZS), with impaired visual and neurological development. Most notable among these is microcephaly; however, recent reports note instances of neuro-ocular pathology among infants independent of microcephaly (182, 183). The multi-modal transmission of ZIKV, coupled with its long-term persistence and impact on brain and eyes, underlies the importance of developing an effective vaccine with potential for worldwide distribution.

The production of autoantibodies in GBS leads to enhanced tissue pathology and clinical symptomatology. As such, progressive paralysis of one or more limbs culminating in hyporeflexia or areflexia are diagnostic hallmarks of GBS, and can be fully manifested within 4 weeks (188). While other pathogens implicated in GBS, such as *Campylobacter jejuni,* develop pathology after pathogen clearance, ZIKV-induced GBS is initiated during infection (189-191). Long-term demyelination of CNS tissues and chronic neuroinflammation is common among GBS patients, and have been linked to T cell infiltration into these tissues (192, 193). However, there is limited knowledge on the putative role of ZIKV-specific antibodies in initiating or sustaining neuro-ocular symptoms and the role that vaccination may play in their development.

Several publications have demonstrated the specific role of T cells in mediating brain pathology, such as synaptic degradation (192), and detailed the role of retinal epithelial cells in maintaining ocular immune-privilege via blood-barrier integrity (95, 99). These studies often rely on a combination of human primary cell cultures and different mouse models. As flavivirus pathology is intricately linked to the host type I and type III interferon (IFN) response, many studies rely on short term observations in wild-type (WT) animals or utilize immunocompromised animals to generate extreme pathology. For example, Singh et al. provided a thorough transcriptional analysis of cellular responses after intra-ocular injection of ZIKV into either WT or ISG15 deficient C57BL/6 mice and demonstrated the rapid induction of inflammation in retinal cells (95). This inflammation corresponded to retinal lesions within WT mice that persisted up to 96 hours after infection. Despite evidence that ZIKV-induced neuro-ocular pathology develops in a variety of murine models, few studies seek to evaluate the synergy between this pathology and humoral immune responses following vaccination.

There are at least 29 ZIKV vaccine candidates in various stages of clinical trials, with 45% of US-based candidates utilizing Zika virus inactivated particles (ZVIP) (173, 241-244) in conjunction with adjuvants, administered subcutaneously (SC) or intramuscularly (IM)(179, 245). These candidates are often are co-administered with an alum adjuvant (242-244). In this study, we generated a Zika virus inactivated particle (ZVIP) vaccine using the Asian lineage PRVABC59 strain and implemented investigated two routes of delivery,: IM and or cutaneous with dissolving polymer microneedle patches (MNP) encapsulating the vaccine (246-248). By targeting the cutaneous vaccine to epidermal keratinocytes, Langerhans cells, and dermal dendritic cells, we aimed to mobilize unique immunological mechanisms and signaling pathways from the vaccination site to draining lymph nodes, enhancing ZIKV-specific B and T cell responses (249,

250). We have previously demonstrated that MNP immunization confers superior immune responses compared to conventional IM vaccination in adult BALB/c mice (251, 252), and in high-risk populations (253). Hence, we considered the MNP approach as more effective for a mosquito-borne infection because epithelial cells are early ZIKV infection targets (254) and protection can be conferred using skin-resident memory T cells (255).

MNP immunization with ZVIP was juxtaposed to IM immunization to test our hypothesis whether vaccine delivery via the skin can induce potent, long-lasting, and broadly protective immune responses using an immunocompetent BALB/c mouse model. This strain was selected over C57BL/6 mice for its ability to generate robust humoral responses in vaccination studies and for the less invasive approach to generate neuro-ocular symptoms; while BALB/c mice can present pathology of these compartments following intravenous infection with ZIKV, C57BL/6 mice require intracranial injection in order to achieve similar ZIKV neuro-ocular pathology(197). Here, we seek to build on existing vaccine candidates by using a prime-boost administration approach to investigate kinetics, magnitude, and quality of immune responses, evaluate if vaccination confers robust protection against infectious challenge, and to correlate reductions in auto-reactive antibodies and neuro-ocular pathology with vaccination routes.

METHODS AND MATERIALS

Cells and virus stocks

Vero cells (ATCC, CCL-81) for virus propagation and titration were maintained in DMEM (Mediatech, 10-013-CV) containing 10% fetal bovine serum (FBS; Hyclone, Thermo Scientific, SH3007103), HEPES (Corning, H3537) and 1% Penicillin/Streptomycin (Corning, 30-002-CI). ZIKV stocks were generated from the African lineage Uganda strain (MR766, B.E.I. resources,

NR-50085) and the Asian lineage, Caribbean isolate from Puerto Rico (PRVABC59, generously provided by Dr. Scott Michael and Dr. Sharon Isern at Florida Gulf Coast University). The FLR strain from Colombia was obtained from B.E.I (B.E.I. resources, NR-50183). Resources. Dengue virus strains (DENV1/Hawaii/1944, DENV2/16681/Thailand/1964, DENV3/H87/Philippines/1956, and DENV4/UNC4019/ Colombia/2006) were generously provided by Dr. Joshy Jacob of Emory University. All viruses were propagated in Vero cells for 7 days at 37°C. After the tenth passage, culture supernatants were collected and cell debris was cleared by centrifugation at 3,000xg for 10 minutes at 4°C. Viral harvest was then filtered using 0.22-micron filters (Sigma, Z741966). Culture supernatants were concentrated using Amicon centrifugal concentration filters (EMD Millipore, C7715) by centrifugation at 4,000xg for 30 minutes. As the ZIKV virion is approximately 50 nm in diameter, we used the 100 NMWL variant filters to maximize the recovery. Finally, viral supernatants were purified by discontinuous 20-60% sucrose gradient, where they were diluted 1:5 with FBS before final storage at -80°C (198).

Virus titration

Viral stocks were titrated by plaque assay performed in Vero cells as previously described (199). Focus-forming assays were performed as previously described (200). Blue foci were counted, and titers were calculated by foci numbers in infectious volume (# of foci x infectious volume x conversion factor to ml x dilution factor). FFU and PFU are equivalent in that both are quantification methods. In this study, PFU assays and FFU assays resulted in similar titers.

Trans-well Focus-Forming Assay: To evaluate if live virus can be isolated from systemic and privileged tissues and bodily fluids, we adapted a trans-well infectious system similar to a monocyte chemotaxis assay used for Japanese Encephalitis Virus (201). Tissue homogenates and

cell suspensions were then added onto 0.4µm trans-well insert systems (Corning, CLS3396) overtop sterile Vero cells. Live virus released from cells in contact with the insert filtered through the membrane to infect permissive Vero cells below to provide a measure of tissue-specific live viral load as opposed to quantifying the amount of vRNA present in tissues.

Vaccine preparation

ZIKV-PRVABC59 stocks were prepared as detailed above and were titrated with plaque assay and FFA (199). Viral stocks were inactivated with 0.04% formalin for 7 days at 22^{o}C and subjected to membrane dialysis (164) to remove formalin (175). Stocks were then tested for successful inactivation by plaque assay and FFA in Vero cells.

ZIKV incorporation into MNP

MNPs were fabricated and underwent quality control testing as previously described (256). Briefly, MNPs containing the vaccine were dissolved in PBS, ran on a 10% SDS-PAGE gel and immune-stained with anti-ZIKV E-protein antibody (EMD Millipore, MAB10216) in order to visualize protein bands and to determine successful incorporation of the inactivated virus. MNPs were fabricated in a two-step process with polydimethylsiloxane (PDMS) molds as previously described (257). MNPs were prepared by sequentially casting the first-cast solution to fill the mold cavities and the second-cast solution to cover the mold surface (corresponding to the MNP patch backing). The MN patches were removed from the molds and attached to adhesive paper discs. Patches were inspected via light microscopy for integrity and uniformity

Animal strains and housing

Female BALB/c mice (Charles River Laboratories) were housed in a biosafety level 1 facility at Emory University's Division of Animal Resources and viral infection experiments were performed on animals housed in a Biosafety Level 3 facility at Emory University's Division of Animal Resources. All experiments were conducted in accordance with protocols (DAR2002950-122617BN) approved by Emory University's Institutional Animal Care and Use Committee (IACUC) and in accordance with guidelines with the United States Federal Animal Welfare Act (PL 89-544) and subsequent amendments. At the time of vaccination, mice were 5-6 weeks old.

Vaccination protocol

BALB/c mice were vaccinated with 4μg of whole, inactivated ZIKV. Vaccine was administered via MNP (258) or IM injections using a prime-boost vaccination schedule. Mice were anesthetized using a ketamine/xylazine cocktail, and MNP patches were administered to the caudal side of the dorsum using direct pressure for 1 minute, and then left for 20 minutes (249). Thirty days after prime vaccination, mice received an identical booster immunization, and were then infected 30 days later. Antibody kinetics were performed on days 7 and 30 post-prime vaccination, and again on days 7, 14 and 30 post-booster vaccination.

Animal infection, tissue and biological fluid sampling

Mice were infected with $1x10^6$ FFU of ZIKV-PR virus intravenously (IV) (202). Serum or platelet-poor plasma (PPP) was collected 0, 3, 6, 10, 30, 40, 60, 80, 100, and 120 days post-challenge; plasma was collected in citrate buffer and stored at -20^{o}C until use. Small groups of mice were euthanized at 10 and 100 DPI. Tissues were collected and processed for histology, homogenized

in protease inhibitors and RNase inhibitors (ThermoFisher Scientific, Waltham, MA) for infectivity and qRT-PCR studies. In the remaining mice, tears were collected via PBS gavage 100 DPI and after euthanasia. Tissues (brain, eyes, genital organs, liver and spleen) were collected and processed for infectivity experiments, histology, and inflammatory markers. Ocular tissues were not perfused prior to harvest to avoid structural and cellular changes induced by the perfusion process (203), as functional morphology of the retina correlates directly with fluid pressure in the choroid. For both FFA and qRT-PCR quantification methods, tissues were homogenized after mincing and passaged through 40µm cell strainers (Fisher Scientific, 08-771-1). They were further digested with 1 mg/ml of Collagenase IV (Worthington, LS004189) for 30 minutes at 37°C, and the purified through 40µm cell strainers. Homogenates were separated using a Percoll (Millipore Sigma, P1644) density gradient (204, 205), and cell suspensions were isolated for qRT-PCR and FFA trans-well studies. One eye from each animal was used for FFA and qRT-PCR experiments, and the other was used for tissue sectioning for microscopy studies.

RNA isolation and qRT-PCR

Total RNA was extracted from tissues using Trizol (Ambion, 15596018). Tissues were homogenized into Trizol reagent using the FastPrep-24 5G homogenizer (MP Biomedicals). Total RNA was isolated using the PureLink RNA mini-kit (Ambion, 12183025). Purified RNA was quantified, checked for quality assurance via NanoDrop Spectrometry (ThermoFisher, ND200), and then reverse transcribed with the qScript Reverse Transcription kit (QuantaBio, 95047). For quantification of vRNA, a standard curve was generated using 10-fold serial dilutions of ZIKV RNA standard. qRT-PCR for ZIKV prM-E was performed with TaqMan Gene Expression Master Mix, ZIKV Primers, and probe as previously described (207). The standard curve had an R^2 value

greater than 0.99. vRNA copies were interpolated from the standard curve using the average Ct value obtained from samples run in triplicate. qRT-PCR for GAPDH, IL-1β, TNF-α, IL-10, SOCS3, MMP2, MMP9, and COX2 were performed with PerfeCTa SYBR Green SuperMix Low Rox (Quantabio, #95056-500). Primers for GAPDH, IL-1 β, TNF- α, IL-10, SOCS3, and COX2 were as previously described (208). MMP2 primers were as follows; forward 5'-AACGGTCGGGAATACAGCAG-3'; reverse 5'-GTAAACAAGGCTTCATGGGGG-3'. MMP9 primers were as follows; forward 5'-AACCTCCAACCTCACGGACA-3'; reverse 5'-AGGTTTGGAATCGACCCACG-3'. Data was analyzed using the ΔΔCt method to determine normalized relative expression.

Ocular and Brain Symptomatology

At the same time points of blood collection post-infection, animals were assessed for ocular and motor/neural symptomatology. Behavioral tests to characterize pathogenesis in our mouse model were adapted from the Department of Molecular & Comparative Pathobiology's 2015 Lab Manual from Johns Hopkins University School of Medicine (209). These assessments were identified and further researched with the explicit aim to evaluate visual and motor function following ZIKV infection.

Visual Placement Reflex: A reaching reflex test, or visual placement assessment measures optic function and can also potentially indicate inflammation in parietal and occipital lobes of the brain (210, 211). It is performed by holding the mouse gently by the tail suspended approximately 1-2 feet above a solid cage grate surface (209). The mouse is then vertically lowered slowly toward the grate, taking note not to allow whiskers to contact the surface. A mouse with normal, average visual capabilities will attempt to reach toward the surface. A mouse that is blind, with impaired

vision, or spatio-temporal problems will not attempt to reach until the whiskers contact the surface. Alternatively, the impaired mouse may also try to bend backwards on itself, in attempt to right itself using its awareness of gravity.

Palpebral Reflex: Alternatively called the corneal reflex, it measures optic function and indicates potential inflammation in central nervous tissue connected to the optic tract, such as the trigeminal nerve, occipital lobe, and parietal lobes of the brain (212, 213). It is performed by using a teased-out cotton tipped applicator. The mouse is held steady, and the cotton is gently touched against the cornea (209). The blinking response is assessed on a scale of 0 to 3. On this scale, 3 represents a hyper-repetitive blinking in response to corneal stimulation; 2 equivocates to a normal, quick blink response; 1 corresponds to a slow blink or a closure response to stimuli; and a score of 0 indicates there was no response to corneal stimuli. Impaired or absent reflex responses suggests deteriorated motor/neural capabilities, eye function, and potential neurological inflammation.

Rear Limb Withdrawal: The limbic withdrawal test measures motor neuron responses in mice, and can indicate arthralgia in limb joints, and/or inflammation of motor neurons (214, 215). The mouse is allowed to grip onto a surface and steadied by the tail (209). One of the hind limbs is gently picked up and pulled taut at a 45˚ angle. The limb is then released, and the withdrawal of the limb is scored on a scale 0 to 3. On this scale, 3 represents a hyper-active response; 2 equivocates to a normal quick withdrawal of the limb back to normal position; 1 corresponds to a slow response to stimulus; and a score of 0 indicates there was no response, and leg drops to the ground and does not return to normal position.

Grip Time Assessment: The grip time assessment quantitatively evaluates mouse muscular capabilities and indicates potential arthralgia and muscular coordination issues (216, 217). The test was performed by placing a mouse on a grated cage lid, and the grate was suspended 1-2 feet above

the bench-top or cage (209). The mouse and grate were gently shaken for 1 minute, and then rapidly inverted to bring the mouse into an upside-down position. The time the mouse could successfully hold on without falling off the grate was recorded. Healthy mice are expected to be able to hold onto the grate for a minimum of 1 minute. Any recordings less than 60 seconds were considered abnormal.

Histopathology and immunofluorescence of eyes and brain

To evaluate tissue infectivity, viral burden, and infection-induced histopathology, eyes and brains were harvested from 5 out of 20 total mice per group at 10 and the remaining at 100 DPI. The tissues were fixed in 10% formalin solution, followed by paraffin embedding for 8 µm sectioning. Sectioning of brain tissues was performed at the Neuropathology/Histochemistry core of the Emory NINDS Neurosciences Core Facility (P30 NS055077), sectioning and H&E staining of eye tissues was performed by the L.F. Montgomery Ophthalmology Pathology core.

Immunofluorescent staining: Slides were de-waxed and rehydrated using sequential washes of xylene, ethanol, and distilled water. Antigens were unmasked and retrieved by submersion in sodium citrate buffer (10mM, pH 6.0) for 10 minutes at 56°C. Aldehyde auto-fluorescence was quenched in a humidified chamber using 3M glycine solution, and lipofuscin auto-fluorescence was quenched using Sudan-Black B. Slides were then blocked in bovine serum albumin (2% BSA)-TBS. Primary antibody diluted in 1% BSA in PBS buffer was added directly on top of each section, and slides were incubated overnight at 4°C. The 4G2 antibody (Millipore, MAB10216) was used for viral infectivity analysis. Myelination studies utilized anti-MBP-Alexa Fluor488 (SantaCruz, sc-271524), anti-Vimentin (Abcam, ab92547), and anti-Myelin PLP (Abcam, 28486) antibodies. Secondary antibodies were fluorescently conjugated (Anti-Mouse Alexa594,

Biolegend #405326; Anti-rabbit Alexa547, Abcam, ab150167; Anti-mouse Alexa488, Invitrogen, A10667), diluted in 1%BSA in PBS solution and incubated for 2 hours at room temperature. Prolong Gold Antifade mounting medium with DAPI (Thermo-Fisher, P36931) was applied, and slides were covered with a coverslip. Images were taken on Zeiss AxioScope microscopes via SPOT-advanced imaging software. Images were processed in Fiji/ImageJ.

TUNEL staining: TUNEL stain was selected because for the broad range of cell death pathways it stains for, i.e. apoptosis, necrosis, and pyroptosis (218-220). While there is no definitive way to discern between these pathways via TUNEL stain, DNA fragmentation does occurs in all of these cell death pathways, making it preferable in this study where we seek to identify cell death induced by infection rather than specific pathways. Terminal deoxynucleotidyl transferase dUTP nick end labeling, or TUNEL, staining was performed according to manufacturer protocol (Abcam, ab66110). Slides were de-waxed and rehydrated using sequential washes of xylene, ethanol, and distilled water. Antigens were unmasked and retrieved by submersion in sodium citrate buffer (10mM, pH 6.0) for 10 minutes at 56°C. Aldehyde auto-fluorescence was quenched in a humidified chamber using 3M glycine solution, and lipofuscin auto-fluorescence was quenched using Sudan-Black B. Slides were then blocked in bovine serum albumin (2% BSA)-TBS. Slides were then washed in PBS and blocked using a proteinase K solution for 5 minutes at room temperature. Wash slides with PBS and then label fragmented DNA using TdT enzyme, enzyme buffer, and Br-dUTP (Abcam, ab66110). Prolong Gold Antifade mounting medium with DAPI (Thermo-Fisher, P36931) was applied, and slides were covered with a coverslip. Images were taken on Zeiss AxioScope microscopes via SPOT-advanced imaging software. Images were processed in Fiji/ImageJ.

Quantification of MBP, Myelin PLP, and 4G2 positive cells: Corrected total cellular fluorescence (CTCF, also called normalized MFI) was determined as described by Lourenço et al. for both MBP, myelin PLP, and vimentin stains (221). Similarly, to determine the percentage of 4G2 positive cells, DAPI foci and 4G2 cells were enumerated both manually and automatically, using the "Threshold" and "Analyze particles" functions in FIJI/ImageJ. The percent of infected cells was then calculated as the number of 4G2 positive cells was divided by the number of DAPI positive foci.

Antibody Titration and Characterization

ELISAs: Anti-ZIKV specific antibodies were determined by coating flat bottom, 96-well Nunc MaxiSorp plates (Thermo-Fisher, 44-2404-21) with 4µg/ml of inactivated virus stocks, diluted in sodium bicarbonate buffer. Plates were incubated overnight at 4°C, washed with PBS-Tween 0.5%and blocked with 2% BSA in PBS for 1 hour. Individual PPP samples were run in duplicate and incubated for 2 hours at 37°C. The standard curves were generated with appropriate purified mouse immunoglobulins and isotype-specific HRP-labeled detection antibodies (Southern Biotech, Birmingham, AL). Sample IgG concentrations were determined by interpolation from standard curves. Anti-ganglioside specific antibody concentrations were determined similarly. Flat bottom, 96-well Nunc MaxiSorp plates were coated with 2µg/ml of either GD1a, GD1b, or GT1a ganglioside (SantaCruz, sc-202621, sc-202622, sc-202629, respectively). Standard wells were coated as described above. PPP samples were diluted. Standard curve antibodies and development of plates was performed as described previously (222). The avidity index was determined using Prism 7.03 Software (GraphPad, La Jolla, CA) by calculating the molar concentration of the

chaotropic agent required to reduce the initial optical density by 50% as previously described (222).

Focus-forming Reduction by Neutralization Assay (FFRNT): Heat-inactivated PPP samples were diluted serially and combined with 100 FFU live virus. Antibody dilutions and virus were co-incubated for 1 hour at 37˚C, and then added over Vero cells for 24 hours. The focus-forming assay was performed as described (200).

Avidity: Competitive ELISA with chaotropic inhibition was performed as described previously (222).

Flow Cytometry identification of activated cellular subsets. Skin draining (inguinal) lymph nodes were collected at 7 and 14 DPV to evaluate the presence of activated T_{FH} cells, $CD8^+$ follicular cells, and GC B-cells. Spleens were also collected at 7 and 14 DPV (-53 and -46 DPI) to evaluate the presence of recently activated T-cell populations, as well as for differentiated B-cell subsets (256). Samples were acquired on an LSR II flow cytometer (BD Biosciences) and data were analyzed with FlowJo (FlowJo LLC, BD, v9.9) (Gating strategies available in SFig 2A, B, and C).

ELISpot: ELISpot assays were performed and quantified as described previously (222).

Antibody-Dependent Enhancement Assay: ADE assay protocol was performed as described using U937 cells (200). The cells were maintained in suspension in complete RPMI medium. Cells were stained with 4G2 antibody (EMD Millipore). Samples were run on a CytoFLEX LX system at Pediatrics/Winship Flow Cytometry Core of Winship Cancer Institute of Emory University, Children's Healthcare of Atlanta and NIH/NCI, which is supported under the award number P30CA138292.

Statistical Analysis

Correlation analysis was performed on vRNA titers determined by qRT-PCR for brain and eyes to determine a relationship with raw reflex scores. Pearson's correlation coefficient with a two-tailed p-value were calculated for each of the four reflexes. For ELISA assays, linear regression tests to interpolate OD values into concentrations. For ELISPOT, flow cytometry, co-culture assays, and qRT-PCR, two-way ANOVA followed by Bonferroni's Post Hoc test for multiple comparisons was used to analyze differences between vaccination groups, as well as between vaccinated and unvaccinated groups following infection. Two-way ANOVA with Bonferroni's post-hoc was also used to determine differences between uninfected and infected groups, as well as between vaccination groups for all reflex assessments performed. For immunofluorescence assays, two-way ANOVA was used to compare difference hippocampal and cortical regions, as well as between early and late timepoints. Non-linear regression analysis was performed to determine the IC_{50} (95% confidence interval) for avidity and neutralization assays. A p-value less than 0.05 was considered significant.

RESULTS

MNP vaccination induced a greater concentration of vaccine-specific antibodies with higher avidity.

The role of autoreactive $CD8^+$ T cells has been well documented in regard to ZIKV neurological pathology, but the putative interplay of autoantibodies has been neglected despite the obvious connection between self-reactive antibodies and GBS (192). Here, we utilized two vaccination strategies to investigate their effect on antibody magnitude, quality, and protective immunity against viral infection. Two cohorts of mice were vaccinated as per the schematic in Supplementary Fig 1A using either intramuscular injection (IM), cutaneously delivery using dissolving polymer microneedle patches (MNP), or an empty MNP as a mock vaccination control. All animals received a primary vaccination of 4µg of ZVIP injected either by IM or MNP, and were then monitored for 30 days. After 30 days, animals received a booster vaccination that was identical to the prime in both dose and administration route, and subsequently monitored for an additional 30 days.

Prior to all vaccination experiments, ZVIP incorporation into the MNPs was confirmed qualitatively by microscopy to visualize ZVIP vaccine combined with sulforhodamine dye and by Western blot (Fig S1B). Patches with –vaccine mixed with vital dye (sulforhodamine) are pictured after patch casting and after needle dissolution in porcine cadaver skin (Fig SB-i and ii, respectively) Vaccine delivery into porcine cadaver skin was verified by the presence of dye deposition (Fig S1B-iii). Vaccine concentration in the new patches and used patches was quantitatively estimated with sandwich ELISA. The difference in concentration between new and used patches allowed us to calculate the percentage of vaccine delivery in the skin and thus adjust the dose to match those delivered with needle and syringe. MNPs are simple-to-administer skin

patches that contain water-soluble, solid, conical needles of microns dimensions that encapsulate vaccine (246-248). Upon painless application to skin, the microneedles dissolve and release the vaccine within minutes, after which the used patch can be discarded as non-sharps waste. To ensure the ZVIP vaccine was successfully incorporated in patches, we ran a western blot to confirm the presence of ZVIP in cast patches (SFig1-Biv).

Antibody kinetics of ZVIP-specific IgG, IgG1, and IgG2a were evaluated by ELISA (Fig 1). MNP vaccination generated at least 10-fold greater total IgG as early as 7 days after vaccination (-53 DPI) compared to IM vaccination (Fig 1A). MNP-induced total IgG concentrations remained 10-fold greater for all time-points prior to infectious challenge. IgG1 induced by MNP showed an immediate spike of antibodies, followed by a plateau of concentration for the remaining time-points. IM-induced IgG1 showed a gradual increase in titer concentration that increased further after the booster vaccination (Fig 1B). MNP and IM vaccinations demonstrated similar kinetic trends for IgG2a concentrations, but MNP vaccine recipients had consistently 4.4- to 50-fold greater concentrations of IgG2a than IM vaccinated mice (Fig 1C). Prior to infectious challenge, 30 days after booster vaccination (0 DPI), we measured antibody avidity as an index of antibody maturation and quality (Fig 1D). MNP generated antibodies demonstrated IC_{50} of 1.365 M, and IM antibodies had an IC_{50} of 0.683 M, a 2.2-fold difference ($p=0.023$). This data demonstrates that MNP patches induce greater concentrations of vaccine-specific antibodies, and that after a prime and booster vaccination animals that received MNPs have antibodies with greater avidity for vaccine-antigen.

MNP vaccinations induced sustained B and T cell responses while IM vaccination induced ephemeral T cell secretory responses.

ZVIP-specific $CD8^+$ and $CD4^+$ T cells impact viral pathogenesis and have established roles in autoreactive demyelination and chronic neuroinflammation; as such, cellular responses after a single vaccination were also evaluated. The frequency of germinal center (GC) B cells, follicular helper T cells (T_{FH}), follicular $CD8^+$ T cells, and $CD4^+$ and $CD8^+$ cells in inguinal lymph nodes (ILN) and spleen suspensions were quantitated (gating strategies in Fig S2). $CD19^+CD3\varepsilon^-GL7^+FAS^+$ ILN GC B cell levels were 10-fold higher in ZVIP-MNP than IM groups as early as 7 days post-vaccination (DPV; -53 DPI) (Fig 2A-i) and 20-fold higher by 14 DPV (-46 DPI) ($p<0.0001$, $p=0.02$ respectively). The frequencies of $TCR\beta^-/B220^+/CD138^+$ splenic plasmablasts were 2-fold 7 DPV (-53 DPI) and 3-fold 14 DPV (-46 DPI) higher in the MNP group compared to IM ($p<0.0001$) (Fig 2A-iv and v). $TCR\beta^-/B220^-/CD138^+$ splenic plasma cells were 3-fold 7 DPV (-53 DPI) and 2-fold 14 DPV (-46 DPI) in the MNP group compared to the IM group ($p<0.0001$).

IM immunization elicited an early, significant spike of $CD19^-/CD3\varepsilon^+/CD4^+/CXCR5^+/PD\text{-}1^+CD4^+$ and $CD19^-/CD3\varepsilon^+/CD8^+/CXCR5^+/PD\text{-}1^+CD8^+$ follicular T cell frequencies. At 14 DPV (-46 DPI), follicular T cell subsets contracted 10-fold in IM vaccinees from 10% to <1% but remained constant at 3% in MNP vaccinees (7 DPV $p<0.0001$; 14 DPV $p=0.0019$; -53 DPI $p=0.0001$) (Fig 2A-ii and iii). IFN- γ, IL-2, IL-4, or TNF-α secretion among $CD4^+$ T cells was 3-fold greater in IM than MNP groups 7 DPV (-53 DPI; $p<0.0001$, $p=0.0013$) (Fig 2B). By 14 DPV (-46 DPI), MNP immunization increased the frequency of $CD4^+$ T cells secreting IFN-γ by 87.1-fold, TNF-α 21.7-fold, IL-2 53.4-fold, and IL-4 26.1-fold (all $p<0.0001$) (Fig 2C), suggesting delayed activation of $CD4^+$ T cells due to an antigen-depot effect (249). MNP-induced $CD8^+$ T cell secretion was low 7 DPV (-53 DPI) but was still 7- to 10-fold higher than IM (IFN-□

p=0.0026; TNF-α p<0.0001; IL-2 p<0.0001; IL-4 p=0.0018) (Fig 2B). Importantly, IM vaccination-induced $CD8^+$ T cells were indistinguishable from blank vaccinated controls, while MNP vaccination-induced $CD8^+$ secreting cells were 16-25% greater than IM groups (all p<0.0001) (Fig 2B).

Overall, our data suggests that MNP vaccination induces greater cellular responses in addition to ZVIP-specific antibodies of superior immunological quality. Systemic vaccination appears to offer an ephemeral $CD4^+$ T cell response that does not persist beyond 7 DPV (-53 DPI), whereas MNP vaccination not only induces elevated and persistent $CD4^+$ and $CD8^+$ T cells in LN and spleen, but that these populations expand continually after vaccination.

Unadjuvanted IM vaccination offered little protection against infectious challenge.

Animals were challenged with live virus that was homologous to the vaccine strain 30 days after receiving a booster vaccination. To evaluate vaccine protective efficacy, weight changes were monitored post-challenge up to 120 DPI; both MNP and IM vaccination protected against weight loss (Fig 3A). MNP vaccinees did not lose weight after infection and IM vaccinees lost a maximum of 5% of their starting weight 6 DPI. Blank controls showed 10% weight loss 6 DPI, followed by a slow recovery of weight (Fig 3A).

As ZIKV has demonstrated persistence in human organs and fluids for ≥200 days(223), we evaluated viral burden in brain, eyes, and plasma 10 and 100 DPI. Thus, we quantified viral burden in tissues and secretions with a focus-forming assay (FFA) co-culture, where homogenized tissues were used in a trans-well system over permissive Vero cells (201). Homogenized tissues shed live virus through the membrane pores, infected permissive sterile cells below, and provided FFU/ml for each tissue. Homogenates were not added directly to monolayers because this does not

discriminate if the cells are permissive to infection and a productive infection. Previous concerns were raised that ZIKV would not propagate in WT BALB/c tissues due to STAT non-homology. Thus, they were evaluated here to specifically identify if live virus was being shed from the tissues. Compared to IM vaccinations, MNP-vaccinees co-cultures exhibited 10- and 15-fold lower viral load for brains and eyes, 24- and 13-fold less for spleen and liver, and 11-fold less for tears and plasma at 100 DPI (all $p<0.0001$) (Fig 3B). qRT-PCR quantification of vRNA mirrored FFA co-culture findings, where MNP vaccinations showed 6.4-, 3.6-, and 4.1- fold less vRNA in brain, eyes, and plasma, respectively at 100 DPI ($p\leq0.0001$ for all groups) (Fig 3C).

The development and severity of neurological and ocular pathology was assessed by clinical reflexes up to 120 days after infectious challenge. For palpebral reflexes, MNP recipients exhibited a nadir at 10 DPI, with approximately 60% of animals showing loss of palpebral reflex ($p=0.0013$ for 6 DPI, $p<0.0001$ for all other time-points), while blank controls show a nadir at 6 DPI (Fig 3D). After this sharp decline, symptoms waned and animals recovered, with only 10% of animals demonstrating hyporeflexia at 120 DPI. IM recipients showed an immediate impairment in reflexes, with 45% of animals showing areflexia as early as 3 DPI, with the lowest score at 10 DPI, and long-term persistence up to 120 DPI. MNP vaccinees showed minimal loss of visual placement reflex, with only 15% of animals showing areflexia in a cyclical pattern, potentially indicating host inability to control viremia long-term and a periodic re-emergence of virus from privileged compartments. In contrast, IM vaccination resulted in a 50% impairment of visual placement reflex within 6 DPI, with 70% of animals showing areflexia at 30 DPI, and persistent loss of visual placement abilities up to 120 DPI (all $p<0.0001$) (Fig 3E).

Rear limb withdrawal kinetics showed a trend similar as that observed with palpebral reflex, where MNP vaccinated animals demonstrated the maximum loss of reflex ability 10 to 30 DPI

with approximately 40% showing hyporeflexia (Fig 3F). Of these, 30% exhibited a partial recovery and ultimately only 10% had persistent hyporeflexia 120 DPI. In contrast, IM vaccinated mice showed two negative peaks at 10 and 40 DPI, with 65% of animals suffering from hyporeflexia (6 DPI $p=0.01$; 10 DPI $p=0.0014$; 40 DPI $p=0.0004$; 80, 100 and 120 DPI $p<0.0001$). These animals underwent a periodic cycle of convalescence and re-emergence of symptoms, and 60% of them showed persistent loss of withdrawal reflexes (Fig 3F). Finally, IM and MNP recipients demonstrated 2.8- and 2.1-fold lower grip times 6 DPI, respectively, with MNP vaccine recipients showing a gradual recovery across the time-course and reaching normal scores by 60 DPI. IM vaccinated animals, on the other hand, maintained reduced grip times significantly lower than uninfected/blank vaccinated control group until 100 DPI (40 DPI $p=0.0002$; 60, 80, and 100 DPI $p<0.0001$) (Fig 3G).

IM vaccination exacerbated intraocular pathology without protecting against infection or cell death.

Ocular pathology was evaluated 10 and 100 DPI in IM, MNP, and uninfected/blank vaccinated animals. After 10 days, IM and blank recipient mice demonstrated stromal inflammation, corneal destruction, complete loss of corneal cellular organization, and a distinct abundance of infiltrating leukocytes in the apical lumen. MNP mice showed mild hyperplasia of corneal epithelia and infiltrating leukocytes in the stroma while controls lacked these pathological features (Fig 4A, left column). Within the retinas, IM and blank vaccination mice had scleral hyperplasia, edema and subsequent degeneration of the inner and outer nuclear layers, as denoted by increases in total neural nuclei present. Additionally, ganglionic cell layers among IM recipients showed a distinct bifurcation with intense hyperplasia, potentially indicating vascular angiogenesis. In contrast,

MNP retinal layers appeared normal with mild edema of RPE and limited scleral inflammation (Fig 4A, right-column).

At 100 DPI, the pathology observed in IM and blank vaccination mice was similar to 10 DPI with increased numbers of leukocytes in the stroma, loss of cellular organization among cuboidal epithelia, and warping of Descemet's and Bowman's layers. MNP corneas demonstrated edema and hyperplasia of cuboidal epithelia (Fig 4B, left column). Retinal layers of IM recipients had visible hyperplasia within the ganglionic layers, and hydropic degeneration of RPE, choroid, and sclera layers, and leukocytes in the tissue posterior to the sclera which were absent in uninfected controls. In contrast, MNP ganglionic, nuclear, and plexiform layers appeared normal, while RPE and sclera exhibited mild edema and inflammation (Fig 4B, right-column).

To assess ZIKV tropism within various tissues of the eye, we performed 4G2 immunohistochemistry on whole eyes. 4G2-positive foci detected in cornea, RPE, and lacrimal glands were enumerated 10 and 100 DPI. MNP recipients demonstrated low levels of infectivity at both time points, with a decrease from 6.5% to 2.8% between 10 and 100 DPI (Fig 4C, SFIG3 A and B). IM vaccinated mice demonstrated 4.6-times higher viral infectivity 10 DPI, and 8.8-times greater infectivity at 100 DPI compared to MNP groups, with an upward trend between early and late time-points (all $p<0.0001$) (Fig 4C-D). TUNEL staining was performed in the optic tract to assess cell death 10 and 100 DPI (SFIG 3C and D). Cornea and retina were TUNEL-positive, with corneal epithelium demonstrating abundant foci in all groups. Cell death was evident at early and late time-points among all groups. MNP vaccination showed no changes in cell death at both time-points, with 2.6 to 2.1-fold higher cell death at 10 and 100 DPI, respectively, when compared to uninfected animals. IM recipients demonstrated 4.6- and 8.8-fold greater cell death compared to uninfected and blank vaccinated mice at the same time-points, doubling the rate of cell death.

Importantly, IM vaccinees showed 1.7-fold greater cell death levels at 10 DPI, and 4.2- fold more 100 DPI compared to MNP (all $p<0.0001$) (Fig 4 E-F).

Transcriptional analysis revealed that MNP vaccination limited expression of proinflammatory cytokines after infection, with 22-times greater transcription of *IL-1β* compared to uninfected animals, whereas IM vaccination resulted in 123-times higher expression ($p=0.0004$) (Fig 7G). Similarly, *TNF-α* transcription was increased 32.5-fold in MNP and 293 -fold in IM vaccinated mice ($p<0.0001$). *COX2* expression was 7.3-fold lower in the eyes of the infected MNP indicating lower inflammation; IM vaccination did not alter *COX2* expression compared to MNP ($p<0.001$) (Fig 4G). MMPs displayed a similar trend, where in the MNP group *MMP2* expression was 35.7-fold greater than uninfected/blank vaccinated controls, and in the IM group expression was 1,138.4-fold greater than in uninfected mice. Additionally, there was a 31.9-fold difference between IM and MNP immunized groups ($p=0.006$) (Fig 4G). Finally, the MNP vaccine recipients showed an increase of 40.2- and 6.5-fold in transcription of anti-inflammatory cytokine, *IL-10* and *SOCS3*, respectively, compared to uninfected/blank vaccinated animals, while IM vaccine recipients demonstrated an increase of 442- and 17-fold compared to uninfected mice. Comparatively, MNP animals exhibited 11-fold less transcription of *IL-10* compared to IM groups, and 2.6-fold less transcription of *SOCS3* ($p=0.0001$) (Fig 4G). Lower expression of anti-inflammatory proteins may point to resolution of ocular infection within MNP groups, while elevated transcription of *IL-10* and *SOCS3* correlates with H&E findings of pathogenic neovascularization. Taken together, our immunofluorescence, H&E, and transcriptional data demonstrate that weakly neutralizing antibodies correlated with intraocular pathology and fail to protect animals from ocular infectivity, persistent ocular inflammation and pronounced cell death.

MNP vaccination protected against ZIKV-induced demyelination and chronic neuroinflammation.

Immunocompetent mice infected with PRVABC59 demonstrated neurological and ocular symptomatology that correlated strongly with viral burden. Viral burden was reduced by MNP vaccination, reducing severity of symptoms and improving overall convalescence and recovery. To further evaluate the impact of vaccine-induced antibodies on neuro-ocular pathology, we quantified hippocampal and cortical myelin levels using fluorescent microscopy, and determined neuro-inflammatory transcriptional responses using qRT-PCR.

Myelination of neural axons allows for electrical conduction and intracellular signaling. Within the CNS, the two most common forms of myelin are Myelin-basic protein and myelin proteolipid protein, and both are regulated by vimentin (259). One hundred days after infection, both hippocampal and cortical regions of the MNP group's brains demonstrated that only 1.5% of cells were infected (Fig 5A). In comparison, the IM group showed identical infection levels in both regions of the brain, although they were 16-fold greater compared to MNP recipients (both $p<0.0001$) (Fig 5A; SFIG4). MBP expression after MNP vaccination in both hippocampus and cortex appeared to be unaffected by infection, as fluorescence was indistinguishable from uninfected animals. IM recipients, however, exhibited 3- and 2.1-fold less MBP expression in hippocampus and cortex, respectively, when compared to both uninfected and MNP vaccinated animals (both $p<0.0001$) (Fig 5B-C; SFIG4A). Both mPLP and Vim expression showed similar patterns, where MNP recipients demonstrated levels similar to uninfected and blank vaccinated animals. mPLP expression was 3.2- and 2.7-fold lower in the hippocampus and cortex, respectively, of the IM group, when compared to uninfected animals; and 4.1- and 2.2-fold lower when compared to MNP recipients (mPLP $p<0.0001$ and $p=0.0006$; Vim both $p<0.0001$) (Fig 5D-

E). Vim expression was 1.7- and 2.3-fold lower in the hippocampus and cortex of IM vaccinated mice when compared to uninfected animals; and 1.6- and 1.7-fold lower when compared to MNP recipients (Fig 5F-G; SFIG4).

Transcriptional analysis of the inflammatory mediators in the brain revealed no change of proinflammatory *IL-1β* or *TNF-α* expression post-infection in the MNP group, comparable to uninfected controls. Infected IM vaccinees however, showed 166- and 281-fold greater transcription, respectively, compared to uninfected animals ($p=0.0462$ and $p=0.0012$) (Fig 5H). Pain mediator and proinflammatory stimulant, *COX2*, showed 1.8-fold greater expression among MNP mice and 678-fold higher expression in IM vaccine recipients ($p<0.0001$) (Fig 5H). Matrix metalloproteinases (MMPs) demonstrated a trend similar to the proinflammatory cytokines, where MNP immunized animals showed transcription levels comparable to uninfected animals, while the IM immunized group demonstrated 477- and 133-fold greater transcription relative to blank vaccinated and uninfected mice for *MMP2* and *MMP9* respectively ($p<0.0001$ and $p=0.0005$) (Fig 5H). Finally, the levels of anti-inflammatory cytokines *IL-10* and *SOCS3* were significantly upregulated among MNP brains, with 838- and 714-fold greater levels than uninfected animals. IM immunized mice also showed elevated anti-inflammatory transcription, with 53- and 112-fold greater expression of *IL-10* and *SOCS3* compared to uninfected animals, but these levels were significantly less than MNP mice ($p<0.001$ and $p=0.002$) (Fig 5H). Collectively, these data demonstrate that highly specific antibodies abrogated demyelination observed during ZIKV infection and limit the chronic neuro-inflammatory response.

MNP antibodies demonstrate greater breadth of neutralization, less ADE, and are less auto-reactive.

As GBS is primarily mediated by auto-reactive antibodies, we next determined if the observed reduction in neuro-ocular pathology following MNP vaccination correlated with antibody neutralization, ADE, and auto-reactivity to ganglioside residues. After infectious challenge, vaccination groups demonstrated a plateau of antibody concentrations, regardless of IgG subtypes, that endured up to 120 DPI (Fig 6A, B, and C).

Antibodies from both vaccination groups, sampled 100 DPI, were evaluated for their ability to neutralize 3 strains of ZIKV and each of 4 DENV serotypes (Fig 7). Neutralization of the homologous strain showed a titer of 11,815 for the MNP group, and a titer of 3,265 for the IM group, a 3.6-fold difference (Fig 7A). For ZIKV-FLR, MNP-induced antibodies had a titer of 1,915 and IM-induced antibodies had a titer of 81, a 23.6-fold difference (Fig 7Bi and ii). Neutralization of MR766 showed titers of 26,887 and 3,313 for the MNP and IM vaccinated mice respectively, an 8.1-fold difference (Fig 7Bii). Among DENV strains, MNP-raised antibodies reached 21,818, 1,702, 9,219, and 30 VN titers for DENV-1 through -4 respectively. IM-induced antibodies had neutralizing titers of 208, 397, 185, and 2 for the same strains. Thus, MNP antibody neutralization titers were 104.9-, 4.3-, 50.2-, and 15-fold greater than IM titers for DENV-1, DENV-2, DENV-3, and DENV-4, respectively (SFIG 5Aiii-vi) (all neutralization titers are listed in Sup Fig 5A).

The capability of vaccination-induced antibodies to enhance homologous and heterologous flavivirus infection were also quantified for both maximum infectivity and the associated endpoint titers (Sup Fig 5B). Ideal vaccine candidates would minimize ZIKV infection by ADE, regardless of strain, and demonstrate limited DENV reactivity. Co-incubation of ZIKV or DENV strains and U937 cells resulted in no detected infection. MNP-induced antibodies limited ADE infection of

the permissive U937 cells. Following antibody co-incubation with PRVABC59, a maximum of 5% of the 10,000 cells assayed were positive for ZIKV infection (Fig 7A). The same antibodies generated a maximum of 10% and 18% of all infected cells when the FLR or MR766 strains were used (Fig 8B- i and ii). Among DENV serotypes, MNP-induced antibodies resulted in a maximum of 22% of all cells labeled positive for DENV-1 infection, 36% of cells were positive for DENV-2, 24% were positive for DENV-3, and 19% were positive for DENV-4 (SFIG 6Aiii-vi). When infectious virus was co-incubated with antibodies generated by IM vaccination, the frequency of cells positive for infection increased dramatically. The IM group showed a maximum of 84.6% of all cells infected with PRVABC59 (Fig 8A), while FLR and MR766 demonstrated a maximum of 70% and 90% cell infectivity, respectively (Fig8 Bi and ii). IM-vaccination antibodies resulted in 72% of cells infected with DENV-1, 54% infected with DENV-2, 41% infected with DENV-3, and 86% infected with DENV-4 (Fig 8Biii –vi).

Collectively, these data demonstrate that antibodies generated via MNP vaccination were of greater immunological quality than those generated by IM, as evidenced by the reduced viral burden and limitation of clinical symptoms and tissue pathology after infection.

To correlate observed neuro-ocular pathology with GBS-like autoantibodies, we determined the relative concentrations of anti-ganglioside autoantibodies generated by MNP and IM vaccinations. Thus, we quantified the total amount of IgG that bound to GD1a, GD1b, and GT1a gangliosides (Fig 9A, B, and C). Each of these correlates with a specific variety of GBS. GD1a reactive IgG correlates with acute motor axonal neuropathy; GD1b corresponds to a sensory ataxic variant; GT1a is connected to Miller-Fisher Syndrome, a variant of GBS affecting the eyes (232). To understand what quantity of these antibodies are auto-reactive, we took the percentage of each ganglioside concentration as a proportion to the total ZIKV-specific IgG. In the MNP vaccinated

group, 12% of all antibodies were GD1a reactive prior to infectious challenge and never exceeded 15% after challenge. Prior to challenge, 16% of IM induced antibodies were GD1a-reactive, and after challenge, a maximum of 25.1% of all antibodies showed autoreactivity 60 DPI (Fig 9A). For all time-points observed, MNP antibodies were significantly less reactive to GD1a than those induced by IM vaccination ($p=0.008$ at 0 DPI, all other $p<0.0001$). Thirteen percent of MNP antibodies prior to vaccination were reactive to GD1b and reached a maximum of 19% 10 DPI (Fig 9B). Twenty-two percent of IM vaccination-induced antibodies were reactive to GD1b prior to challenge, and reached a maximum of 25% after challenge 10 DPI. Again, for all time-points observed, MNP antibodies were significantly less reactive to GD1b than those induced by IM vaccination ($p=0.001$ at 10 DPI, all other $p<0.0001$). Twelve percent of MNP antibodies prior to vaccination were reactive to GT1a and reached a maximum of 38% 60 DPI (Fig9C). Sixteen percent of IM vaccination-induced antibodies were reactive to GT1a prior to challenge and reached a maximum of 25% after challenge 10 DPI. Similarly, MNP antibodies were significantly less reactive to GD1b than those induced by IM vaccination throughout the observation period ($p=0.001$ at 10 DPI, all other $p<0.0001$).

DISCUSSION

ZIKV has remained as an international health concern since its re-appearance in 2015. It is increasingly apparent that the impact of ZIKV extends beyond microcephaly, as children born to infected mothers continually present new neurological and ocular clinical manifestations (93, 260). As a result, there has been substantial interest in understanding the mechanisms behind ZIKV invasion and persistence in immune-privileged tissues, as well as a sustained interest in viable vaccine candidates. Ocular and neurological pathology observed in humans has successfully been

recapitulated in both WT and immunocompromised murine models, but has not been utilized to evaluate vaccine efficacy despite the potential correlation between GBS and ZIKV-induced long-term pathology. Here, we demonstrated that immunocompetent BALB/c mice developed unique ocular and neuro-motor pathology as a result of ZIKV infection, and that this pathology can be abrogated with cutaneous immunization using MNPs encapsulating unadjuvanted whole, particle vaccine.

Importantly, we demonstrate that this route of vaccination can generate broadly neutralizing antibodies against multiple strains of ZIKV and DENV, while limiting antibody-mediated infection among non-permissive Fcγ-R bearing macrophages. We also show that the same unadjuvanted vaccine delivered intramuscularly induces weak and short-lived cellular responses, which ultimately result in broadly cross-reactive antibodies with limited neutralizing activity and elevated ADE capabilities compared to MNP vaccination. IM vaccination induced antibodies that enhanced ADE -similarly to infected controls that received blank vaccinations; further supporting the hypothesis that antibodies generated by an IM delivered unadjuvanted ZIKV were of low immunological quality. This hypothesis was validated by our avidity analysis showing that antibodies in the IM vaccinated cohort had lower avidity than the MNP cohort. Collectively, this data indicates the necessity of adjuvants in conventional vaccination routes to stimulate more robust cellular and humoral responses. Indeed, recent studies point to the importance of a strong $CD4^+$ and $CD8^+$ T cell responses, where $CD4^+$ T cells are critical in systemic clearance of ZIKV and prevent ZIKV neuro-invasion(202), while $CD8^+$ T cells and T cell-derived IFN-γ are essential to protecting microglia during ZIKV infection(192).

The observed neuroinflammation and neuro-ocular pathology was consistent with published data showing how flavivirus infections culminate in chronic neurological inflammation that

directly contributes to lethal motor/cognitive diseases, such as GBS (115). MNP vaccination conferred protection of ocular and brain micro-environments against viral infection, as shown by a reduction of *COX2*, *TNF-α,* and *IL-1β* transcription, which was consistently lower than IM vaccination counterparts. These three pro-inflammatory markers created a positive feedback loop in the context of microglial secretion, where IL-1β and TNF-α secretion by glial cells is stimulated by COX2 (116), and paracrine or autocrine IL-1β signaling through NF-κB signaling (117) (118). Similar to the reduction of pro-inflammatory transcription, MNP vaccination resulted in lower transcription of *MMP2* and *MMP9* than IM vaccination after infectious challenge. MMPs are endopeptidases with vital functions such as neural network remodeling, tissue destruction and restructure, and BBB integrity regulation (119, 120). Thus, infection that induces increased permeability of the BBB via elevated transcription of *MMP2* and *MMP9* corresponds to increased inflammatory leukocyte trafficking into the brain (121, 122). For both brain and eyes, the relative transcription levels of *COX2*, *IL-1β, TNF-α, MMP2*, and *MMP9* among ZIKV-infected MNP vaccinated animals never exceeded a 2-fold difference and were statistically similar to blank vaccinated control mice, indicating a robust protection of these tissues using the MNP vaccination platform. Conversely, IM vaccination-induced transcription levels of these same markers were at least 100-fold higher than MNP vaccinations, but were not statistically different from animals that received blank vaccinations, indicating the cellular and humoral responses generated by IM immunizations were not protective in immune-privileged compartments.

Even though the eye and brain are intricately linked immune-privileged compartments, our data demonstrated that vaccination differentially impacted the anti-inflammatory responses within these tissues. Anti-inflammatory proteins IL-10 and SOCS3 form a unique pathway, whereby following stimulation with TNF-α and IL-6 by local resident and infiltrating immune cells

producing IL-10 (236). The latter then stimulates SOCS3 production, and both work in concert to block intracellular signaling of IL-6 and IL-23, to prevent STAT3 phosphorylation and directly influence ocular T cell repertoire (240). Infected brain tissues showed that MNP elevated both IL-10 and SOCS3 more than IM counterparts. As IL-10 has demonstrated the ability to protect astrocytes from excessive inflammation (237, 238), our data demonstrated that MNP vaccination conferred protection against long-term neuro-inflammation in a manner that IM vaccination did not. Within the eye, IL-10 and SOCS3 have a counter-intuitive mechanism. Previous studies have demonstrated that high intraocular concentrations of these anti-inflammatory cytokines could stimulate angiogenesis via Müller-cell mediated neovascularization (239). Of particular note, IM vaccination appeared to exacerbate ocular pathology 10 DPI, with intense infiltration of monocytes and granulocytes into both the vitreous and apical lumen. Leukocyte infiltration occurred alongside a bifurcation of the ganglionic cell layers of infected retinas, demonstrating ocular pathology was not specific to a single tissue layer of the eye.

Our study is the first to report on MNP vaccination used against ZIKV, and that autoreactive antibodies to GD1a, GD1b, and GT1a gangliosides are increased following unadjuvanted IM vaccination, which contributed to myelin degradation in immunocompetent BALB/c mice following infection (111). GBS has been correlated with antibody cross-reactivity to host gangliosides in other flaviviruses (261, 262), but is rarely studied as a consequence of flavivirus vaccination. We observed that 25-75% of all PRVABC59-specfic antibodies generated by ZIKV infection that were specific PRVABC59 were autoreactive, and that MNP vaccination lower this proportion to 14-19%, while IM vaccination had 25-40% of autoreactive antibodies. Gangliosides are vital to synaptic transmissions, intercellular adhesion and communication, equilibrium, immune signaling, and nervous system and motor/neural network maintenance (113). Anti-

ganglioside antibodies have been previously shown to lead to the absence or fragmentation of MBP, myelin PLP, and vimentin, all contributing to persistent neuroinflammation within the brain by releasing damage associated molecular patterns (DAMPs) (114). Myelin or myelin-debris signals in macrophages via complement/opsonization or phagocytosis and facilitates M1 (macrophage type-1) polarization and proinflammatory secretion (114). This M1 microglia polarization is associated with prolonged secretion of TNF-α at high levels and can lead to permanent neural degeneration. This observation, correlated with our transcriptional data of blank vaccinated and IM vaccinated animals demonstrating chronic neuro-inflammation and demyelination.

Our study points to the need for a more comprehensive, systems biology approach to understand how antibodies influence long-term neurological pathogenesis of flaviviruses. Our data suggests that low specificity of ZIKV antibodies may initiate a demyelination cascade that ultimately results in chronic neuroinflammation and persistent neuro/ocular impairments. This adverse pathology can be circumvented by novel vaccination approaches that generate highly specific, strongly neutralizing antibodies despite the absence of an adjuvant. These antibodies limit infection of Fcγ-R bearing macrophages via ADE mechanisms and demonstrated limited autoreactivity to GBS-associated residues. Importantly, we demonstrated here that immunocompetent animals can serve as models for long-term vaccination studies, and denote highlight that the need for adjuvants depends on the antigen administration route. Our findings point to the need of exploring alternative vaccination platforms and imposing stringent qualifications for ZIKV vaccine candidates: vaccines must that would confer breadth and longevity of protection while minimizing the risk of autoimmunity and ADE. Future studies should include investigation of demyelination sequelae after passive transfer of ZIKV-induced antibodies, and the

putative role of maternal antibodies on vertical transmission. Additionally, future studies duplicating this work in C57BL/6 mice will determine if similar pathology can be observed in a Th1-skewed background and investigating antibody neutralization via passive antibody transfer.

Acknowledgements

We thank Dr. Sharon Isern, Dr. Scott Michael, and Lauren Paul for providing the ZIKV PRVABC59 strain for propagation. We thank Dr. Micah Chrenek, Dr. Hans Grossniklaus, and Dr. John Nickerson from Emory Ophthalmology Clinic for their advice on optic histology and staining. We thank Dr. Eugenia Scountzou and Dr. Nikolaos Papaioannou for their expertise in veterinary ophthalmology and for detailed assistance in evaluating animal ocular pathology. We thank Dr. Kiran Gill at Emory Vaccine Center core facility for her expert advice with flow cytometry. We thank Vidisha Singh and Aaron Scanlon for assistance running qRT-PCR experiments.

Funding Source

This work was supported by NIAID and CEIRS – HHSN272201400004C NIAID

Author contribution

J.T.B., N.L., I.S., E.S. Project conceptualization and experimental design

J.T.B., L.K.M., E.S.E., D.S., N.L., O.Q.A., E.Q.L., I.S.: Execution of experiments

E.S. and N.P. Assessment of ocular pathology

J.T.B, N.L., D.S., and I.S. Data analysis.

A.R.: Development and fabrication of MNP

J.T.B., D.S. and I.S. Manuscript preparation

M.R.P.: Overseeing ZVIP-MNP development

R.W.C. Manuscript feedback.

All authors read and provided feedback prior to submission

Competing financial interests

M.R.P. is an inventor of patents licensed to companies developing microneedle-based products, is a paid advisor to companies developing microneedle-based products and is a founder/shareholder of companies developing microneedle-based products (Micron Biomedical). This potential conflict of interest has been disclosed and is managed by Georgia Tech and Emory University.

J.T.B., L.K.M., E.S.E., D.S., N.L., O.Q.A., E.S., N.P., D.T.W., A.R., R.W.C., and I.S. declare that they have no conflicts of interest.

FIGURE 1

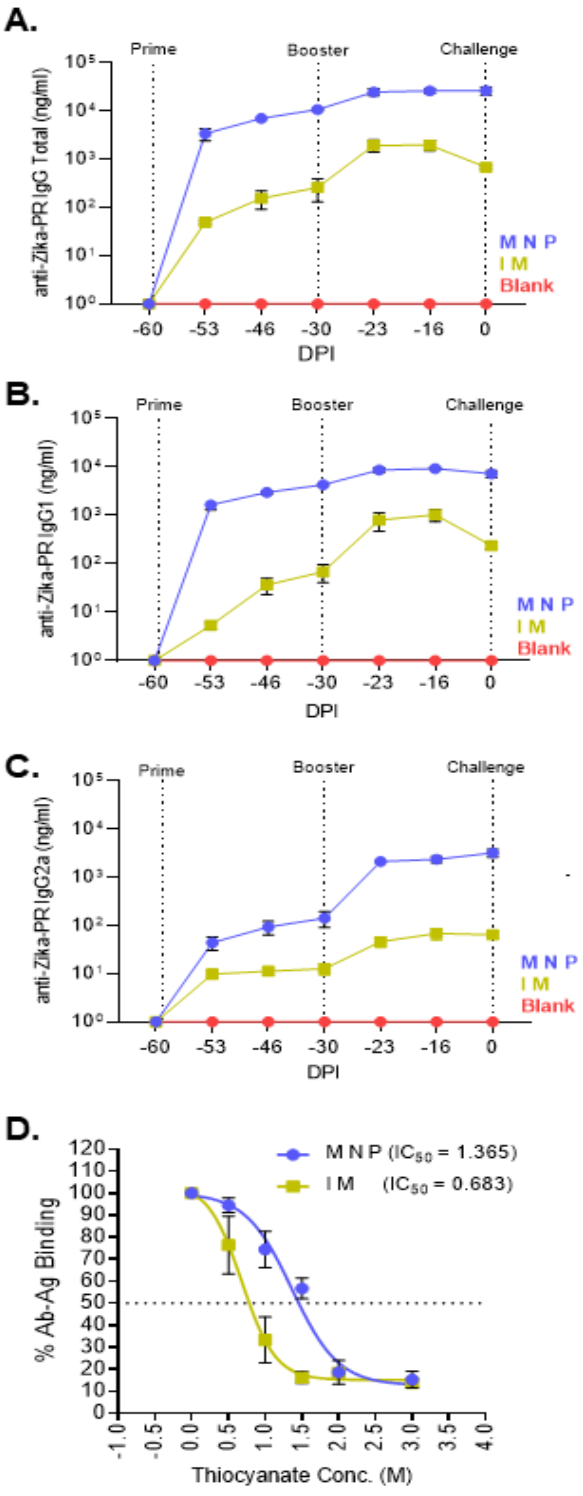
A.
Prime
Booster
Challenge
anti-Zika-PR IgG Total (ng/ml)
M N P
I M
Blank
DPI
B.
anti-Zika-PR IgG1 (ng/ml)
C.
anti-Zika-PR IgG2a (ng/ml)
D.
% Ab-Ag Binding
M N P (IC50 = 1.365)
I M (IC50 = 0.683)
Thiocyanate Conc. (M)

Figure 1. Cutaneous vaccinations induced greater antibody concentrations that bind with higher avidity.

Animals received a prime vaccination 60 days prior to infectious challenge (-60 DPI) by either IM or MNP, and were then monitored 7 and 14 days after vaccination (-53 and -46 DPI). Animals received a duplicate vaccination that was identical in route and dosage, termed booster, 30 days after vaccination (-30 DPI). After booster vaccination, animals were again monitored 7 and 14 days (-23 and -16 DPI). Vaccine-specific IgG total (A), IgG1 (B), and IgG2a (C). Vertical lines denote prime and booster vaccination administration and also identify 0 DPI as the day animals were challenged. (All N=10) (D) Antibody avidity was determined by chaotropic competitive ELISA (N=10). The dotted horizontal line denotes the IC_{50}, or the concentration of thiocyanate needed to remove 50% of antibodies bound to vaccine-antigen. Antibody-antigen binding (Ab-Ag) is analyzed using a non-linear analysis (Log (inhibitor) vs response with a variable slope) to determine the $logIC_{50}$. Error bars represent standard deviation for all panels.

FIGURE 2

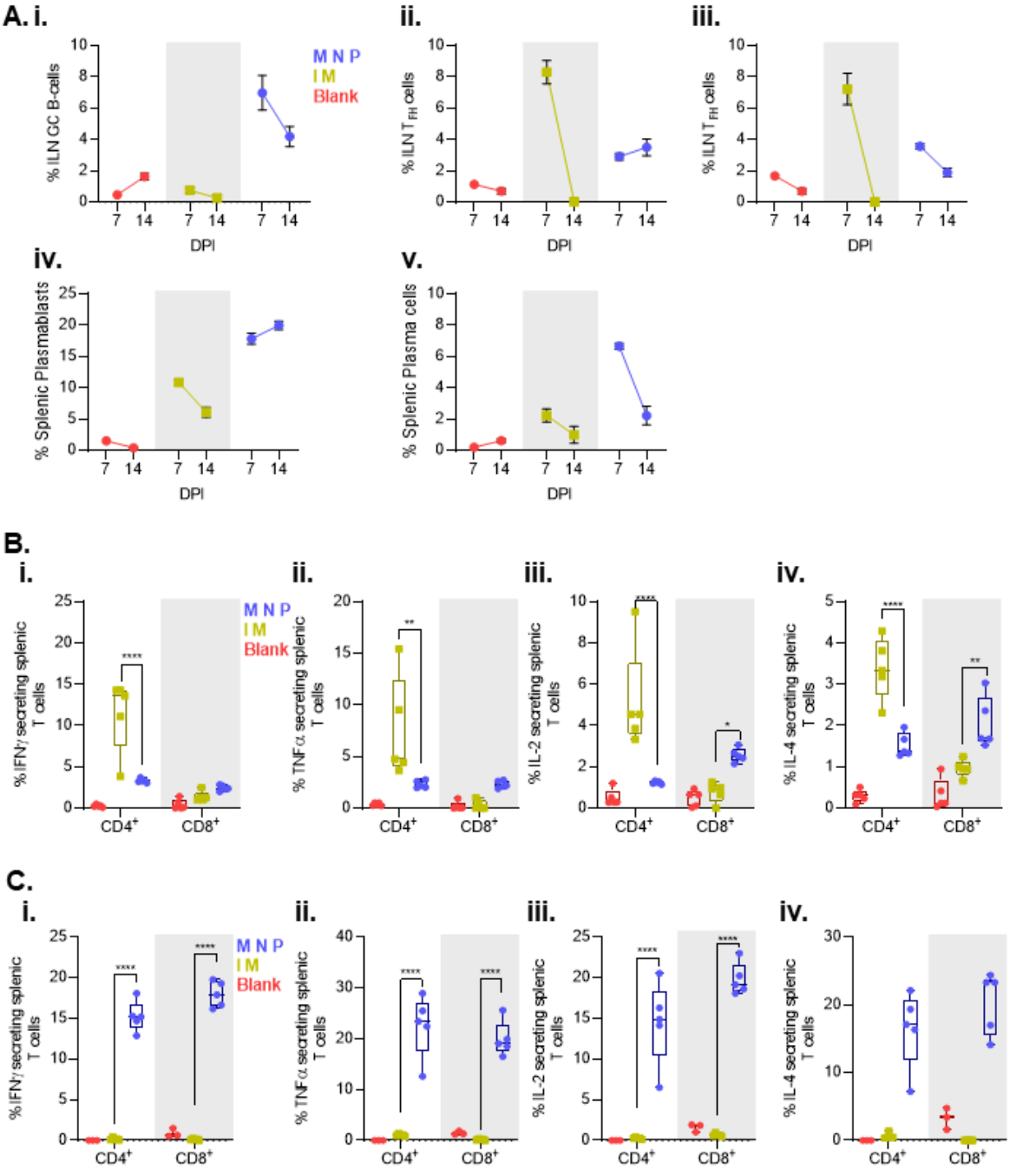
A. i.
ii.
iii.
iv.
v.
% ILN GC B-cells
% ILN T FH cells
% Splenic Plasmablasts
% Splenic Plasma cells
DPI
M N P
I M
Blank
B.
i.
ii.
iii.
iv.
% IFNγ secreting splenic T cells
% TNFα secreting splenic T cells
% IL-2 secreting splenic T cells
% IL-4 secreting splenic T cells
CD4+
CD8+
C.
i.
ii.
iii.
iv.

Figure 2. Cutaneous vaccination generated greater B and T cell responses within 2 weeks after of vaccination.

(A) Kinetics of cellular responses to a single vaccination were evaluated in immune competent female BALB/c mice 7 and 14 DPV (-53 and -46 DPI). Germinal center B cell (i), T_{FH} cell (ii), and follicular $CD8^+$ cell (iii) kinetics were evaluated in inguinal lymph nodes, ILN, (N=10 for -53 DPI; 5 for -46 DPI). Splenic plasmablasts (iv) plasma cell frequencies (v) were also evaluated for systemic humoral responses (N=5 for -53 and -46 DPI). Two-way ANOVA test was used to compare vaccine administration routes between vaccination groups and corrected using Sidak post-host analysis. $CD4^+$ and $CD8^+$ T cell subsets at 7 (B) and 14 (C) days post prime vaccination (-53 and -46 DPI) were analyzed for secretion of IFNγ (i), TNFα (ii), IL-2 (iii), and IL-4 (iv) (N=5). Two-Way ANOVA test was used to compare vaccine administration routes and corrected using Sidak post-host analysis. For all panels, * is $p<0.05$, ** is $p<0.01$, *** is $p<0.001$, and **** is $p<0.0001$. Error bars represent standard deviation for all panels.

FIGURE 3

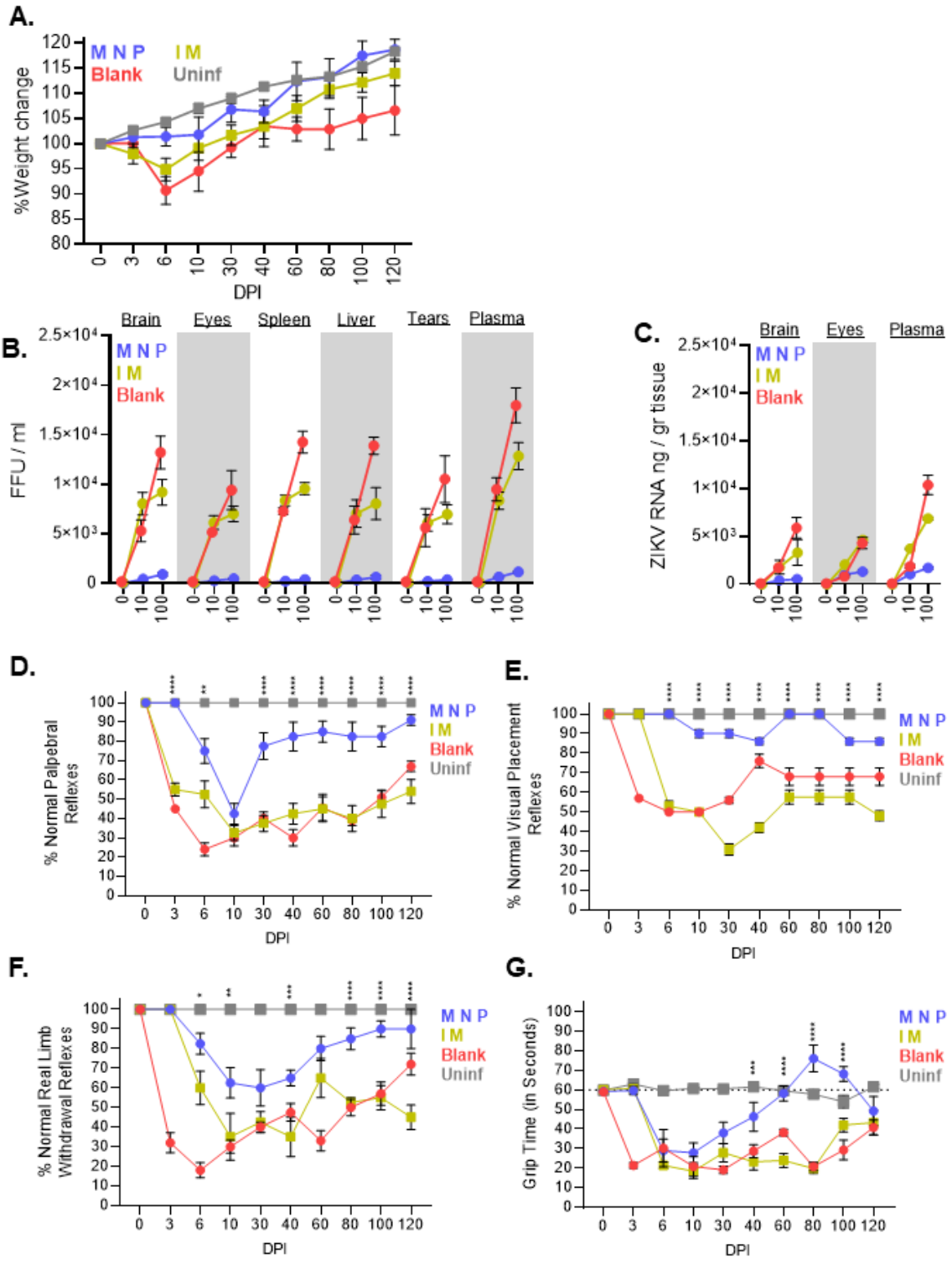
A.
% Weight change
DPI
M N P
I M
Blank
Uninf
B.
FFU / ml
Brain
Eyes
Spleen
Liver
Tears
Plasma
C.
ZIKV RNA ng / gr tissue
D.
% Normal Palpebral Reflexes
E.
% Normal Visual Placement Reflexes
F.
% Normal Real Limb Withdrawal Reflexes
G.
Grip Time (in Seconds)

Figure 3. Cutaneous vaccination reduced viral burden and protected against pathogenic weight loss and neuro-ocular symptoms.

(A) Body weight changes were monitored for 120 DPI (N=10 for all timepoints). (B) Replication competent viral load among systemic organs, immune privileged tissues, and bodily fluids was determined by infectious co-culture (C) at 0, 10, and 100 DPI. (C) Total ZIKV genomic RNA was quantified by qRT-PCR at 0, 10, and 100 DPI (D) (Two-way ANOVA with Sidak's post-hoc; N=5). Ocular clinical scores were determined via palpebral (D) and visual placement (E) reflex tests. (Two-way ANOVA with Sidak's post-hoc; N=10). Motor/neural clinical scores were evaluated by rear-limb withdrawal reflex tests (F) and by grip time tests (G). The horizontal line in panel G denotes the average time a normal mouse should be able to endure test conditions. (Two-way ANOVA with Sidak's post-hoc; N=10). For all panels, * is $p<0.05$, ** is $p<0.01$, *** is $p<0.001$, and **** is $p<0.0001$. P values represent the comparative differences between IM and MNP groups. Error bars represent standard deviation for all panels.

FIGURE 4

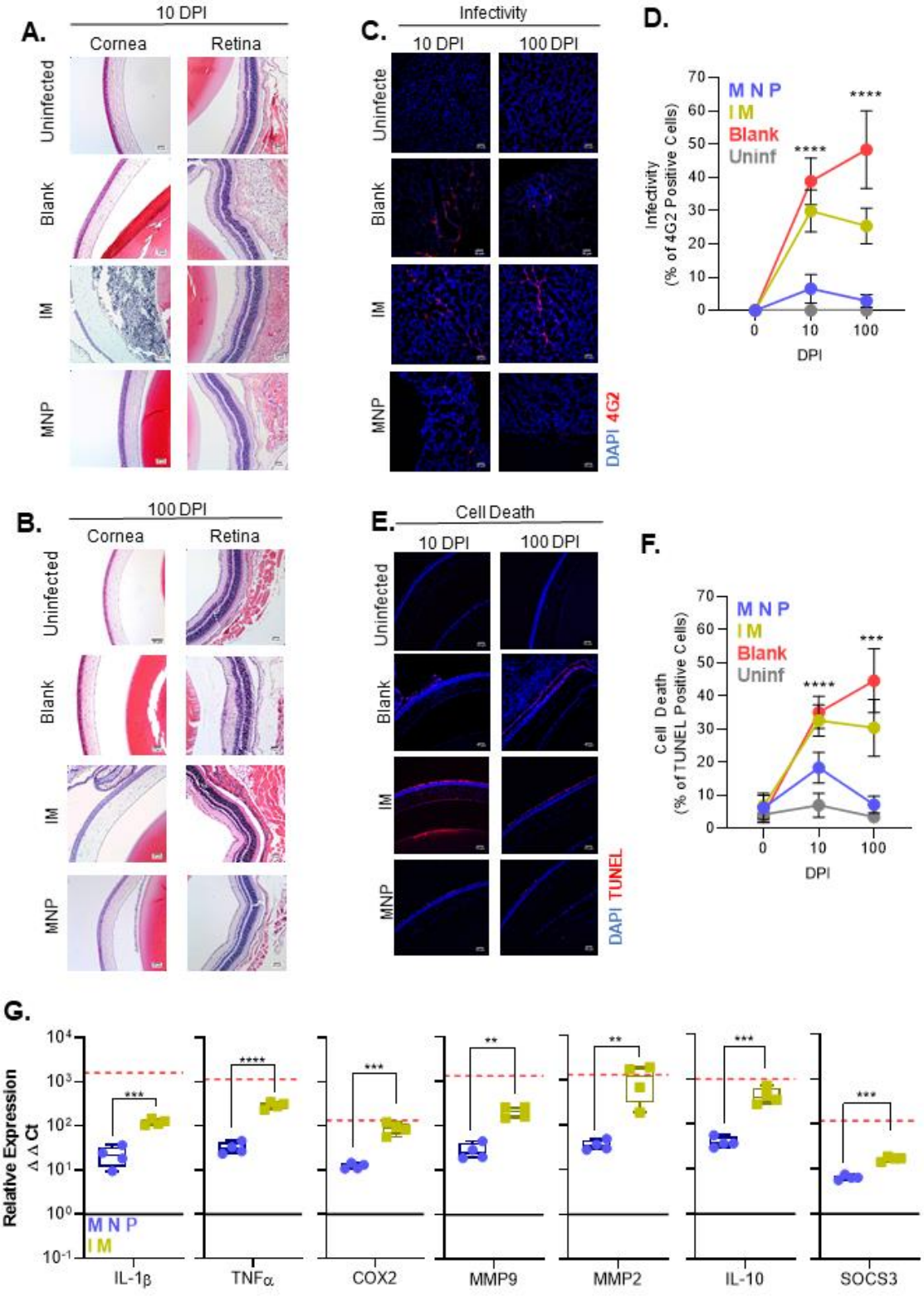
A.
10 DPI
Cornea
Retina
Uninfected
Blank
IM
MNP
B.
100 DPI
Cornea
Retina
Uninfected
Blank
IM
MNP
C.
Infectivity
10 DPI
100 DPI
Uninfecte
Blank
IM
MNP
DAPI 4G2
D.
M N P
I M
Blank
Uninf
Infectivity (% of 4G2 Positive Cells)
DPI
E.
Cell Death
10 DPI
100 DPI
Uninfected
Blank
IM
MNP
DAPI TUNEL
F.
M N P
I M
Blank
Uninf
Cell Death (% of TUNEL Positive Cells)
DPI
G.
Relative Expression Δ Δ Ct
M N P
I M
IL-1β
TNFα
COX2
MMP9
MMP2
IL-10
SOCS3

Figure 4. Low-quality antibodies triggered acute ocular pathology, increased ocular infectivity, and elevated cell death persisting up to 100 DPI.

(A-B) Eyes from infected and uninfected mice were harvested 10 (A) and 100 (B) DPI for H&E and immunofluorescent staining. H&E images of corneal and retinal layers were taken at 20x to assess pathology. (C-D) ZIKV infectivity was determined by immunofluorescent staining for flavivirus antigens. The number antigen foci relative to the number of total cells in the field was calculated for both time points (Two-way ANOVA with Sidak's post-hoc; N=10). (E-F) Similarly, TUNEL staining for cell death was performed at 10 and 100 DPI. Foci were quantified to assess infection-induced cell death (Two-way ANOVA with Sidak's post-hoc; N=10). (G) qRT-PCR on pro-inflammatory proteins, pain mediators, MMPs, and anti-inflammatory proteins among infected brains were normalized to GAPDH and then to expression levels of uninfected controls using the ΔΔCt method. (Two-way ANOVA with Sidak's post-hoc; N=5) Red dashed lines indicate relative expression levels detected in infected mice that received blank vaccinations. For all panels, * is $p<0.05$, ** is $p<0.01$, *** is $p<0.001$, and **** is $p<0.0001$. Error bars in all panels denote standard deviation.

FIGURE 5

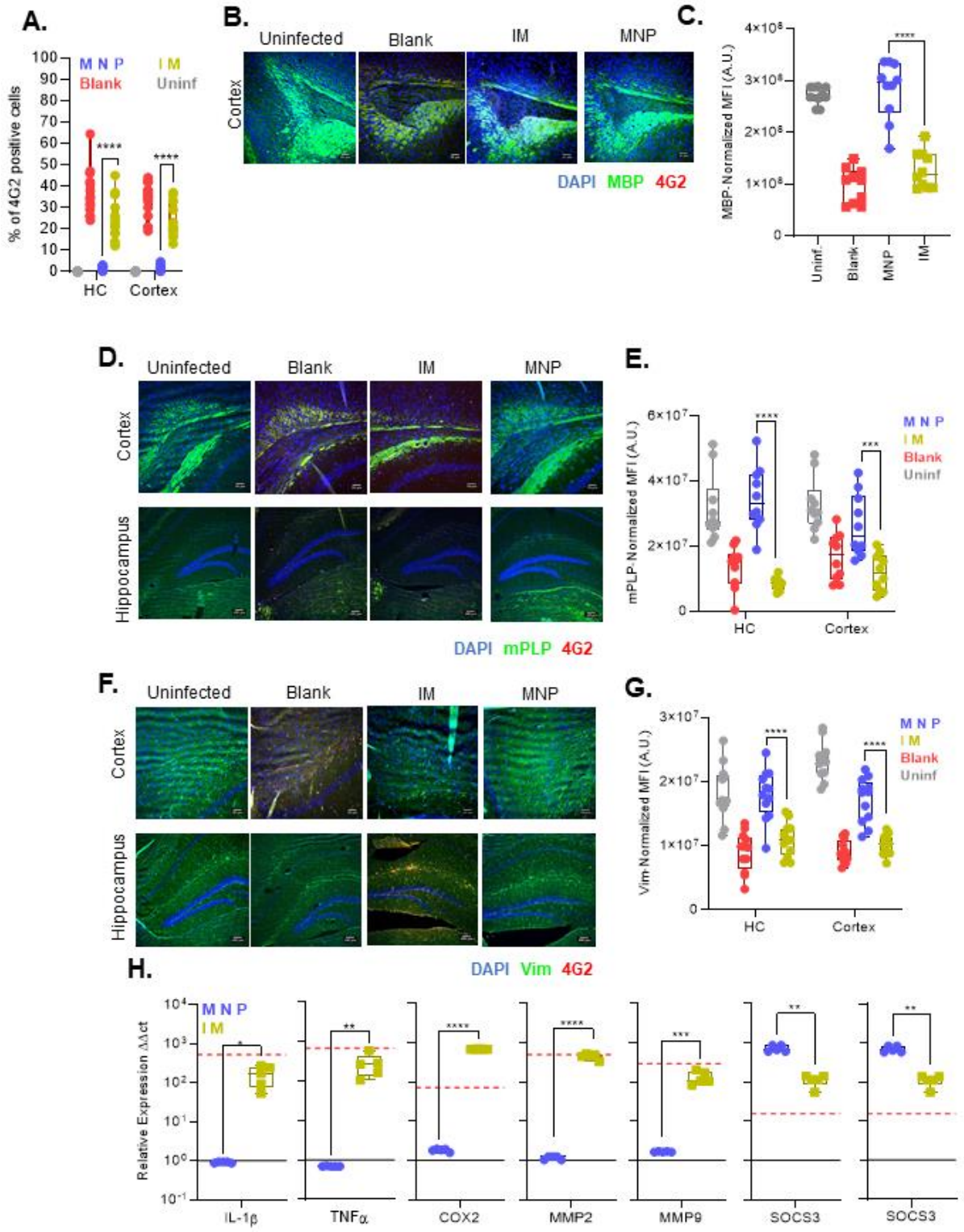
A.
% of 4G2 positive cells
M N P
Blank
I M
Uninf
HC
Cortex
B.
Uninfected
Blank
IM
MNP
Cortex
DAPI MBP 4G2
C.
MBP-Normalized MFI (A.U.)
Uninf.
Blank
MNP
IM
D.
Uninfected
Blank
IM
MNP
Cortex
Hippocampus
DAPI mPLP 4G2
E.
mPLP-Normalized MFI (A.U.)
M N P
I M
Blank
Uninf
HC
Cortex
F.
Uninfected
Blank
IM
MNP
Cortex
Hippocampus
DAPI Vim 4G2
G.
Vim-Normalized MFI (A.U.)
M N P
I M
Blank
Uninf
HC
Cortex
H.
Relative Expression ΔΔct
M N P
I M
IL-1β
TNFα
COX2
MMP2
MMP9
SOCS3
SOCS3

Figure 5. Low-quality antibodies elevated infection, lower myelin expression, and chronically stimulate pro-inflammatory cytokine expression.

(A) Infectivity was determined by analyzing the number of 4G2 positive cells relative to the number of total cells in the field (Two-way ANOVA with Sidak's post-hoc; N=14). (B-C) MBP expression was quantified in mid-brain cortex and hippocampus regions of infected mice (B), and was normalized to background using the CTCF method and was enumerated as normalized MFI (C; One-way ANOVA with Sidak's post-hoc analysis; N=8). (D-E) mPLP expression was similarly quantified in mid-brain cortex (D) and hippocampus (E) regions of infected mice and was normalized to background (Two-way ANOVA with Sidak's post-hoc analysis; N=10). (F-G) Vim expression was quantified in mid-brain cortex and hippocampus regions of infected mice using the CTCF method (F) and was normalized to background (G; Two-way ANOVA with Sidak's post-hoc analysis; N=12). (H) qRT-PCR on pro-inflammatory proteins, pain mediators, MMPs, and anti-inflammatory proteins among infected brains were normalized to GAPDH and then to expression levels of uninfected controls using the ΔΔCt method. (Two-way ANOVA with Sidak's post-hoc; N=5). Red dashed lines indicate relative expression levels detected among infected mice that received blank vaccination controls. For all panels, * is $p<0.05$, ** is $p<0.01$, *** is $p<0.001$, and **** is $p<0.0001$. Error bars in all panels denote standard deviation.

FIGURE 6

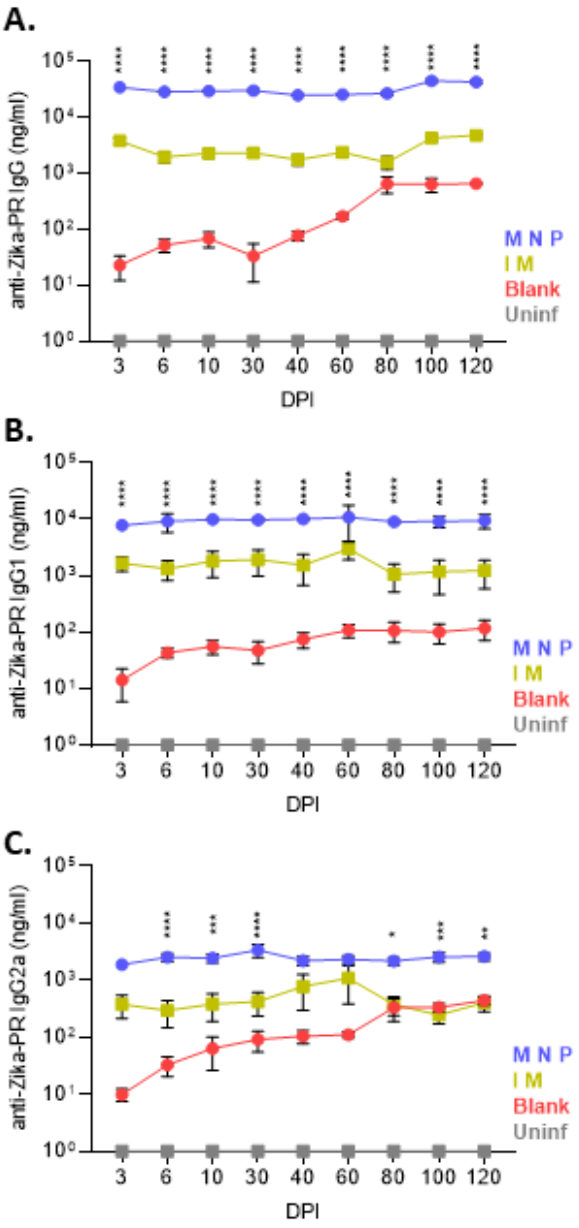
A.
anti-Zika-PR IgG (ng/ml)
DPI
M N P
I M
Blank
Uninf
B.
anti-Zika-PR IgG1 (ng/ml)
DPI
M N P
I M
Blank
Uninf
C.
anti-Zika-PR IgG2a (ng/ml)
DPI
M N P
I M
Blank
Uninf

Figure 6. Antibodies generated by MNP vaccination remain elevated after infection challenge.

ZIKV-specific antibody kinetics were quantified up to 120 DPI for IgG total (A), IgG1 (B), and IgG2a (C). Time-points were analyzed using Two-way ANOVA with Sidak's post-hoc correction (N=10). For all panels, * is $p<0.05$, ** is $p<0.01$, *** is $p<0.001$, and **** is $p<0.0001$. Error bars in all panels denote standard deviation.

FIGURE 7

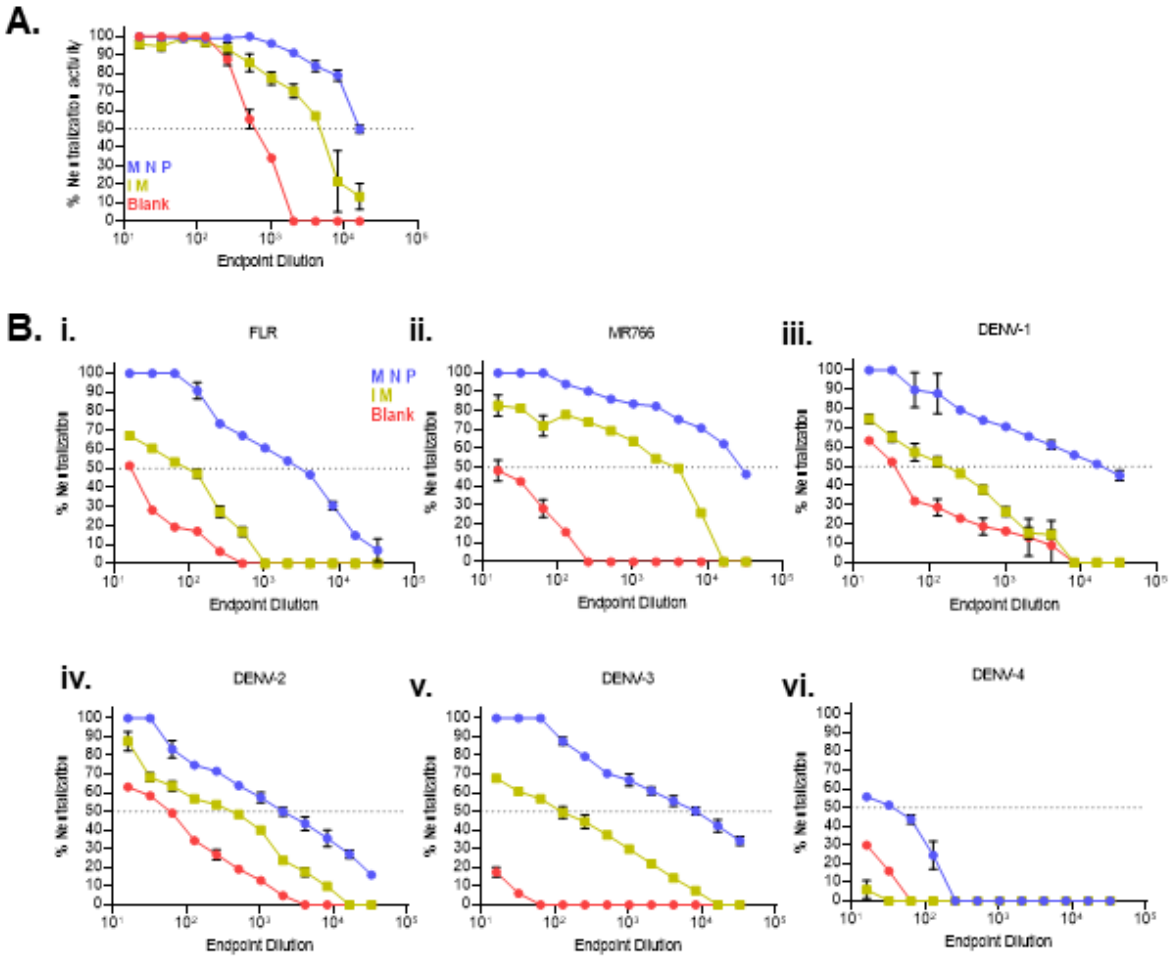

Figure 7. IM-induced antibodies demonstrated lower neutralizing activity than those generated by MNP.

(A) Endpoint IC_{50} antibody dilutions were determined for MNP and IM vaccinated animals 100 DPI using the PRVABC59 strain of ZIKV. (B) Neutralization was also determined using the (i) FLR, and (ii) MR766 strains of ZIKV in addition to (iii) DENV1/Hawaii/1944, (iv) DENV2/16681/Thailand/1964, (v) DENV3/H87/Philippines/1956, and (vi) DENV4/UNC4019/Colombia/2006. The dotted line denotes 50% neutralization. Error bars represent standard deviation for all panels.

FIGURE 8

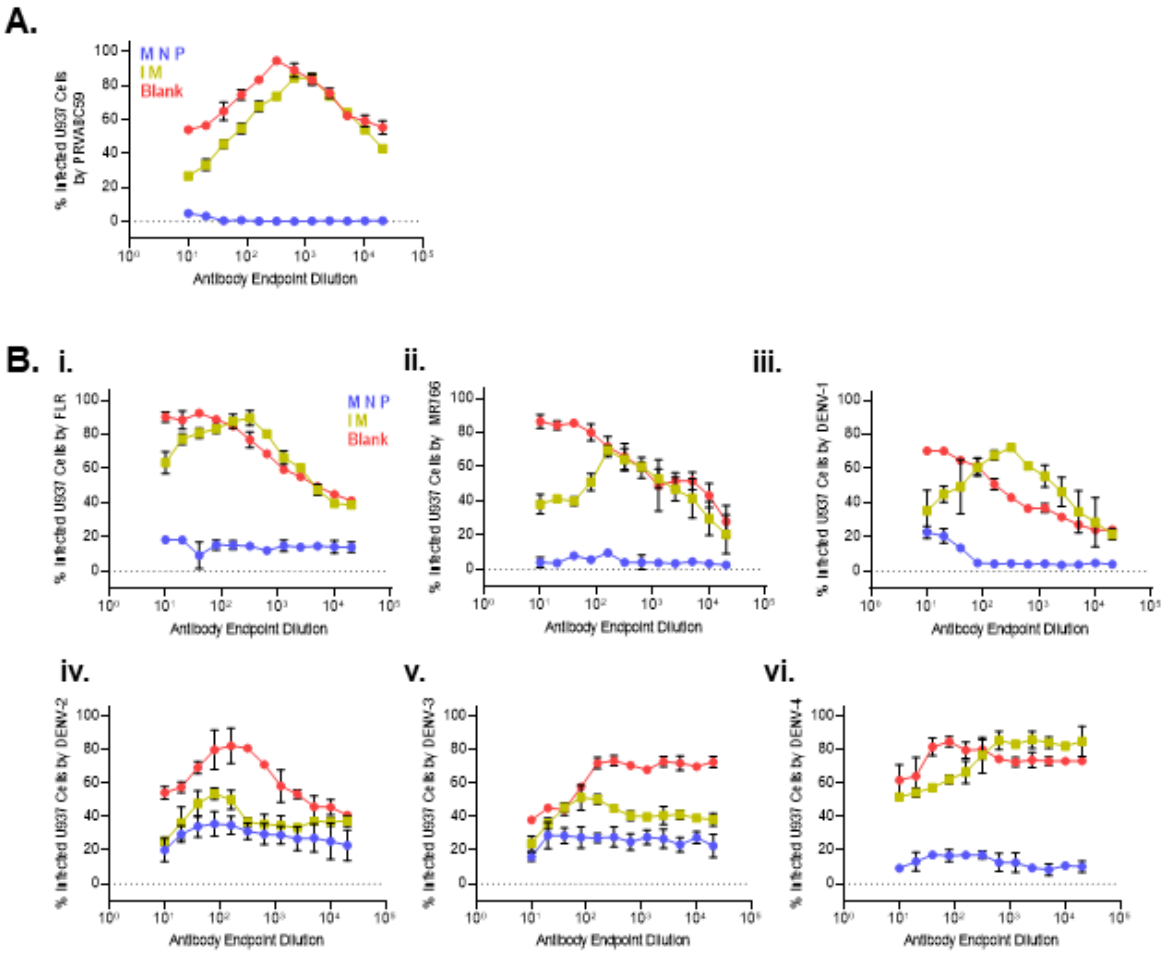

Figure 8. IM-induced antibodies enhanced infection among non-permissive FcγR-bearing cells, whereas MNP antibodies limit ADE. (A) ADE capacity was measured for MNP and IM vaccinated antibodies 100 DPI for the PRVABC59 strain of ZIVK. (B) ADE was also determined using the (i) FLR, and (ii) MR766 strains of ZIKV in addition to (iii) DENV1/Hawaii/1944, (iv) DENV2/16681/Thailand/1964, (v) DENV3/H87/Philippines/1956, and (vi) DENV4/UNC4019/Colombia/2006. The dotted line denotes background fluorescence determined by cells combined with virus but no antibodies. Error bars represent standard deviation for all panels.

FIGURE 9

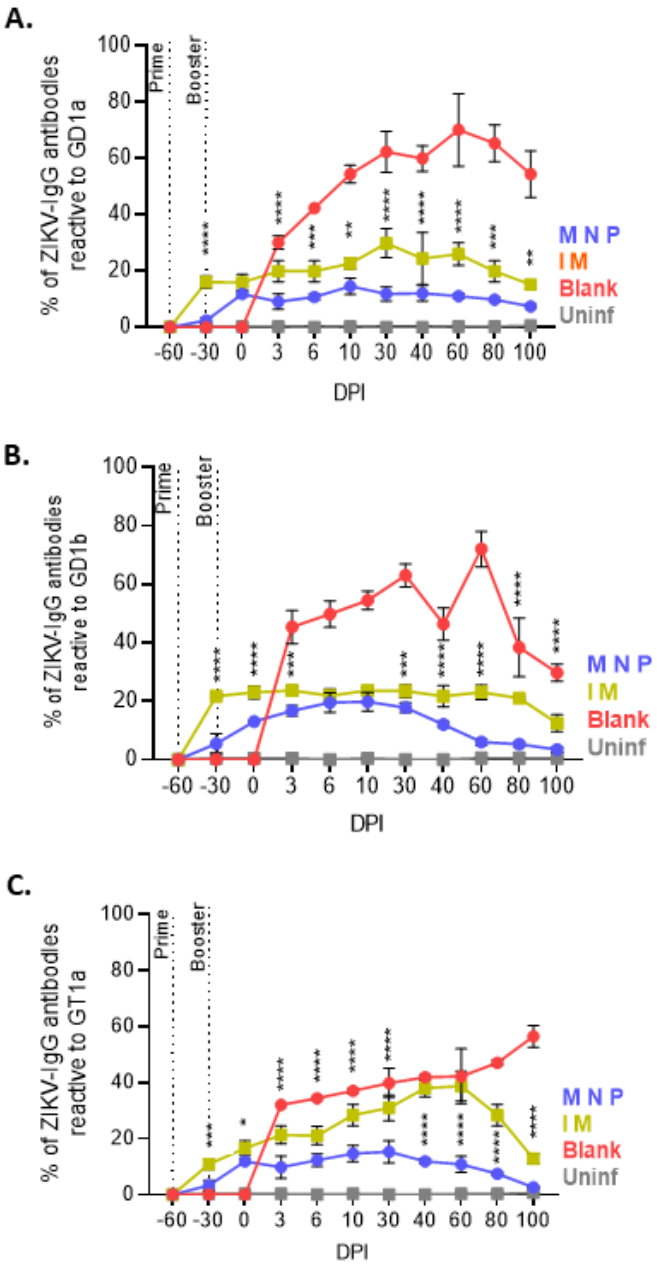

Figure 9. Antibodies generated by MNP vaccination were less auto-reactive to gangliosides. ZIKV-specific antibodies were evaluated for autoreactivity to host gangliosides GD1a (A), GD1b (B), and GT1a (C). (Two-way ANOVA with Sidak's post-hoc; N=5). For all panels, * is $p<0.05$, ** is $p<0.01$, *** is $p<0.001$, and **** is $p<0.0001$. Error bars in all panels denote standard deviation.

SUPPLEMENTARY FIGURE 1

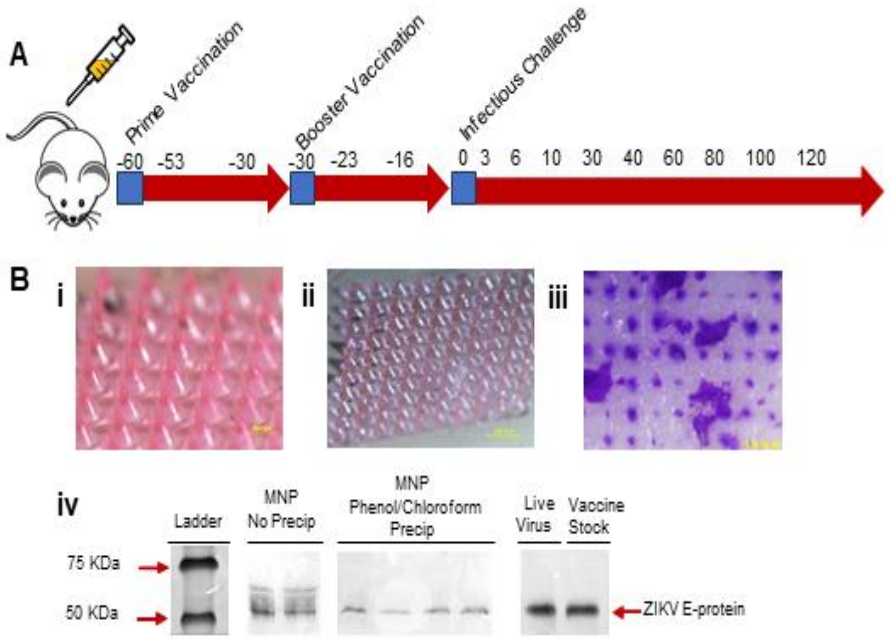

Supplementary Fig 1. ZVIP incorporation into MNP for cutaneous vaccination maintained antigen functionality.

(A) A schematic representation of the prime and booster vaccination schedule used for all vaccinated mice. Animals were given a prime vaccination of 4µg of ZIKV-PRVABC59 inactivated particles by either IM or MNP administration, or a blank MNP as a control (on -60 DPI). Thirty days after prime administration 30 DPV (-30 DPI), all animals received a booster vaccination, identical to their first. Animals were challenged with live virus homologous to the vaccine 30 days after booster vaccination (0 DPI). (B) ZVIP was successfully integrated into polymer patches (i) and did not interfere with patch dissolution (ii). Vaccine-loaded patches demonstrated rigidity by successful insertion in porcine cadaver skin as evidenced by the tissue-marking dye after patch removal (iii). Western blot analysis demonstrated successful incorporation and isolation of ZVIP in MNP after staining for ZIKV E-protein (iv).

SUPPLEMENTARY FIGURE 2

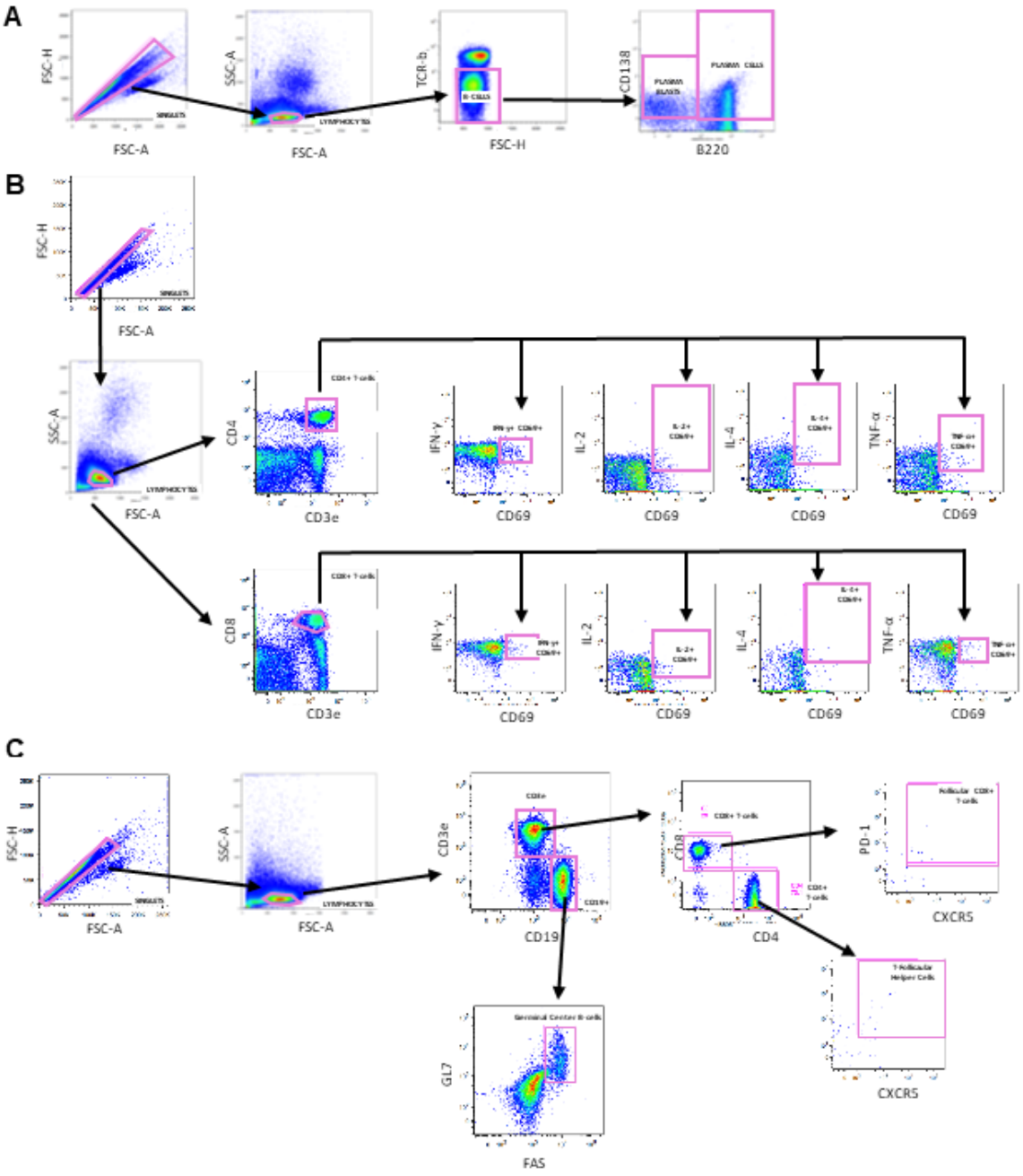

Supplementary Fig 2. Gating strategies utilized for flow cytometry experiments.

(A) Singlets were isolated, and then lymphocytes were selected. Splenic plasma cells and plasmablasts were identified as TCRβ$^-$/B220$^-$/CD138$^+$ plasma cells and TCRβ$^-$/B220$^+$/CD138$^+$ plasmablasts. (B) Singlets were isolated, and then lymphocytes were selected. CD4$^+$ T cells (CD3ε$^+$/CD4$^+$), and CD8$^+$ T cells (CD3ε$^+$/CD8$^+$). were gated as CD69+/IFNγ+, CD69+/TNF-α+, CD69$^+$/IL-2$^+$, and CD69$^+$/IL-4$^+$secreting CD4$^+$ and CD8$^+$ T cells. (C) Singlets were isolated, and then lymphocytes were gated as either CD19$^+$ or CD3ε$^+$ cells. CD3ε$^+$ cells were gated for CD4$^+$ or CD8$^+$ T cells populations and further gated for follicular cells (PD-1$^+$/CXCR5$^+$). CD19$^+$ cells were then gated as GL7$^+$/FAS$^+$ germinal center (GC).

SUPPLEMENTARY FIGURE 3

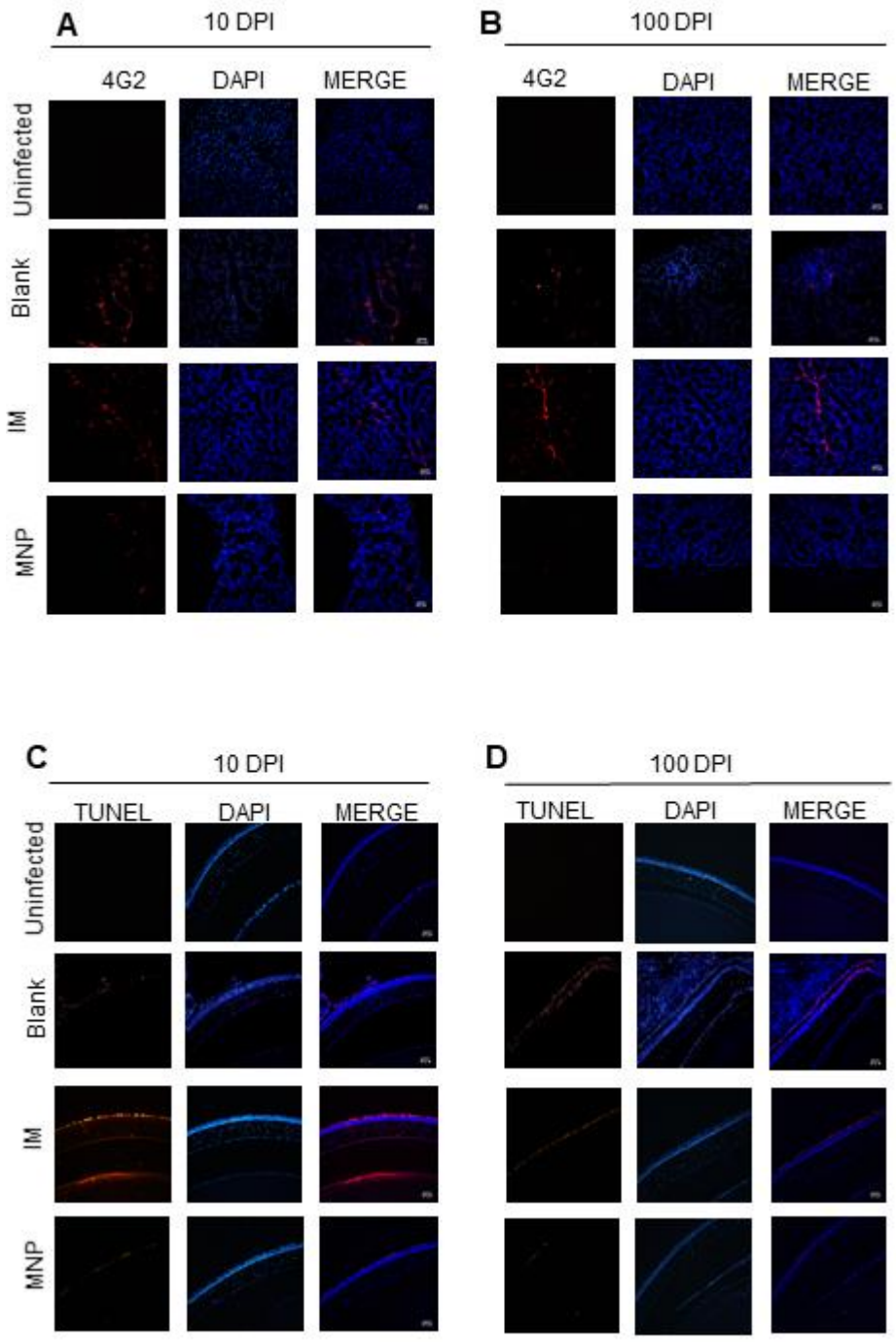

Supplementary Fig 3. MNP conferred protection against intraocular apoptosis and necroptosis induced by ZIKV infection.

(A-B) Infectivity among eye tissues was determined via 4G2 immunofluorescent labeling of ZIKV E-protein in cells at 10 (A) and 100 (B) DPI. Individual panels show 4G2 ZIKV-antigen in red, DAPI in blue, and a final merge. (C-D) Immunofluorescent cell death was determined via TUNEL stain for fragmented DNA at 10 (C) and 100 (D) DPI. Individual panels show TUNEL-positive cells in red, DAPI in blue, and a final merge. Images were taken at 20x magnification with a scale-bar of 100 μm (bottom right corner).

SUPPLEMENTARY FIGURE 4

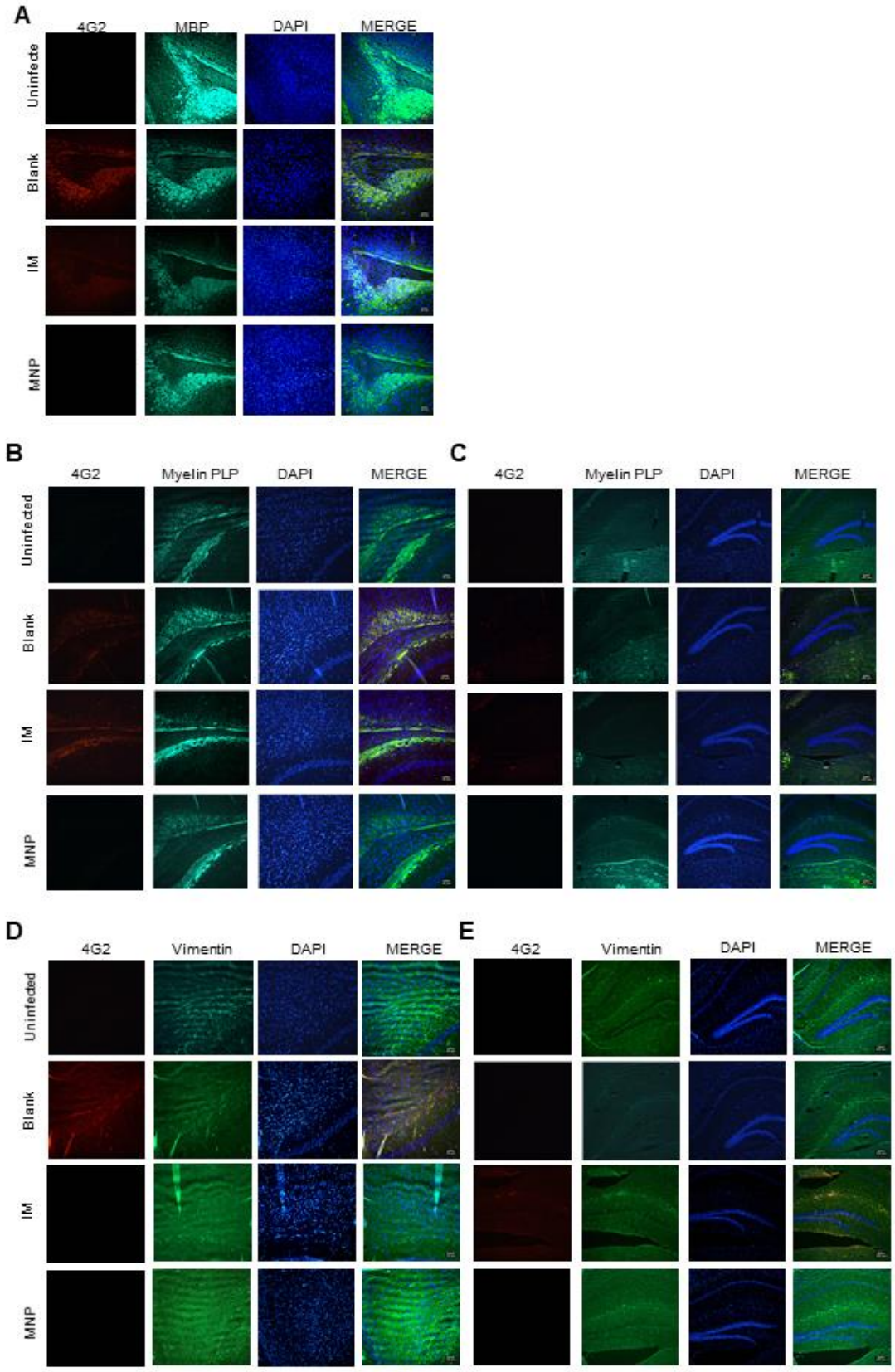

Supplementary Fig 4. MNP protected against ZIKV-induced demyelination.

(A) Individual fluorescent panels show MBP expression in cortex regions of infected animals 100 DPI. Images were taken at 20x magnification with a scale-bar of 100 μm (bottom right corner). (B-C) Individual fluorescent panels show myelin PLP expression in cortex (B) and hippocampus (C) regions of infected animals 100 DPI. Images were taken at 20x magnification with a scale-bar of 100 μm (bottom right corner). (D-E) Individual fluorescent panels show vimentin expression in cortex (D) and hippocampus (E) regions of infected animals 100 DPI. All images were stained with DAPI (blue); MBP, myelin PLP, or vimentin (green); and the ZIKV E-protein via 4G2 (red). Images were taken at 20x magnification with a scale-bar of 100 μm (bottom right corner).

A.

	Endpoint Antibody Titer		
Virus / Strain	**MNP**	**IM**	**Blank**
ZIKV – PRVABC59	11,815	3,265	628
ZIKV – FLR	1,915	81	16
ZIKV – MR766	26,887	3,313	16
DENV - 1	21,818	208	33
DENV - 2	1,702	397	61
DENV - 3	9,291	185	0
DENV - 4	30	2	0

B.

	Maximum Infectivity			Antibody Titer of Max Infectivity		
Virus / Strain	**MNP**	**IM**	**Blank**	**MNP**	**IM**	**Blank**
ZIKV – PRVABC59	5%	84.6%	95%	10	640	320
ZIKV – FLR	10%	70%	86%	160	160	40
ZIKV – MR766	18%	90%	92%	20	320	40
DENV - 1	22%	72%	70%	10	320	20
DENV - 2	36%	54%	85%	80	80	160
DENV - 3	24%	41%	64%	160	40	320
DENV - 4	19%	86%	84%	40	640	80

Supplementary Tables summarizing the neutralization and ADE qualities of vaccination induced antibodies.

(A) Table of IC_{50} antibody titers for MNP and IM vaccinations, and for PRVABC59 infection following blank vaccination. (B) Table detailing the maximum infectivity observed for MNP, IM, and infection only groups for each virus used. Antibody titers for each corresponding infectivity are also provided.

CHAPTER IV: CONCLUSIONS

ZIKV garnered international attention because of its rapid international expansion since 2015 when an epidemic struck Brazil, resulting in a newly identified pathology including severe neurological impairments such as microcephaly, which is now part of the congenital ZIKV syndrome, as well as Guillain-Barré syndrome afflicting adult population (1). The World Health Organization declared ZIKV a Public Health Emergency of International Concern in February 2016, during which time ZIKV was spreading rapidly across South America, the Caribbean, and into the United States (1). This precarious outbreak in Brazil spread across the western continents raising critical questions regarding virus evolution. Prior to 2015, ZIKV infections were limited geographically to Africa and Asia and were reported to be asymptomatic, and approximately 20% mildly symptomatic represented as a self-limiting febrile illness with most common symptoms maculopapular rash, conjunctivitis, and joint pain (2). In 2020, ZIKV has receded into the background amid the global coronavirus pandemic, with minimal cases reported from major endemic countries (263). While the number of reported cases may be directly attributed to herd immunity against ZIKV and better regional control of arbovirus vectors, the impact of ZIKV still echoes today as infants born from ZIKV-infected mothers provide a unique window into fetal-maternal transmission, immunity, and into the long-term impacts of viral infection among neonates and infants as they develop into toddlers and small children.

This dissertation focused on the long-term impacts of ZIKV infection, as the most severe symptoms and consequences of ZIKV often only manifest at late timepoints following infection. In short, this dissertation focused on defining a long-term mouse model for ZIKV pathogenesis and then utilizing it to evaluate efficacy of differential vaccine delivery platforms.

In Chapter II, I found treating mice with a monoclonal antibody that functionally blocked IFNAR signaling, resulting in a dramatic skewing of survival and pathology data. Indeed, animals that received the α-IFNAR antibody reached moribund endpoints that required euthanasia within 14 days of infection, while animals that were immune competent demonstrated these same endpoints at frequencies similar to human infections (264). My research revealed neuro-ocular pathology manifested within 3 days after infection among competent mice and persisted with variable severity up to 120 days after infection. The ocular sequelae observed in this dissertation were comparable to other studies investigating ZIKV infections in eye tissues in suckling mice (98), and to studies investigating mechanisms of ocular infiltration by ZIKV via infection of the blood-retinal barrier and the trabecular meshwork (95, 234).

While most research on ZIKV-induced neuro-ocular pathology focuses on quantifying specific phenomena, such as single limb paralysis (142), only at one timepoint, to demonstrate the presence of ZIKV-CNS pathology, I wanted to develop a more comprehensive diagnostic method to evaluate inflammatory damage and functional aberrations that result ZIKV in the neuro-ocular compartment. The optimization of these clinical tests revealed that inflammation in immune-privileged compartments lasted up to 120 days. Even at late timepoints, neuro-ocular clinical scoring abnormalities correlated with strong pro-inflammatory transcription and intracranial demyelination. Demyelination and intracranial inflammation correlate strongly with work published by Garber et al., which suggests that flavivirus infection-induced neuronal damage is mediated by T cells infiltrating the brain and responding to virally-infected neurons (192).

In this dissertation, I did not investigate T cell specific responses in immune privileged compartments at early or late stages of infection; my research mainly focused on evaluating known biomarkers of GBS among infected mice, namely autoreactive anti-ganglioside antibodies.

Gangliosides are a class of sphingoceramides, or heavily glycosylated lipids, that are present on CNS cell surfaces and play critical roles in myelin sheath function, regulating axon growth and regeneration, and the function of neural networks (265, 266). During GBS, naturally occurring glycosylation moieties on the pathogen's surface resemble ganglioside residues, and thus early response antibodies may be directed against these mimetic surface patterns (267). While several variant forms of GBS exist, in this dissertation I chose to investigate 3 specific gangliosides, GD1a, GD1b, and GT1awhich are linked to acute motor axonal neuropathy, sensory ataxia, and an ocular form of GBS called Miller-Fisher syndrome, respectively (232). The work in this dissertation is the first to evaluate the autoreactivity of host antibodies following ZIKV infection, as a correlate of host immunity, following infection or vaccination. While elevated levels of host antibodies were found in unvaccinated infected mice to be reactive to gangliosides, it is important to emphasize that they are a subset of antibodies generated by ZIKV, therefore we presented ganglioside antibodies as a proportion of total anti-ZIKV antibodies.

In synopsis, my dissertation bridges knowledge gaps in both ZIKV pathogenesis and host immune responses, by highlighting adverse, antibody mediated pathology during ZIKV infection in long-term studies and amelioration of side effects following skin vaccination. I demonstrate that competent mice can be used to investigate neuro-ocular, GBS-like pathology and that the same model can be utilized for prophylactic vaccination studies. I show that IM vaccinations without an adjuvant provide a transient germinal center response, with B and T cells that do not endure beyond 7 days after vaccination. Antibodies generated by 2 sequential IM vaccinations demonstrated elevated breadth of immunity among non-homologous ZIKV and DENV viruses, albeit with little functional protection against non-resolving intracranial demyelination and ocular hydropic retinal degeneration. The same IM-induced antibodies appeared to offer no protection against viral

tropism in cells that are usually non-permissive to infection but can be infected by ADE mechanisms. Cutaneous vaccination using dissolving MNPs demonstrated germinal center B cell and T cell populations continuous expansion 14 days after infection. Skin vaccination demonstrated superior results in effector vaccine-specific CD4 and CD8 populations compared to their IM counterparts. Antibodies generated by MNP vaccination showed elevated antibody-antigen avidity and higher total vaccine-specific titers at all timepoints before and after infectious challenge. These antibodies also showed greater breadth of immunity among ZIKV and DENV viruses and limited ADE infection among non-permissive Fcγ-R.

REFERENCES

1. Dowall SD, Graham VA, Rayner E, Hunter L, Atkinson B, Pearson G, et al. Lineage-dependent differences in the disease progression of Zika virus infection in type-I interferon receptor knockout (A129) mice. PLoS Negl Trop Dis. 2017;11(7):e0005704.
2. Wang L, Valderramos SG, Wu A, Ouyang S, Li C, Brasil P, et al. From Mosquitos to Humans: Genetic Evolution of Zika Virus. Cell Host Microbe. 2016;19(5):561-5.
3. Dick GW, Haddow AJ. Uganda S virus; a hitherto unrecorded virus isolated from mosquitoes in Uganda. I. Isolation and pathogenicity. Trans R Soc Trop Med Hyg. 1952;46(6):600-18.
4. Weaver SC, Costa F, Garcia-Blanco MA, Ko AI, Ribeiro GS, Saade G, et al. Zika virus: History, emergence, biology, and prospects for control. Antiviral Res. 2016;130:69-80.
5. Costa F, Sarno M, Khouri R, de Paula Freitas B, Siqueira I, Ribeiro GS, et al. Emergence of Congenital Zika Syndrome: Viewpoint From the Front Lines. Ann Intern Med. 2016;164(10):689-91.
6. Macnamara FN. Zika virus: a report on three cases of human infection during an epidemic of jaundice in Nigeria. Trans R Soc Trop Med Hyg. 1954;48(2):139-45.
7. Duffy MR, Chen T-H, Hancock WT, Powers AM, Kool JL, Lanciotti RS, et al. Zika Virus Outbreak on Yap Island, Federated States of Micronesia. New England Journal of Medicine. 2009;360(24):2536-43.
8. Horwood P, Bande G, Dagina R, Guillaumot L, Aaskov J, Pavlin B. The threat of chikungunya in Oceania. Western Pac Surveill Response J. 2013;4(2):8-10.
9. Buathong R, Hermann L, Thaisomboonsuk B, Rutvisuttinunt W, Klungthong C, Chinnawirotpisan P, et al. Detection of Zika Virus Infection in Thailand, 2012-2014. Am J Trop Med Hyg. 2015;93(2):380-3.
10. Oehler E, Watrin L, Larre P, Leparc-Goffart I, Lastere S, Valour F, et al. Zika virus infection complicated by Guillain-Barre syndrome--case report, French Polynesia, December 2013. Euro Surveill. 2014;19(9).
11. Faria NR, Azevedo RD, Kraemer MU, Souza R, Cunha MS, Hill SC, et al. Zika virus in the Americas: Early epidemiological and genetic findings. Science. 2016.
12. WHO. Zika virus, Microcephaly and Guillain-Barré syndrome. 2016.
13. Tognarelli J, Ulloa S, Villagra E, Lagos J, Aguayo C, Fasce R, et al. A report on the outbreak of Zika virus on Easter Island, South Pacific, 2014. Arch Virol. 2016;161(3):665-8.
14. Cao-Lormeau VM, Roche C, Teissier A, Robin E, Berry AL, Mallet HP, et al. Zika virus, French polynesia, South pacific, 2013. Emerg Infect Dis. 2014;20(6):1085-6.
15. Passos SRL, Borges Dos Santos MA, Cerbino-Neto J, Buonora SN, Souza TML, de Oliveira RVC, et al. Detection of Zika Virus in April 2013 Patient Samples, Rio de Janeiro, Brazil. Emerg Infect Dis. 2017;23(12):2120-1.
16. Brasil P, Calvet GA, Siqueira AM, Wakimoto M, de Sequeira PC, Nobre A, et al. Zika Virus Outbreak in Rio de Janeiro, Brazil: Clinical Characterization, Epidemiological and Virological Aspects. PLoS Negl Trop Dis. 2016;10(4):e0004636.
17. Mattar S, Ojeda C, Arboleda J, Arrieta G, Bosch I, Botia I, et al. Case report: microcephaly associated with Zika virus infection, Colombia. BMC Infect Dis. 2017;17(1):423.
18. Zonneveld R, Roosblad J, Staveren JW, Wilschut JC, Vreden SG, Codrington J. Three atypical lethal cases associated with acute Zika virus infection in Suriname. IDCases. 2016;5:49-53.
19. Benjamin I, Fernandez G, Figueira JV, Parpacen L, Urbina MT, Medina R. Zika virus detected in amniotic fluid and umbilical cord blood in an in vitro fertilization-conceived pregnancy in Venezuela. Fertil Steril. 2017;107(6):1319-22.
20. Calvet G, Aguiar RS, Melo AS, Sampaio SA, de Filippis I, Fabri A, et al. Detection and sequencing of Zika virus from amniotic fluid of fetuses with microcephaly in Brazil: a case study. The Lancet Infectious diseases. 2016.

21. Oliveira Melo AS, Malinger G, Ximenes R, Szejnfeld PO, Alves Sampaio S, Bispo de Filippis AM. Zika virus intrauterine infection causes fetal brain abnormality and microcephaly: tip of the iceberg? Ultrasound Obstet Gynecol. 2016;47(1):6-7.
22. Mlakar J, Korva M, Tul N, Popovic M, Poljsak-Prijatelj M, Mraz J, et al. Zika Virus Associated with Microcephaly. N Engl J Med. 2016.
23. Sarno M, Sacramento GA, Khouri R, do Rosario MS, Costa F, Archanjo G, et al. Zika Virus Infection and Stillbirths: A Case of Hydrops Fetalis, Hydranencephaly and Fetal Demise. PLoS Negl Trop Dis. 2016;10(2):e0004517.
24. Martines RB, Bhatnagar J, Keating MK, Silva-Flannery L, Muehlenbachs A, Gary J, et al. Notes from the Field: Evidence of Zika Virus Infection in Brain and Placental Tissues from Two Congenitally Infected Newborns and Two Fetal Losses - Brazil, 2015. MMWR Morbidity and mortality weekly report. 2016;65(6):159-60.
25. Brasil P, Nielsen-Saines K. More pieces to the microcephaly-Zika virus puzzle in Brazil. The Lancet Infectious diseases. 2016;16(12):1307-9.
26. Wang L, Zhao H, Oliva SM, Zhu H. Modeling the transmission and control of Zika in Brazil. Sci Rep. 2017;7(1):7721.
27. Ye Q, Liu ZY, Han JF, Jiang T, Li XF, Qin CF. Genomic characterization and phylogenetic analysis of Zika virus circulating in the Americas. Infect Genet Evol. 2016;43:43-9.
28. Smith DR, Sprague TR, Hollidge BS, Valdez SM, Padilla SL, Bellanca SA, et al. African and Asian Zika Virus Isolates Display Phenotypic Differences Both In Vitro and In Vivo. Am J Trop Med Hyg. 2018;98(2):432-44.
29. Fritz R, Blazevic J, Taucher C, Pangerl K, Heinz FX, Stiasny K. The unique transmembrane hairpin of flavivirus fusion protein E is essential for membrane fusion. J Virol. 2011;85(9):4377-85.
30. Goertz GP, Abbo SR, Fros JJ, Pijlman GP. Functional RNA during Zika virus infection. Virus Res. 2017.
31. Akiyama BM, Laurence HM, Massey AR, Costantino DA, Xie X, Yang Y, et al. Zika virus produces noncoding RNAs using a multi-pseudoknot structure that confounds a cellular exonuclease. Science. 2016;354(6316):1148-52.
32. Filomatori CV, Carballeda JM, Villordo SM, Aguirre S, Pallares HM, Maestre AM, et al. Dengue virus genomic variation associated with mosquito adaptation defines the pattern of viral non-coding RNAs and fitness in human cells. PLoS Pathog. 2017;13(3):e1006265.
33. Donald CL, Brennan B, Cumberworth SL, Rezelj VV, Clark JJ, Cordeiro MT, et al. Full Genome Sequence and sfRNA Interferon Antagonist Activity of Zika Virus from Recife, Brazil. PLoS Negl Trop Dis. 2016;10(10):e0005048.
34. Haddow AD, Schuh AJ, Yasuda CY, Kasper MR, Heang V, Huy R, et al. Genetic characterization of Zika virus strains: geographic expansion of the Asian lineage. PLoS Negl Trop Dis. 2012;6(2):e1477.
35. Yokoyama S, Starmer WT. Possible Roles of New Mutations Shared by Asian and American Zika Viruses. Mol Biol Evol. 2017;34(3):525-34.
36. Metsky HC, Matranga CB, Wohl S, Schaffner SF, Freije CA, Winnicki SM, et al. Zika virus evolution and spread in the Americas. Nature. 2017;546(7658):411-5.
37. Weaver SC. Emergence of Epidemic Zika Virus Transmission and Congenital Zika Syndrome: Are Recently Evolved Traits to Blame? MBio. 2017;8(1).
38. Gong Z, Xu X, Han GZ. The Diversification of Zika Virus: Are There Two Distinct Lineages? Genome Biol Evol. 2017;9(11):2940-5.
39. Anfasa F, Siegers JY, van der Kroeg M, Mumtaz N, Stalin Raj V, de Vrij FMS, et al. Phenotypic Differences between Asian and African Lineage Zika Viruses in Human Neural Progenitor Cells. mSphere. 2017;2(4).

40. Enfissi A, Codrington J, Roosblad J, Kazanji M, Rousset D. Zika virus genome from the Americas. Lancet. 2016;387(10015):227-8.
41. Gong Z, Gao Y, Han GZ. Zika Virus: Two or Three Lineages? Trends Microbiol. 2016;24(7):521-2.
42. Faye O, Freire CC, Iamarino A, Faye O, de Oliveira JV, Diallo M, et al. Molecular evolution of Zika virus during its emergence in the 20(th) century. PLoS Negl Trop Dis. 2014;8(1):e2636.
43. Lin SR, Zou G, Hsieh SC, Qing M, Tsai WY, Shi PY, et al. The helical domains of the stem region of dengue virus envelope protein are involved in both virus assembly and entry. J Virol. 2011;85(10):5159-71.
44. Yuan L, Huang XY, Liu ZY, Zhang F, Zhu XL, Yu JY, et al. A single mutation in the prM protein of Zika virus contributes to fetal microcephaly. Science. 2017;358(6365):933-6.
45. Dai L, Song J, Lu X, Deng YQ, Musyoki AM, Cheng H, et al. Structures of the Zika Virus Envelope Protein and Its Complex with a Flavivirus Broadly Protective Antibody. Cell Host Microbe. 2016;19(5):696-704.
46. Kostyuchenko VA, Lim EX, Zhang S, Fibriansah G, Ng TS, Ooi JS, et al. Structure of the thermally stable Zika virus. Nature. 2016;533(7603):425-8.
47. Naik NG, Wu HN. Mutation of Putative N-Glycosylation Sites on Dengue Virus NS4B Decreases RNA Replication. J Virol. 2015;89(13):6746-60.
48. Grard G, Caron M, Mombo IM, Nkoghe D, Mboui Ondo S, Jiolle D, et al. Zika virus in Gabon (Central Africa)--2007: a new threat from Aedes albopictus? PLoS Negl Trop Dis. 2014;8(2):e2681.
49. Musso D, Nilles EJ, Cao-Lormeau VM. Rapid spread of emerging Zika virus in the Pacific area. Clin Microbiol Infect. 2014;20(10):O595-6.
50. Lourenco-de-Oliveira R, Rua AV, Vezzani D, Willat G, Vazeille M, Mousson L, et al. Aedes aegypti from temperate regions of South America are highly competent to transmit dengue virus. BMC Infect Dis. 2013;13:610.
51. Chouin-Carneiro T, Vega-Rua A, Vazeille M, Yebakima A, Girod R, Goindin D, et al. Differential Susceptibilities of Aedes aegypti and Aedes albopictus from the Americas to Zika Virus. PLoS Negl Trop Dis. 2016;10(3):e0004543.
52. Dick GW, Kitchen SF, Haddow AJ. Zika virus. I. Isolations and serological specificity. Trans R Soc Trop Med Hyg. 1952;46(5):509-20.
53. Hayes EB. Zika virus outside Africa. Emerg Infect Dis. 2009;15(9):1347-50.
54. Berthet N, Nakoune E, Kamgang B, Selekon B, Descorps-Declere S, Gessain A, et al. Molecular characterization of three Zika flaviviruses obtained from sylvatic mosquitoes in the Central African Republic. Vector Borne Zoonotic Dis. 2014;14(12):862-5.
55. Guedes DR, Paiva MH, Donato MM, Barbosa PP, Krokovsky L, Rocha S, et al. Zika virus replication in the mosquito Culex quinquefasciatus in Brazil. Emerg Microbes Infect. 2017;6(8):e69.
56. Brasil P, Pereira JP, Jr., Moreira ME, Ribeiro Nogueira RM, Damasceno L, Wakimoto M, et al. Zika Virus Infection in Pregnant Women in Rio de Janeiro. N Engl J Med. 2016;375(24):2321-34.
57. Services DCHaH. DCHHS reports first Zika virus case in the Dallas Country acquired through sexual transmission. Online: DCHHS; 2016 [Available from: http://www.dallascounty.org/department/hhs/press/documents/PR2-216DCHHSReportsFirstCaseofZikaVirusThroughSexualTransmission.pdf
58. Foy BD KK, Chilson Foy JL, Blitvich BJ, Travassos da Rosa A, Haddow AD, et al. Probable non-vector-borne transmission of Zika virus, Colorado, USA. Online: Emerging Infectious Diseases; 2016 [
59. Musso D RC, Robin E, Nhan T, Teissier A, CaoLormeau VM. Potential sexual transmission of Zika virus. Emerging Infectious Diseases: Online; 2015 [
60. Atkinson B HP, Afrough B, Lumley S, Carter D, Aarons EJ, et al. Detection of Zika virus in semen Online [17:[

61. Calvez E, Guillaumot L, Millet L, Marie J, Bossin H, Rama V, et al. Genetic Diversity and Phylogeny of Aedes aegypti, the Main Arbovirus Vector in the Pacific. PLoS Negl Trop Dis. 2016;10(1):e0004374.
62. Hills SL RK, Hennessey M, Williams C, Oster AM, Fischer M, et al. Transmission of Zika virus through sexual contact with travelers to areas of ongoing transmission – continental United States, 2016. Online: Centers for Disease Control and Prevention; 2016 [
63. Mansuy JM, Dutertre M, Mengelle C, Fourcade C, Marchou B, Delobel P, et al. Zika virus: high infectious viral load in semen, a new sexually transmitted pathogen? The Lancet Infectious diseases. 2016;16(4):405.
64. Organization PAH. PAHO statement on Zika virus transmission and prevention. Washington D.C.: Pan American Health Organization; 2016. Online: Pan American Health Organization; 2016 [Available from: http://www.paho.org/ hq/index.php?option=com_content&view=article&id=11605% 3A2016-paho-statement-on-zika-transmission-prevention- &catid=8424%3Acontent&lang=en
65. Oster AM BJ, Stryker JE, Kachur RE, Mead P, Pesik NT, et al. Interim guidelines for prevention of sexual transmission of Zika virus – United States, 2016. Online2016 [
66. Oster AM RK, Stryker JE, Friedman A, Kachur RE, Petersen EE, et al. Update: interim guidance for prevention of sexual transmission of Zika virus – United States, 2016. Online: Centers for Disease Control and Prevention; 2016 [
67. Prevention CfDCa. CDC encourages following guidance to prevent sexual transmission of Zika virus. DeKalb County: Centers for Disease Control and Prevention Online: Centers for Disease Control and Prevention; 2016 [Available from: http://www.cdc.gov/media/ releases/2016/s0223-zika-guidance.html.
68. Venturi G, Zammarchi L, Fortuna C, Remoli ME, Benedetti E, Fiorentini C, et al. An autochthonous case of Zika due to possible sexual transmission, Florence, Italy, 2014. Euro Surveill. 2016;21(8):30148.
69. Mead PS, Duggal NK, Hook SA, Delorey M, Fischer M, Olzenak McGuire D, et al. Zika Virus Shedding in Semen of Symptomatic Infected Men. N Engl J Med. 2018;378(15):1377-85.
70. Barreto-Vieira DF, Jacome FC, da Silva MAN, Caldas GC, de Filippis AMB, de Sequeira PC, et al. Structural investigation of C6/36 and Vero cell cultures infected with a Brazilian Zika virus. PLoS One. 2017;12(9):e0184397.
71. Cugola FR, Fernandes IR, Russo FB, Freitas BC, Dias JL, Guimaraes KP, et al. The Brazilian Zika virus strain causes birth defects in experimental models. Nature. 2016;534(7606):267-71.
72. Liu Y, Liu J, Du S, Shan C, Nie K, Zhang R, et al. Evolutionary enhancement of Zika virus infectivity in Aedes aegypti mosquitoes. Nature. 2017;545(7655):482-6.
73. El Costa H, Gouilly J, Mansuy JM, Chen Q, Levy C, Cartron G, et al. ZIKA virus reveals broad tissue and cell tropism during the first trimester of pregnancy. Sci Rep. 2016;6:35296.
74. Foo SS, Chen W, Chan Y, Bowman JW, Chang LC, Choi Y, et al. Asian Zika virus strains target CD14(+) blood monocytes and induce M2-skewed immunosuppression during pregnancy. Nat Microbiol. 2017;2(11):1558-70.
75. Lin HZ, Tambyah PA, Yong EL, Biswas A, Chan SY. A review of Zika virus infections in pregnancy and implications for antenatal care in Singapore. Singapore Med J. 2017;58(4):171-8.
76. Caires-Junior LC, Goulart E, Melo US, Araujo BHS, Alvizi L, Soares-Schanoski A, et al. Discordant congenital Zika syndrome twins show differential in vitro viral susceptibility of neural progenitor cells. Nat Commun. 2018;9(1):475.
77. Shu C, Sankaran B, Chaton CT, Herr AB, Mishra A, Peng J, et al. Structural insights into the functions of TBK1 in innate antimicrobial immunity. Structure. 2013;21(7):1137-48.
78. Marinho PS, Kroon E. Flaviviruses as agents of childhood central nervous system infections in Brazil. New microbes and new infections. 2019;30:100539.
79. van den Pol AN, Mao G, Yang Y, Ornaghi S, Davis JN. Zika Virus Targeting in the Developing Brain. J Neurosci. 2017;37(8):2161-75.

80. Lin MY, Wang YL, Wu WL, Wolseley V, Tsai MT, Radic V, et al. Zika Virus Infects Intermediate Progenitor Cells and Post-mitotic Committed Neurons in Human Fetal Brain Tissues. Sci Rep. 2017;7(1):14883.
81. Aliota MT, Bassit L, Bradrick SS, Cox B, Garcia-Blanco MA, Gavegnano C, et al. Zika in the Americas, year 2: What have we learned? What gaps remain? A report from the Global Virus Network. Antiviral Res. 2017;144:223-46.
82. Singh MS, Marquezan MC, Omiadze R, Reddy AK, Belfort R, Jr., May WN. Inner retinal vasculopathy in Zika virus disease. Am J Ophthalmol Case Rep. 2018;10:6-7.
83. Tan JJL, Balne PK, Leo YS, Tong L, Ng LFP, Agrawal R. Persistence of Zika virus in conjunctival fluid of convalescence patients. Sci Rep. 2017;7(1):11194.
84. Fernandez MP, Parra Saad E, Ospina Martinez M, Corchuelo S, Mercado Reyes M, Herrera MJ, et al. Ocular Histopathologic Features of Congenital Zika Syndrome. JAMA Ophthalmol. 2017;135(11):1163-9.
85. Nayak S, Lei J, Pekosz A, Klein S, Burd I. Pathogenesis and Molecular Mechanisms of Zika Virus. Semin Reprod Med. 2016;34(5):266-72.
86. Valentine G, Marquez L, Pammi M. Zika Virus-Associated Microcephaly and Eye Lesions in the Newborn. J Pediatric Infect Dis Soc. 2016;5(3):323-8.
87. Jampol LM, Goldstein DA. Zika Virus, Microcephaly, and Ocular Findings-Reply. JAMA Ophthalmol. 2016;134(8):946.
88. Jampol LM, Goldstein DA. Zika Virus Infection and the Eye. JAMA Ophthalmol. 2016.
89. Ventura CV, Maia M, Bravo-Filho V, Gois AL, Belfort R, Jr. Zika virus in Brazil and macular atrophy in a child with microcephaly. Lancet. 2016;387(10015):228.
90. Ventura CV, Maia M, Dias N, Ventura LO, Belfort R, Jr. Zika: neurological and ocular findings in infant without microcephaly. Lancet. 2016;387(10037):2502.
91. Ventura CV, Maia M, Ventura BV, Linden VV, Araujo EB, Ramos RC, et al. Ophthalmological findings in infants with microcephaly and presumable intra-uterus Zika virus infection. Arq Bras Oftalmol. 2016;79(1):1-3.
92. Ventura LO, Ventura CV, Dias NC, Vilar IG, Gois AL, Arantes TE, et al. Visual impairment evaluation in 119 children with congenital Zika syndrome. J AAPOS. 2018.
93. Ventura CV, Ventura LO. Ophthalmologic Manifestations Associated With Zika Virus Infection. Pediatrics. 2018;141(Suppl 2):S161-S6.
94. Clark DC, Brault AC, Hunsperger E. The contribution of rodent models to the pathological assessment of flaviviral infections of the central nervous system. Archives of virology. 2012;157(8):1423-40.
95. Singh PK, Guest JM, Kanwar M, Boss J, Gao N, Juzych MS, et al. Zika virus infects cells lining the blood-retinal barrier and causes chorioretinal atrophy in mouse eyes. JCI Insight. 2017;2(4):e92340.
96. Zhao Z, Yang M, Azar SR, Soong L, Weaver SC, Sun J, et al. Viral Retinopathy in Experimental Models of Zika Infection. Invest Ophthalmol Vis Sci. 2017;58(10):4075-85.
97. Mohr EL, Block LN, Newman CM, Stewart LM, Koenig M, Semler M, et al. Ocular and uteroplacental pathology in a macaque pregnancy with congenital Zika virus infection. PLoS One. 2018;13(1):e0190617.
98. Miner JJ, Sene A, Richner JM, Smith AM, Santeford A, Ban N, et al. Zika Virus Infection in Mice Causes Panuveitis with Shedding of Virus in Tears. Cell Rep. 2016;16(12):3208-18.
99. Simonin Y, Erkilic N, Damodar K, Cle M, Desmetz C, Bollore K, et al. Zika virus induces strong inflammatory responses and impairs homeostasis and function of the human retinal pigment epithelium. EBioMedicine. 2019;39:315-31.
100. Dowall SD, Graham VA, Rayner E, Atkinson B, Hall G, Watson RJ, et al. A Susceptible Mouse Model for Zika Virus Infection. PLoS Negl Trop Dis. 2016;10(5):e0004658.

101. Simonin Y, van Riel D, Van de Perre P, Rockx B, Salinas S. Differential virulence between Asian and African lineages of Zika virus. PLoS Negl Trop Dis. 2017;11(9):e0005821.
102. Vielle NJ, Zumkehr B, Garcia-Nicolas O, Blank F, Stojanov M, Musso D, et al. Silent infection of human dendritic cells by African and Asian strains of Zika virus. Sci Rep. 2018;8(1):5440.
103. Himmelsbach K, Hildt E. Identification of various cell culture models for the study of Zika virus. World J Virol. 2018;7(1):10-20.
104. Simonin Y, Loustalot F, Desmetz C, Foulongne V, Constant O, Fournier-Wirth C, et al. Zika Virus Strains Potentially Display Different Infectious Profiles in Human Neural Cells. EBioMedicine. 2016;12:161-9.
105. Hamel R, Ferraris P, Wichit S, Diop F, Talignani L, Pompon J, et al. African and Asian Zika virus strains differentially induce early antiviral responses in primary human astrocytes. Infect Genet Evol. 2017;49:134-7.
106. Zhang F, Wang HJ, Wang Q, Liu ZY, Yuan L, Huang XY, et al. American Strain of Zika Virus Causes More Severe Microcephaly Than an Old Asian Strain in Neonatal Mice. EBioMedicine. 2017;25:95-105.
107. Qian X, Nguyen HN, Song MM, Hadiono C, Ogden SC, Hammack C, et al. Brain-Region-Specific Organoids Using Mini-bioreactors for Modeling ZIKV Exposure. Cell. 2016;165(5):1238-54.
108. Zhu Z, Chan JF, Tee KM, Choi GK, Lau SK, Woo PC, et al. Comparative genomic analysis of pre-epidemic and epidemic Zika virus strains for virological factors potentially associated with the rapidly expanding epidemic. Emerg Microbes Infect. 2016;5:e22.
109. Charles B Stauft OG, Jeronimo Cello, Eckard Wimmer, Bruce Futcher. Comparison of African, Asian, and American Zika Viruses in Swiss Webster mice: Virulence, neutralizing antibodies, and serotypes. Cold Spring Harbor Laboratory - BioRxiv. 2016.
110. Willard KA, Demakovsky L, Tesla B, Goodfellow FT, Stice SL, Murdock CC, et al. Zika Virus Exhibits Lineage-Specific Phenotypes in Cell Culture, in Aedes aegypti Mosquitoes, and in an Embryo Model. Viruses. 2017;9(12).
111. Ponomarenko NA, Durova OM, Vorobiev, II, Belogurov AA, Jr., Kurkova IN, Petrenko AG, et al. Autoantibodies to myelin basic protein catalyze site-specific degradation of their antigen. Proc Natl Acad Sci U S A. 2006;103(2):281-6.
112. Paul LM, Carlin ER, Jenkins MM, Tan AL, Barcellona CM, Nicholson CO, et al. Dengue virus antibodies enhance Zika virus infection. Clin Transl Immunology. 2016;5(12):e117.
113. Komagamine T, Matsuno K, Sakumoto Y, Takahashi H, Kokubun N, Yuki N, et al. Immunohistochemical localization of the GM1, GD1a, GD1b and GQ1b gangliosides in the neuronal endings of rat muscle spindles. Archives of Histology and Cytology. 2013;74(1):31-40.
114. Kopper TJ, Gensel JC. Myelin as an inflammatory mediator: Myelin interactions with complement, macrophages, and microglia in spinal cord injury. J Neurosci Res. 2018;96(6):969-77.
115. Frankola KA, Greig NH, Luo W, Tweedie D. Targeting TNF-alpha to elucidate and ameliorate neuroinflammation in neurodegenerative diseases. CNS Neurol Disord Drug Targets. 2011;10(3):391-403.
116. Wang P, Dai J, Bai F, Kong KF, Wong SJ, Montgomery RR, et al. Matrix metalloproteinase 9 facilitates West Nile virus entry into the brain. J Virol. 2008;82(18):8978-85.
117. Mori T, Miyamoto T, Yoshida H, Asakawa M, Kawasumi M, Kobayashi T, et al. IL-1beta and TNFalpha-initiated IL-6-STAT3 pathway is critical in mediating inflammatory cytokines and RANKL expression in inflammatory arthritis. Int Immunol. 2011;23(11):701-12.
118. Samad TA, Moore KA, Sapirstein A, Billet S, Allchorne A, Poole S, et al. Interleukin-1beta-mediated induction of Cox-2 in the CNS contributes to inflammatory pain hypersensitivity. Nature. 2001;410(6827):471-5.
119. Ashley SL, Pretto CD, Stier MT, Kadiyala P, Castro-Jorge L, Hsu TH, et al. Matrix Metalloproteinase Activity in Infections by an Encephalitic Virus, Mouse Adenovirus Type 1. J Virol. 2017;91(6).

120. Konnecke H, Bechmann I. The role of microglia and matrix metalloproteinases involvement in neuroinflammation and gliomas. Clin Dev Immunol. 2013;2013:914104.
121. Rempe RG, Hartz AMS, Bauer B. Matrix metalloproteinases in the brain and blood-brain barrier: Versatile breakers and makers. J Cereb Blood Flow Metab. 2016;36(9):1481-507.
122. Song J, Wu C, Korpos E, Zhang X, Agrawal SM, Wang Y, et al. Focal MMP-2 and MMP-9 activity at the blood-brain barrier promotes chemokine-induced leukocyte migration. Cell Rep. 2015;10(7):1040-54.
123. Randall RE, Goodbourn S. Interferons and viruses: an interplay between induction, signalling, antiviral responses and virus countermeasures. J Gen Virol. 2008;89(Pt 1):1-47.
124. Phoo WW, Li Y, Zhang Z, Lee MY, Loh YR, Tan YB, et al. Structure of the NS2B-NS3 protease from Zika virus after self-cleavage. Nat Commun. 2016;7:13410.
125. Wu Y, Liu Q, Zhou J, Xie W, Chen C, Wang Z, et al. Zika virus evades interferon-mediated antiviral response through the co-operation of multiple nonstructural proteins in vitro. Cell Discov. 2017;3:17006.
126. Wang B, Thurmond S, Hai R, Song J. Structure and function of Zika virus NS5 protein: perspectives for drug design. Cell Mol Life Sci. 2018;75(10):1723-36.
127. Liu J, Liu Y, Nie K, Du S, Qiu J, Pang X, et al. Flavivirus NS1 protein in infected host sera enhances viral acquisition by mosquitoes. Nat Microbiol. 2016;1(9):16087.
128. Grant A, Ponia SS, Tripathi S, Balasubramaniam V, Miorin L, Sourisseau M, et al. Zika Virus Targets Human STAT2 to Inhibit Type I Interferon Signaling. Cell Host Microbe. 2016;19(6):882-90.
129. Bowen JR, Quicke KM, Maddur MS, O'Neal JT, McDonald CE, Fedorova NB, et al. Zika Virus Antagonizes Type I Interferon Responses during Infection of Human Dendritic Cells. PLoS Pathog. 2017;13(2):e1006164.
130. Mladinich MC, Schwedes J, Mackow ER. Zika Virus Persistently Infects and Is Basolaterally Released from Primary Human Brain Microvascular Endothelial Cells. MBio. 2017;8(4).
131. Xia H, Luo H, Shan C, Muruato AE, Nunes BTD, Medeiros DBA, et al. An evolutionary NS1 mutation enhances Zika virus evasion of host interferon induction. Nat Commun. 2018;9(1):414.
132. Hamel R, Liegeois F, Wichit S, Pompon J, Diop F, Talignani L, et al. Zika virus: epidemiology, clinical features and host-virus interactions. Microbes Infect. 2016;18(7-8):441-9.
133. Frumence E, Roche M, Krejbich-Trotot P, El-Kalamouni C, Nativel B, Rondeau P, et al. The South Pacific epidemic strain of Zika virus replicates efficiently in human epithelial A549 cells leading to IFN-beta production and apoptosis induction. Virology. 2016;493:217-26.
134. Rossi SL, Tesh RB, Azar SR, Muruato AE, Hanley KA, Auguste AJ, et al. Characterization of a Novel Murine Model to Study Zika Virus. Am J Trop Med Hyg. 2016.
135. Sumathy K, Kulkarni B, Gondu RK, Ponnuru SK, Bonguram N, Eligeti R, et al. Protective efficacy of Zika vaccine in AG129 mouse model. Sci Rep. 2017;7:46375.
136. Huang H, Li S, Zhang Y, Han X, Jia B, Liu H, et al. CD8(+) T Cell Immune Response in Immunocompetent Mice during Zika Virus Infection. J Virol. 2017;91(22).
137. McGrath EL, Rossi SL, Gao J, Widen SG, Grant AC, Dunn TJ, et al. Differential Responses of Human Fetal Brain Neural Stem Cells to Zika Virus Infection. Stem Cell Reports. 2017;8(3):715-27.
138. Kam YW, Leite JA, Lum FM, Tan JJL, Lee B, Judice CC, et al. Specific Biomarkers Associated With Neurological Complications and Congenital Central Nervous System Abnormalities From Zika Virus-Infected Patients in Brazil. J Infect Dis. 2017;216(2):172-81.
139. Silveira ELV, Rogers KA, Gumber S, Amancha P, Xiao P, Woollard SM, et al. Immune Cell Dynamics in Rhesus Macaques Infected with a Brazilian Strain of Zika Virus. J Immunol. 2017;199(3):1003-11.
140. Sironi M, Forni D, Clerici M, Cagliani R. Nonstructural Proteins Are Preferential Positive Selection Targets in Zika Virus and Related Flaviviruses. PLoS Negl Trop Dis. 2016;10(9):e0004978.
141. Elong Ngono A, Vizcarra EA, Tang WW, Sheets N, Joo Y, Kim K, et al. Mapping and Role of the CD8(+) T Cell Response During Primary Zika Virus Infection in Mice. Cell Host Microbe. 2017;21(1):35-46.

142. Tripathi S, Balasubramaniam VR, Brown JA, Mena I, Grant A, Bardina SV, et al. A novel Zika virus mouse model reveals strain specific differences in virus pathogenesis and host inflammatory immune responses. PLoS Pathog. 2017;13(3):e1006258.
143. Chaudhary V, Yuen KS, Chan JF, Chan CP, Wang PH, Cai JP, et al. Selective Activation of Type II Interferon Signaling by Zika Virus NS5 Protein. J Virol. 2017;91(14).
144. Costa VV, Ye W, Chen Q, Teixeira MM, Preiser P, Ooi EE, et al. Dengue Virus-Infected Dendritic Cells, but Not Monocytes, Activate Natural Killer Cells through a Contact-Dependent Mechanism Involving Adhesion Molecules. MBio. 2017;8(4).
145. Cimini E, Castilletti C, Sacchi A, Casetti R, Bordoni V, Romanelli A, et al. Human Zika infection induces a reduction of IFN-gamma producing CD4 T-cells and a parallel expansion of effector Vdelta2 T-cells. Sci Rep. 2017;7(1):6313.
146. Pardy RD, Rajah MM, Condotta SA, Taylor NG, Sagan SM, Richer MJ. Analysis of the T Cell Response to Zika Virus and Identification of a Novel CD8+ T Cell Epitope in Immunocompetent Mice. PLoS Pathog. 2017;13(2):e1006184.
147. Li J, Wang Y, Wang X, Ye L, Zhou Y, Persidsky Y, et al. Immune activation of human brain microvascular endothelial cells inhibits HIV replication in macrophages. Blood. 2013;121(15):2934-42.
148. Li J, Hu S, Zhou L, Ye L, Wang X, Ho J, et al. Interferon lambda inhibits herpes simplex virus type I infection of human astrocytes and neurons. Glia. 2011;59(1):58-67.
149. Douam F, Soto Albrecht YE, Hrebikova G, Sadimin E, Davidson C, Kotenko SV, et al. Type III Interferon-Mediated Signaling Is Critical for Controlling Live Attenuated Yellow Fever Virus Infection In Vivo. MBio. 2017;8(4).
150. Miner JJ, Cao B, Govero J, Smith AM, Fernandez E, Cabrera OH, et al. Zika Virus Infection during Pregnancy in Mice Causes Placental Damage and Fetal Demise. Cell. 2016;165(5):1081-91.
151. Noronha L, Zanluca C, Azevedo ML, Luz KG, Santos CN. Zika virus damages the human placental barrier and presents marked fetal neurotropism. Mem Inst Oswaldo Cruz. 2016;111(5):287-93.
152. Yockey LJ, Varela L, Rakib T, Khoury-Hanold W, Fink SL, Stutz B, et al. Vaginal Exposure to Zika Virus during Pregnancy Leads to Fetal Brain Infection. Cell. 2016;166(5):1247-56 e4.
153. Zorrilla CD, Garcia Garcia I, Garcia Fragoso L, De La Vega A. Zika Virus Infection in Pregnancy: Maternal, Fetal, and Neonatal Considerations. J Infect Dis. 2017;216(suppl_10):S891-S6.
154. Gude NM, Roberts CT, Kalionis B, King RG. Growth and function of the normal human placenta. Thromb Res. 2004;114(5-6):397-407.
155. Corry J, Arora N, Good CA, Sadovsky Y, Coyne CB. Organotypic models of type III interferon-mediated protection from Zika virus infections at the maternal-fetal interface. Proc Natl Acad Sci U S A. 2017;114(35):9433-8.
156. Schwartz DA. Viral infection, proliferation, and hyperplasia of Hofbauer cells and absence of inflammation characterize the placental pathology of fetuses with congenital Zika virus infection. Arch Gynecol Obstet. 2017;295(6):1361-8.
157. Jurado KA, Simoni MK, Tang Z, Uraki R, Hwang J, Householder S, et al. Zika virus productively infects primary human placenta-specific macrophages. JCI Insight. 2016;1(13).
158. Weisblum Y, Oiknine-Djian E, Vorontsov OM, Haimov-Kochman R, Zakay-Rones Z, Meir K, et al. Zika Virus Infects Early- and Midgestation Human Maternal Decidual Tissues, Inducing Distinct Innate Tissue Responses in the Maternal-Fetal Interface. J Virol. 2017;91(4).
159. Bayer A, Lennemann NJ, Ouyang Y, Bramley JC, Morosky S, Marques ET, Jr., et al. Type III Interferons Produced by Human Placental Trophoblasts Confer Protection against Zika Virus Infection. Cell Host Microbe. 2016;19(5):705-12.
160. Quicke KM, Bowen JR, Johnson EL, McDonald CE, Ma H, O'Neal JT, et al. Zika Virus Infects Human Placental Macrophages. Cell Host Microbe. 2016;20(1):83-90.

161. Simoni MK, Jurado KA, Abrahams VM, Fikrig E, Guller S. Zika virus infection of Hofbauer cells. Am J Reprod Immunol. 2017;77(2).
162. Durbin AP. Vaccine Development for Zika Virus-Timelines and Strategies. Semin Reprod Med. 2016.
163. Lagunas-Rangel FA, Viveros-Sandoval ME, Reyes-Sandoval A. Current trends in Zika vaccine development. J Virus Erad. 2017;3(3):124-7.
164. Durbin A, Wilder-Smith A. An update on Zika vaccine developments. Expert Rev Vaccines. 2017;16(8):781-7.
165. Durham DP, Fitzpatrick MC, Ndeffo-Mbah ML, Parpia AS, Michael NL, Galvani AP. Evaluating Vaccination Strategies for Zika Virus in the Americas. Ann Intern Med. 2018.
166. Yang M, Dent M, Lai H, Sun H, Chen Q. Immunization of Zika virus envelope protein domain III induces specific and neutralizing immune responses against Zika virus. Vaccine. 2017;35(33):4287-94.
167. Liang H, Yang R, Liu Z, Li M, Liu H, Jin X. Recombinant Zika virus envelope protein elicited protective immunity against Zika virus in immunocompetent mice. PLoS One. 2018;13(3):e0194860.
168. To A, Medina LO, Mfuh KO, Lieberman MM, Wong TAS, Namekar M, et al. Recombinant Zika Virus Subunits Are Immunogenic and Efficacious in Mice. mSphere. 2018;3(1).
169. Pradhan D, Yadav M, Verma R, Khan NS, Jena L, Jain AK. Discovery of T-cell Driven Subunit Vaccines from Zika Virus Genome: An Immunoinformatics Approach. Interdiscip Sci. 2017;9(4):468-77.
170. Richner JM, Himansu S, Dowd KA, Butler SL, Salazar V, Fox JM, et al. Modified mRNA Vaccines Protect against Zika Virus Infection. Cell. 2017;168(6):1114-25 e10.
171. Larocca RA, Abbink P, Peron JP, Zanotto PM, Iampietro MJ, Badamchi-Zadeh A, et al. Vaccine protection against Zika virus from Brazil. Nature. 2016;536(7617):474-8.
172. Muthumani K, Griffin BD, Agarwal S, Kudchodkar SB, Reuschel EL, Choi H, et al. In vivo protection against ZIKV infection and pathogenesis through passive antibody transfer and active immunisation with a prMEnv DNA vaccine. NPJ Vaccines. 2016;1:16021.
173. Shan C, Muruato AE, Nunes BTD, Luo H, Xie X, Medeiros DBA, et al. A live-attenuated Zika virus vaccine candidate induces sterilizing immunity in mouse models. Nat Med. 2017;23(6):763-7.
174. Shan C, Muruato AE, Jagger BW, Richner J, Nunes BTD, Medeiros DBA, et al. A single-dose live-attenuated vaccine prevents Zika virus pregnancy transmission and testis damage. Nat Commun. 2017;8(1):676.
175. Abbink P, Larocca RA, De La Barrera RA, Bricault CA, Moseley ET, Boyd M, et al. Protective efficacy of multiple vaccine platforms against Zika virus challenge in rhesus monkeys. Science. 2016;353(6304):1129-32.
176. Li XF, Dong HL, Wang HJ, Huang XY, Qiu YF, Ji X, et al. Development of a chimeric Zika vaccine using a licensed live-attenuated flavivirus vaccine as backbone. Nat Commun. 2018;9(1):673.
177. Brault AC, Domi A, McDonald EM, Talmi-Frank D, McCurley N, Basu R, et al. A Zika Vaccine Targeting NS1 Protein Protects Immunocompetent Adult Mice in a Lethal Challenge Model. Sci Rep. 2017;7(1):14769.
178. Paz-Bailey G, Rosenberg ES, Doyle K, Munoz-Jordan J, Santiago GA, Klein L, et al. Persistence of Zika Virus in Body Fluids - Preliminary Report. N Engl J Med. 2017.
179. Beaver JT, Lelutiu N, Habib R, Skountzou I. Evolution of Two Major Zika Virus Lineages: Implications for Pathology, Immune Response, and Vaccine Development. Front Immunol. 2018;9:1640.
180. Araujo LM, Ferreira ML, Nascimento OJ. Guillain-Barre syndrome associated with the Zika virus outbreak in Brazil. Arq Neuropsiquiatr. 2016;74(3):253-5.
181. da Silva IRF, Frontera JA, Bispo de Filippis AM, Nascimento O, Group R-G-ZR. Neurologic Complications Associated With the Zika Virus in Brazilian Adults. JAMA Neurol. 2017;74(10):1190-8.
182. Bandyopadhyay D, Hajra A. ZIKA virus: A new threat to the eyes. Eur J Intern Med. 2017;44:e9-e10.

183. Prakalapakorn SG, Meaney-Delman D, Honein MA, Rasmussen SA. The eyes as a window to improved understanding of the prenatal effects of Zika virus infection. J AAPOS. 2017;21(4):259-61.
184. Ramakrishnan S, Kannan B, Kannan A, Venkatesan EP. Vision Loss in Guillain-Barre Syndrome: Is it a Complication of Guillain-Barre Syndrome or Just a Coincidence? J Ophthalmic Vis Res. 2016;11(3):340-1.
185. Barzon L, Pacenti M, Franchin E, Lavezzo E, Trevisan M, Sgarabotto D, et al. Infection dynamics in a traveller with persistent shedding of Zika virus RNA in semen for six months after returning from Haiti to Italy, January 2016. Euro Surveill. 2016;21(32).
186. Murray KO, Gorchakov R, Carlson AR, Berry R, Lai L, Natrajan M, et al. Prolonged Detection of Zika Virus in Vaginal Secretions and Whole Blood. Emerg Infect Dis. 2017;23(1):99-101.
187. Bautista LE. Zika virus infection and risk of Guillain-Barre syndrome: A meta-analysis. J Neurol Sci. 2019;403:99-105.
188. Munoz LS, Parra B, Pardo CA, Neuroviruses Emerging in the Americas S. Neurological Implications of Zika Virus Infection in Adults. J Infect Dis. 2017;216(suppl_10):S897-S905.
189. Barbi L, Coelho AVC, Alencar LCA, Crovella S. Prevalence of Guillain-Barre syndrome among Zika virus infected cases: a systematic review and meta-analysis. Braz J Infect Dis. 2018;22(2):137-41.
190. Dimachkie MM, Barohn RJ. Guillain-Barre syndrome and variants. Neurol Clin. 2013;31(2):491-510.
191. Nachamkin I, Allos BM, Ho T. Campylobacter species and Guillain-Barre syndrome. Clin Microbiol Rev. 1998;11(3):555-67.
192. Garber C, Soung A, Vollmer LL, Kanmogne M, Last A, Brown J, et al. T cells promote microglia-mediated synaptic elimination and cognitive dysfunction during recovery from neuropathogenic flaviviruses. Nat Neurosci. 2019;22(8):1276-88.
193. McDonald EM, Duggal NK, Delorey MJ, Oksanish J, Ritter JM, Brault AC. Duration of seminal Zika viral RNA shedding in immunocompetent mice inoculated with Asian and African genotype viruses. Virology. 2019;535:1-10.
194. Munoz-Jordan JL, Fredericksen BL. How flaviviruses activate and suppress the interferon response. Viruses. 2010;2(2):676-91.
195. Lazear HM, Govero J, Smith AM, Platt DJ, Fernandez E, Miner JJ, et al. A Mouse Model of Zika Virus Pathogenesis. Cell Host Microbe. 2016;19(5):720-30.
196. Morrison TE, Diamond MS. Animal Models of Zika Virus Infection, Pathogenesis, and Immunity. J Virol. 2017;91(8).
197. Nazerai L, Scholler AS, Rasmussen POS, Buus S, Stryhn A, Christensen JP, et al. A New In Vivo Model to Study Protective Immunity to Zika Virus Infection in Mice With Intact Type I Interferon Signaling. Front Immunol. 2018;9:593.
198. Coelho SVA, Neris RLS, Papa MP, Schnellrath LC, Meuren LM, Tschoeke DA, et al. Development of standard methods for Zika virus propagation, titration, and purification. J Virol Methods. 2017;246:65-74.
199. Matrosovich M, Matrosovich T, Garten W, Klenk HD. New low-viscosity overlay medium for viral plaque assays. Virol J. 2006;3:63.
200. Priyamvada L, Quicke KM, Hudson WH, Onlamoon N, Sewatanon J, Edupuganti S, et al. Human antibody responses after dengue virus infection are highly cross-reactive to Zika virus. Proc Natl Acad Sci U S A. 2016;113(28):7852-7.
201. Garcia-Nicolas O, Braun RO, Milona P, Lewandowska M, Dijkman R, Alves MP, et al. Targeting of the Nasal Mucosa by Japanese Encephalitis Virus for Non-Vector-Borne Transmission. J Virol. 2018;92(24).
202. Hassert M, Wolf KJ, Schwetye KE, DiPaolo RJ, Brien JD, Pinto AK. CD4+T cells mediate protection against Zika associated severe disease in a mouse model of infection. PLoS Pathog. 2018;14(9):e1007237.
203. Flammer J, Konieczka K, Bruno RM, Virdis A, Flammer AJ, Taddei S. The eye and the heart. Eur Heart J. 2013;34(17):1270-8.

204. Grabert K, McColl BW. Isolation and Phenotyping of Adult Mouse Microglial Cells. Methods Mol Biol. 2018;1784:77-86.
205. Lee JK, Tansey MG. Microglia isolation from adult mouse brain. Methods Mol Biol. 2013;1041:17-23.
206. Sapparapu G, Fernandez E, Kose N, Bin C, Fox JM, Bombardi RG, et al. Neutralizing human antibodies prevent Zika virus replication and fetal disease in mice. Nature. 2016;540(7633):443-7.
207. Mavigner M, Raper J, Kovacs-Balint Z, Gumber S, O'Neal JT, Bhaumik SK, et al. Postnatal Zika virus infection is associated with persistent abnormalities in brain structure, function, and behavior in infant macaques. Sci Transl Med. 2018;10(435).
208. Taib T, Leconte C, Van Steenwinckel J, Cho AH, Palmier B, Torsello E, et al. Neuroinflammation, myelin and behavior: Temporal patterns following mild traumatic brain injury in mice. PLoS One. 2017;12(9):e0184811.
209. Brayton C, McBean, N.F., Watson, J. JHU Mouse Pathobiology & Phenotyping Short Course. Johns Hopkins University School of Medicine, Department of Molecular & Comparative Pathology 2015;4.
210. Drapeau E, Riad M, Kajiwara Y, Buxbaum JD. Behavioral Phenotyping of an Improved Mouse Model of Phelan-McDermid Syndrome with a Complete Deletion of the Shank3 Gene. eNeuro. 2018;5(3).
211. Olsen CM, Childs DS, Stanwood GD, Winder DG. Operant sensation seeking requires metabotropic glutamate receptor 5 (mGluR5). PLoS One. 2010;5(11):e15085.
212. Ferrari G, Chauhan SK, Ueno H, Nallasamy N, Gandolfi S, Borges L, et al. A novel mouse model for neurotrophic keratopathy: trigeminal nerve stereotactic electrolysis through the brain. Invest Ophthalmol Vis Sci. 2011;52(5):2532-9.
213. Ronca SE, Smith J, Koma T, Miller MM, Yun N, Dineley KT, et al. Mouse Model of Neurological Complications Resulting from Encephalitic Alphavirus Infection. Front Microbiol. 2017;8:188.
214. Blivis D, Haspel G, Mannes PZ, O'Donovan MJ, Iadarola MJ. Identification of a novel spinal nociceptive-motor gate control for Adelta pain stimuli in rats. Elife. 2017;6.
215. Plotnikov MB, Chernysheva GA, Aliev OI, Smol'iakova VI, Fomina TI, Osipenko AN, et al. Protective Effects of a New C-Jun N-terminal Kinase Inhibitor in the Model of Global Cerebral Ischemia in Rats. Molecules. 2019;24(9).
216. Neugebauer V, Han JS, Adwanikar H, Fu Y, Ji G. Techniques for assessing knee joint pain in arthritis. Mol Pain. 2007;3:8.
217. O'Leary TP, Robertson A, Chipman PH, Rafuse VF, Brown RE. Motor function deficits in the 12 month-old female 5xFAD mouse model of Alzheimer's disease. Behav Brain Res. 2018;337:256-63.
218. Fink SL, Cookson BT. Apoptosis, pyroptosis, and necrosis: mechanistic description of dead and dying eukaryotic cells. Infect Immun. 2005;73(4):1907-16.
219. Miao EA, Rajan JV, Aderem A. Caspase-1-induced pyroptotic cell death. Immunol Rev. 2011;243(1):206-14.
220. Yang M, Antoine DJ, Weemhoff JL, Jenkins RE, Farhood A, Park BK, et al. Biomarkers distinguish apoptotic and necrotic cell death during hepatic ischemia/reperfusion injury in mice. Liver Transpl. 2014;20(11):1372-82.
221. Lourenco T, Paes de Faria J, Bippes CA, Maia J, Lopes-da-Silva JA, Relvas JB, et al. Modulation of oligodendrocyte differentiation and maturation by combined biochemical and mechanical cues. Sci Rep. 2016;6:21563.
222. Esser ES, Romanyuk A, Vassilieva EV, Jacob J, Prausnitz MR, Compans RW, et al. Tetanus vaccination with a dissolving microneedle patch confers protective immune responses in pregnancy. J Control Release. 2016;236:47-56.
223. Titilope Oduyebo MKDP, MPH1; Henry T. Walke, MD1; Sarah Reagan-Steiner, MD1; Eva Lathrop, MD1; Ingrid B. Rabe, MBChB1;, Wendi L. Kuhnert-Tallman PSWM, MSc1; Allison T. Walker, PhD1; Christopher J. Gregory, MD1; Edwin W. Ades, PhD1; Darin S., Carroll PMR, MPH1; Janice Perez-Padilla,

MPH1; Carolyn Gould, MD1; Jeffrey B. Nemhauser, MD1; C. Ben Beard, PhD1; Jennifer L., Harcourt PLV, MD1; Michael Johansson, PhD1; Sascha R. Ellington, MSPH1; Emily Petersen, MD1; Laura A. Smith, MA1; Jessica, Reichard MJM-J, PhD1; Michael J. Beach, PhD1; Dale A. Rose, PhD1; Ezra Barzilay, MD1; Michelle Noonan-Smith1; Denise J., Jamieson MSRZ, MD1; Lyle R. Petersen, MD1; Margaret A. Honein, PhD1; Dana Meaney-Delman, MD1. Update: Interim Guidance for Health Care Providers Caring for Pregnant

Women with Possible Zika Virus Exposure — United States

(Including U.S. Territories), July 2017. Morbidity and Mortality Weekly Report Surveillance Summaries. 2017;66(29):781-93.

224. Cao-Lormeau VM, Blake A, Mons S, Lastere S, Roche C, Vanhomwegen J, et al. Guillain-Barre Syndrome outbreak associated with Zika virus infection in French Polynesia: a case-control study. Lancet. 2016;387(10027):1531-9.

225. Yun H, Rowe AM, Lathrop KL, Harvey SA, Hendricks RL. Reversible nerve damage and corneal pathology in murine herpes simplex stromal keratitis. J Virol. 2014;88(14):7870-80.

226. Chucair-Elliott AJ, Zheng M, Carr DJ. Degeneration and regeneration of corneal nerves in response to HSV-1 infection. Invest Ophthalmol Vis Sci. 2015;56(2):1097-107.

227. Martin-Acebes MA, Saiz JC, Jimenez de Oya N. Antibody-Dependent Enhancement and Zika: Real Threat or Phantom Menace? Front Cell Infect Microbiol. 2018;8:44.

228. Langford DJ, Bailey AL, Chanda ML, Clarke SE, Drummond TE, Echols S, et al. Coding of facial expressions of pain in the laboratory mouse. Nat Methods. 2010;7(6):447-9.

229. Matsumiya LC, Sorge RE, Sotocinal SG, Tabaka JM, Wieskopf JS, Zaloum A, et al. Using the Mouse Grimace Scale to reevaluate the efficacy of postoperative analgesics in laboratory mice. J Am Assoc Lab Anim Sci. 2012;51(1):42-9.

230. Ubogu EE. Inflammatory neuropathies: pathology, molecular markers and targets for specific therapeutic intervention. Acta Neuropathol. 2015;130(4):445-68.

231. Fulton D, Paez PM, Campagnoni AT. The multiple roles of myelin protein genes during the development of the oligodendrocyte. ASN Neuro. 2010;2(1):e00027.

232. Naik GS, Meena AK, Reddy BAK, Mridula RK, Jabeen SA, Borgohain R. Anti-ganglioside antibodies profile in Guillain-Barre syndrome: Correlation with clinical features, electrophysiological pattern, and outcome. Neurol India. 2017;65(5):1001-5.

233. Bell BA, Kaul C, Bonilha VL, Rayborn ME, Shadrach K, Hollyfield JG. The BALB/c mouse: Effect of standard vivarium lighting on retinal pathology during aging. Exp Eye Res. 2015;135:192-205.

234. Singh PK, Kasetti RB, Zode GS, Goyal A, Juzych MS, Kumar A. Zika Virus Infects Trabecular Meshwork and Causes Trabeculitis and Glaucomatous Pathology in Mouse Eyes. mSphere. 2019;4(3).

235. Manangeeswaran M, Kielczewski JL, Sen HN, Xu BC, Ireland DDC, McWilliams IL, et al. ZIKA virus infection causes persistent chorioretinal lesions. Emerg Microbes Infect. 2018;7(1):96.

236. DiSabato DJ, Quan N, Godbout JP. Neuroinflammation: the devil is in the details. J Neurochem. 2016;139 Suppl 2:136-53.

237. Burmeister AR, Marriott I. The Interleukin-10 Family of Cytokines and Their Role in the CNS. Front Cell Neurosci. 2018;12:458.

238. Khaiboullina S, Uppal T, Kletenkov K, St Jeor SC, Garanina E, Rizvanov A, et al. Transcriptome Profiling Reveals Pro-Inflammatory Cytokines and Matrix Metalloproteinase Activation in Zika Virus Infected Human Umbilical Vein Endothelial Cells. Front Pharmacol. 2019;10:642.

239. Nakamura R, Sene A, Santeford A, Gdoura A, Kubota S, Zapata N, et al. IL10-driven STAT3 signalling in senescent macrophages promotes pathological eye angiogenesis. Nat Commun. 2015;6:7847.

240. Baker BJ, Akhtar LN, Benveniste EN. SOCS1 and SOCS3 in the control of CNS immunity. Trends Immunol. 2009;30(8):392-400.

241. Pardi N, Hogan MJ, Pelc RS, Muramatsu H, Andersen H, DeMaso CR, et al. Zika virus protection by a single low-dose nucleoside-modified mRNA vaccination. Nature. 2017;543(7644):248-51.
242. Calvet GA, Kara EO, Giozza SP, Botto-Menezes CHA, Gaillard P, de Oliveira Franca RF, et al. Study on the persistence of Zika virus (ZIKV) in body fluids of patients with ZIKV infection in Brazil. BMC Infect Dis. 2018;18(1):49.
243. Gaudinski MR, Houser KV, Morabito KM, Hu Z, Yamshchikov G, Rothwell RS, et al. Safety, tolerability, and immunogenicity of two Zika virus DNA vaccine candidates in healthy adults: randomised, open-label, phase 1 clinical trials. Lancet. 2018;391(10120):552-62.
244. Modjarrad K, Lin L, George SL, Stephenson KE, Eckels KH, De La Barrera RA, et al. Preliminary aggregate safety and immunogenicity results from three trials of a purified inactivated Zika virus vaccine candidate: phase 1, randomised, double-blind, placebo-controlled clinical trials. Lancet. 2018;391(10120):563-71.
245. Barrett ADT. Current status of Zika vaccine development: Zika vaccines advance into clinical evaluation. NPJ Vaccines. 2018;3:24.
246. Moffatt K, Wang Y, Raj Singh TR, Donnelly RF. Microneedles for enhanced transdermal and intraocular drug delivery. Curr Opin Pharmacol. 2017;36:14-21.
247. Nguyen TT, Park JH. Human studies with microneedles for evaluation of their efficacy and safety. Expert Opin Drug Deliv. 2018;15(3):235-45.
248. Prausnitz MR. Engineering Microneedle Patches for Vaccination and Drug Delivery to Skin. Annu Rev Chem Biomol Eng. 2017;8:177-200.
249. del Pilar Martin M, Weldon WC, Zarnitsyn VG, Koutsonanos DG, Akbari H, Skountzou I, et al. Local response to microneedle-based influenza immunization in the skin. MBio. 2012;3(2):e00012-12.
250. Pulit-Penaloza JA, Esser ES, Vassilieva EV, Lee JW, Taherbhai MT, Pollack BP, et al. A protective role of murine langerin(+) cells in immune responses to cutaneous vaccination with microneedle patches. Sci Rep. 2014;4:6094.
251. Sullivan SP, Koutsonanos DG, Del Pilar Martin M, Lee JW, Zarnitsyn V, Choi SO, et al. Dissolving polymer microneedle patches for influenza vaccination. Nat Med. 2010;16(8):915-20.
252. Koutsonanos DG, Vassilieva EV, Stavropoulou A, Zarnitsyn VG, Esser ES, Taherbhai MT, et al. Delivery of subunit influenza vaccine to skin with microneedles improves immunogenicity and long-lived protection. Sci Rep. 2012;2:357.
253. Vassilieva EV, Wang S, Li S, Prausnitz MR, Compans RW. Skin immunization by microneedle patch overcomes statin-induced suppression of immune responses to influenza vaccine. Sci Rep. 2017;7(1):17855.
254. Hamel R, Dejarnac O, Wichit S, Ekchariyawat P, Neyret A, Luplertlop N, et al. Biology of Zika Virus Infection in Human Skin Cells. J Virol. 2015;89(17):8880-96.
255. Mackay LK, Rahimpour A, Ma JZ, Collins N, Stock AT, Hafon ML, et al. The developmental pathway for CD103(+)CD8+ tissue-resident memory T cells of skin. Nat Immunol. 2013;14(12):1294-301.
256. Littauer EQ, Mills LK, Brock N, Esser ES, Romanyuk A, Pulit-Penaloza JA, et al. Stable incorporation of GM-CSF into dissolvable microneedle patch improves skin vaccination against influenza. J Control Release. 2018;276:1-16.
257. Vassilieva EV, Kalluri H, McAllister D, Taherbhai MT, Esser ES, Pewin WP, et al. Improved immunogenicity of individual influenza vaccine components delivered with a novel dissolving microneedle patch stable at room temperature. Drug Deliv Transl Res. 2015;5(4):360-71.
258. Rouphael NG, Paine M, Mosley R, Henry S, McAllister DV, Kalluri H, et al. The safety, immunogenicity, and acceptability of inactivated influenza vaccine delivered by microneedle patch (TIV-MNP 2015): a randomised, partly blinded, placebo-controlled, phase 1 trial. Lancet. 2017;390(10095):649-58.

259. Triolo D, Dina G, Taveggia C, Vaccari I, Porrello E, Rivellini C, et al. Vimentin regulates peripheral nerve myelination. Development. 2012;139(7):1359-67.
260. Guevara JG, Agarwal-Sinha S. Ocular abnormalities in congenital Zika syndrome: a case report, and review of the literature. J Med Case Rep. 2018;12(1):161.
261. Al-Fifi YSY, Kadkhoda K, Drebot M, Wudel B, Bow EJ. The First Case Report of West Nile Virus-Induced Acute Flaccid Quadriplegia in Canada. Case Rep Infect Dis. 2018;2018:4361706.
262. Van Gerpen JA. Neurologic sequelae of west nile virus infection. Ochsner J. 2003;5(3):18-20.
263. Cohen J. 10.1126/science.aao6984. Science. 2017.
264. Souza INO, Barros-Aragao FGQ, Frost PS, Figueiredo CP, Clarke JR. Late Neurological Consequences of Zika Virus Infection: Risk Factors and Pharmaceutical Approaches. Pharmaceuticals (Basel). 2019;12(2).
265. Schnaar RL. Gangliosides of the Vertebrate Nervous System. J Mol Biol. 2016;428(16):3325-36.
266. Yu RK, Tsai YT, Ariga T, Yanagisawa M. Structures, biosynthesis, and functions of gangliosides--an overview. J Oleo Sci. 2011;60(10):537-44.
267. Rivera-Correa J, de Siqueira IC, Mota S, do Rosario MS, Pereira de Jesus PA, Alcantara LCJ, et al. Anti-ganglioside antibodies in patients with Zika virus infection-associated Guillain-Barre Syndrome in Brazil. PLoS Negl Trop Dis. 2019;13(9):e0007695.